Amplitudes in the Spin Foam Approach to Quantum Gravity

by

Lin-Qing Chen

A thesis
presented to the University of Waterloo
in fulfillment of the
thesis requirement for the degree of
Doctor of Philosophy
in
Physics

Waterloo, Ontario, Canada, 2017

Examining Committee Membership

The following served on the Examining Committee for this thesis. The decision of the Examining Committee is by majority vote.

External Examiner   Jesus Fernando Barbero Gonzalez
                                             Prof.

Supervisor   Lee Smolin
                                             Prof.

Co-supervisor   Laurent Freidel
                                             Prof.

Internal Member   Niayesh Afshordi
                                             Prof.

Committee Member   Bianca Dittrich
                                           Prof.

Internal-external Examiner   Eduardo Martin-Martinez
                                             Prof.

This thesis consists of material all of which I authored or co-authored: see Statement of Contributions included in the thesis. This is a true copy of the thesis, including any required final revisions, as accepted by my examiners.

I understand that my thesis may be made electronically available to the public.

Statement of Contributions

The construction of the holomorphic Spin Foam model and the calculation of Pachner Moves have been done in collaboration with Andrzej Banburski and Jeff Hnybida, which was supervised by Laurent Freidel. The asymptotics is based on work in collaboration with Andrzej Banburski. The rest of the original results are based solely on my own work.

The publications related with this thesis:

L. Q. Chen, "Bulk amplitude and degree of divergence in 4d spin foams," Phys. Rev. D 94, no. 10, 104025 (2016)

A. Banburski and L. Q. Chen, "Simpler way of imposing simplicity constraints," Phys. Rev. D 94, no. 10, 104003 (2016)

A. Banburski, L. Q. Chen, L. Freidel and J. Hnybida, "Pachner moves in a 4d Riemannian holomorphic Spin Foam model," Phys. Rev. D 92, no. 12, 124014 (2015)

Other publications during PhD:

L. Q. Chen, "Causal loop in the theory of Relative Locality," Phys. Rev. D 88, 024052 (2013)

L. Q. Chen,"Orientability of loop processes in relative locality," Phys. Rev. D 88, 124003 (2013)

Abstract

In this thesis, we study a Spin Foam model for 4D Riemannian quantum gravity, and propose a new way of imposing the simplicity constraints that uses the recently developed holomorphic representation. Rather than imposing the constraints on the boundary spin network, one can impose the constraints directly on the Spin Foam propagator. We find that the two approaches have the same leading asymptotic behaviour. This allows us to obtain a model that greatly simplifies calculations, but still has Regge Calculus as its semi-classical limit.

Based on this newly developed model, we aim at answering the following questions that previously has never been properly addressed in the field: how to efficiently evaluate arbitrary Spin Foam amplitudes in 4D? Do we have residual diffeomorphism invariance of the model? What happens to the amplitudes under coarse graining? Can we learn the degree of divergence of an amplitude simply by its graphic properties? What type of geometry in the bulk has the dominant contribution to the partition function?

Using the power of the holomorphic integration techniques, and with the introduction of new methods: the homogeneity map, the loop identity and a natural truncation scheme, for the first time we give the analytical expressions for the behaviour of the Spin Foam amplitudes under 4-dimensional Pachner moves. The model considered is not invariant under the 5–1 Pachner Move, as the configuration of five 4-simplices reduces to a single 4-simplex with an insertion of a nonlocal operator inside. Similar behaviour occurs also for the 4–2 move. The non-invariance under 5–1 move means that the vertex translation symmetry, the residual of diffeomorphism invariance for discrete gravity, is broken in this path integral formalism. We also developed a natural truncation scheme that captures the dominant contribution and preserves the geometrical structures, while at the same time efficiently reduces the complexity.

We then push the result to be more general – evaluating arbitrary amplitudes. We study the amplitudes on arbitrary connected 2-complexes and their degrees of divergence. First we derive a compact expression for a certain class of graphs, which allows us to write down the value of bulk amplitudes simply based on graph properties. We then generalize the result to arbitrary connected 2-complexes and extract a formula for the degree of divergence only in terms of combinatorial properties and topological invariants. By regulating the model, this result allows us to find the dominant contributions to the partition function, which gives us some valuable hints about the continuum limit. The distinct behaviors of the model in different regions of parameter space signal phase transitions. However, in the regime which is of physical interest for recovering diffeomorphism symmetry in the continuum limit, the most divergent contributions are from geometrically degenerate configurations. We finish with discussing possible resolutions, the physical implications for different scenarios of defining the continuum limit and the analytical insights we have gained into the behavior of Spin Foam amplitudes.

Acknowledgements

Dedication

In memory of my grandparents.

Table of Contents

x

List of Tables

List of Figures

Chapter 1

Introduction

1.1   The challenge of finding quantum gravity

Quantum mechanics and general relativity are distinct frameworks trying to describe our universe from the two different aspects – microscopical and astrophysical. The two frameworks meet when we confine a large amount of energy into a tiny region of space. So far we have yet to find a consistent theory that could describe this regime.

We have however learnt valuable lessons from three different intersections of gravity with quantum mechanics: quantum field theory on curved spacetime, gravitons on a fixed spacetime background, and the conjecture of holographic duality. By studying quantum field theory on curved spacetimes, we have understood how the cosmic microwave background could encode information from the early universe, but this approach fails when we try to describe physics close to the cosmological singularity [1, 2]. We also learnt that black holes radiate, but we still do not fully understand whether the radiation encodes information of the collapsed matter as well as what the end-stage of this evaporation is [3, 4, 5]. We have learnt that non-inertial observers

measure Unruh tempreature in vacuum, but we do not know whether an inertial observer is still a valid concept in quantum spacetime[6]. From the perturbative approach of treating gravity like a quantum field theory on a fixed background, we have understood the structure of graviton scattering amplitudes, but we also know that gravity is perturbatively nonrenormalizable, and also the ambiguity of choosing background versus the perturbation brings ambiguity of causal structure [7, 8, 9, 10]. This implies that either new degrees of freedom are yet to be discovered, like the W bosons in the Fermi's four-fermion interaction, or that new nonperturbative methods need to be developed. Lastly, through the AdS/CFT correspondence, we have gained insights into strongly coupled quantum systems by studying AdS black hole solutions and obtained interesting results of probing geometry in the bulk using entanglement entropy on the boundary, but we have not yet learnt anything new about the black hole interior itself [11, 12, 13, 14, 15].

Nature never fails to surprise us when we try to go beyond the current knowledge and pursue a more fundamental theory. Quantum gravity lies in the heart of this pursuit. We expect a theory of quantum gravity to be able to provide a description of the microstructure and dynamics of quantum spacetime, while at the same time surprise us with novel predictions in the regions of high curvature, such as the interior of black holes and the beginning of our universe. The central questions of quantum gravity are about the very nature of spacetime, hence we are at the same time facing some of the biggest philosophical questions regarding the existence of our universe, its origin and its fate.

A unique challenge of such a research field is that we lack the guidance from experimental data. The relevant scale of quantum gravity is very remote from our current technological capabilities[16]. However, we are guided by the strong constraints of the known physics, such as the structure of Hilbert space, diffeomorphism invariance, unitarity, semiclassical dynamics etc. The theory needs to be UV complete, mathematically well-defined, and at the same time consistently bridge a vast range of scales to connect to the known physics. Due to these strict constraints, we do not have many theories on the market to get confused about which is the right one yet. Indeed, one could argue that we have none that satisfy all the requirements yet.

Different approaches to quantization of gravity take different subsets of the known principles as the starting point. However, we have to keep in mind that while the known physical principles can provide guidance, they can also be misleading at the same time: the framework we will need for quantum gravity might be so dramatically different with what we have known that certain assumptions we have previously taken for granted might have to be dropped. For example, locality, which has been central to the construction of quantum field theories, has been shown to be relaxed in several approaches of quantum gravity [17, 18, 19, 20]

The successful framework of quantum field theory cannot be directly applicable to quantum gravity. One crucial reason is that standard field theory needs a rigid pre-established spacetime

geometry, since even the inner product on Fock space depends on a background metric. Hence, a key step for formulating quantum gravity is to invent a framework of quantum theory that does not refer to the pre-existent notion of background. Loop quantum gravity aims at addressing this task [21, 22, 23, 24]. It has had a great success in constructing the kinematical Hilbert space for quantum gravity: the state space of the theory consistently solves the spatial diffeomorphisms constraints [23, 25, 26]. However, solving the dynamics of the theory, namely the Hamiltonian constraint, has turned out to be a great challenge. The Spin Foam approach was invented to tackle the dynamics via the path integral formalism[27]. It is this covariant approach that we will focus on in this thesis.

1.2   A brief history of Spin Foams

Spin Foam models attempt to rigorously define a path integral formalism of Quantum Gravity. Their construction was inspired by the discretization of general relativity á la Regge, loop quantum gravity and topological quantum field theories. Historically, the very first spin foam model was proposed by G. Ponzano and T. Regge in 1968 as a state sum model for 3-d quantum gravity [28], long before the term *Spin Foams* was introduced [30]. In 90's a path integral formalism of quantum gravity was invented to tackle the dynamics of loop quantum gravity from the covariant perspective, through defining transition amplitudes between spin network states as "sums over surfaces.[29].

It is a hope that the path integral formalism would not only provide a mathematical tool to implement the projector on physical states satisfying the Hamiltonian constraint, but also provide a physical picture of the quantum spacetime for loop gravity. It was later that the state-sum models obtained from discretizing the path integral for 3D BF theory were shown to be related to the Spin Foam amplitudes from the "sum-over-surfaces path integral formalism [30]. Along this path, inspired by the relation between gravity and topological field theories, various 4 dimensional Spin Foam models were proposed [35][36] [37] [38] [41][42]. These early Spin Foam models had certain insights, but also limitations. The proposal which has stimulated a lot of explorations was the Barrett-Crane model in both Euclidean and Lorentzian signatures [33, 34, 37, 38]. It was constructed by using geometric quantization techniques [39][40]. The model has remarkable simplicity, however, it over-constrains the solution space and results in the wrong semi-classical limit.

After many years of clarifying the foundations of Spin Foams, and introducing new techniques – using coherent intertwiners to build Spin Foam amplitudes, labelling boundary states with classical geometric data and using saddle-point techniques to study asymptotics – finally

3

a new class of Spin Foam models was invented, which is now known as Engle-Pereira-Rovelli-Livine and Freidel-Krasnov (EPRL-FK) models [43, 44, 45, 46]. At the level of a single 4-simplex, this class of models provides the desired semiclassical limit – Regge Calculus. It has been suggested in [47, 48] that we can bring the models closer to reality by including the cosmological constant with deforming the underlying group structure to quantum groups. In 3-d this has been achieved by Turaev and Viro [32, 49], while in 4-d the work is ongoing, see for example [50, 51, 52, 53]. An alternative construction by using Chern-Simons theory has been given in [54].

Having defined the EPRL-FK models, a lot of effort has been made in recent years towards obtaining physical predictions, such as studying graviton propagators, the resolution of spacetime singularities, Planck stars and attempting cosmological predictions [55, 56, 57, 58, 59]. While many interesting results have been obtained, their validity is questionable because some very fundamental questions at the heart of the model have not been fully understood yet.

The first question is the gauge symmetry of the model. In 3D Spin Foams this is not an issue, because the model does not have local propagating degrees of freedom – any discretization captures the continuum physics. In 4D however, discretization in general breaks diffeomorphism invariance [60, 61, 62]. One open question is whether the EPRL-FK model has any residual diffeomorphism symmetry and how to check it. The next question would be whether we can recover the full diffeomorphisms in the continuum limit.

The crucially related question is about the renormalization of the model. The Spin Foam paradigm is essentially a bottom-up approach – postulating the dynamics of quantum spacetime at the smallest scales. To see whether the theory recovers general relativity in the large scale limit and whether we can connect predictions with any observable phenomena, we need to bridge the gap of scales. The physical predictions we can get from the model will not be reliable without a consistent renormalization procedure relating observables at different scales [62].

Before we even attempt renormalizing the Spin Foam models, we have to first be able to evaluate the divergences of Spin Foam amplitudes. A crucial aspect of studying quantum field theory is understanding the behavior of divergence. Ultraviolet divergence comes from integrating degrees of freedom to arbitrarily high energy scales and should be removed through renormalization, while infrared divergence is due to an infinite number of soft massless particles and does not influence measurable quantities. The generic divergences in Spin Foams are very different to those in quantum field theory. In Spin Foams, the existence of minimum length scale removes the ultraviolet divergence [10, 24, 27]. However, the arbitrarily large length scale degrees of freedom in the path integral can in principle lead to infrared divergences. The divergences from self-energy and radiative corrections in 4-d models have been studied in [74, 75, 76]. The general structure has been studied in 3-d [79, 80, 81, 82, 83] and also in 4-d topological group

4

field theory [84, 85]. Understanding the general behavior of divergences is a basis for studying renormalization in Spin Foams.

As a Spin Foam model is defined by a path integral over all the geometrical degrees of freedom with a given boundary, it is crucial to understand what type of geometry has the dominant contribution to the partition function. It will give us hints as to whether the theory will lead to smooth 4-d geometry in its continuum limit. In the colored tensor models [86, 87, 88, 89, 91], as it has been shown in the 1/N expansion, the dominant contribution to the partition function comes from melonic graphs, which leads to branched polymers phase [91, 92]. Such a complete analysis of dominant contributions has always been missing in non-topological 4-d Spin Foam models.

Only achieving the correct semi-classical limit without addressing the above points does not quantum gravity make. One crucial reason of why they have not yet been answered is the technical difficulty of precisely evaluating amplitudes for more than one single building block.

1.3 The aspirations of this research

The main goal of this thesis is answering the following questions:

- How to evaluate arbitrary amplitudes efficiently?

- Do we have residual diffeomorphism invariance?

- What happens to the amplitudes under coarse graining?

- Can we learn the degree of divergence of an amplitude simply by its graphic properties?

- What type of geometry in the bulk has the dominant contribution to the partition function?

1.4 Plan of the thesis

Chapter 2 serves as the background and basis. I will introduce the basic idea of Spin Foam models. We start with a topological field theory, known as BF theory, which at the classical level can be constrained to a first-order formulation of General Relativity. A Spin Foam model is a proposal for a discretized version of these constraints at the quantum level, which are imposed on the partition function of BF theory. The desired semi-classical limit of a Spin Foam model

is the Regge calculus, which is a discrete approximation of the smooth geometrical solutions in General Relativity by piece-wise flat simplicial manifolds.

In the discrete approaches towards 4-d quantum gravity, a subtlety is the gauge symmetry. This is even present at the classical level: the discretization breaks diffeomorphism invariance in general[60, 61]. I will review a series of works identifying gauge symmetry in Regge Calculus. At the quantum level, in the canonical formalism the difficulty is solving the Hamiltonian constraint, which generates the diffeomorphisms in the time direction. In the path integral formalism, the challenge of finding the correct continuum limit is deeply related to recovering the diffeomorphism invariance through renormalization[99, 100, 101, 102, 103, 62].

The divergences in Spin Foam models (with vanishing cosmological constant) are expected to encode information about gauge symmetry [93, 94, 95, 96, 97]. Diffeomorphism symmetry leads to non-compact gauge orbits, thus a path integral over such orbits leads to divergence. This is known exactly in the 3-d Ponzano-Regge Model. Residual action of the diffeomorphism group acts at the vertices of triangulation of a 3D manifold as a vertex translation symmetry. In the Ponzano-Regge Model, the divergences which are due to this translation symmetry can be removed by using the Faddeev-Poppov procedure [93]. 3D gravity is topological and has no local degrees of freedom, hence its continuum limit is fully described by the discrete model, which is not the case for 4D gravity. In the case of 4D models, the situation is non-trivial, because the diffeomorphism symmetry in discrete models is broken[60, 61] and is only expected to be recovered in the continuum limit through renormalization [62]. Nevertheless, the discretized 4D Regge action has the vertex translation symmetry under the 1–5 refining Pachner Move [61]. Therefore, understanding the behavior of divergence in 4D Spin Foam models can give us hints about the residue of diffeomorphisms present in the model.

In Chapter 3, I will go through the construction of a Spin Foam model with the holomorphic representation. It is a 4D Riemannian model with vanishing cosmological constant [105, 106]. The model arose from rewriting Spin Foams in terms of coherent states using the SU(2) holomorphic representation beginning with the work in [108, 109] and continued in [110, 111, 112, 113, 114, 115, 116, 117, 119, 121, 122, 123]. In the holomorphic representation complicated integrals over SU(2) irreducible representations can be rewritten as spinor integrals over the complex plane. This allows for exact evaluations of complicated spin network functions [121, 123].

The standard framework for imposing the simplicity constraints corresponding to the EPRL/FK models was implemented in the holomorphic framework by Dupuis and Livine in [115], which we will refer to as the DL model. In the Riemannian case of the gauge group $SU(2)_L \times SU(2)_R$, the constraint imposes left and right spinors to be proportional to each other on the boundary spinor network of a 4-simplex. Different with the conventional approach, we impose the simplic-

ity constraints on the Spin Foam propagators rather than on the boundary spinor networks. This effectively imposes the constraints not only on the boundary, but also in the bulk. This choice allows us to calculate the Spin Foam amplitudes much more efficiently. Naively it is not obvious that imposing more constraints does not spoil the semi-classical limit of the Spin Foam model. We will show that with the alternative way of imposing the simplicity constraints, the model still has the same semiclassical limit as the EPRL/FK model [126, 127, 63, 64, 65, 66, 67, 70] at the leading order [106], but the computability of the model has been tremendously simplified. The differences in asymptotics between the models reside in the Hessian, the overall normalization and the higher order terms as well as on the off-shell trajectories.

Chapter 4 is a whole package of newly developed techniques and methods which enable us to evaluate amplitudes beyond one single 4-simplex. As the partition function is defined on the dual of simplicial lattice – the 2-complex, we will first analyze the graph structure. We will introduce the concepts of a *spanning tree*, a *fundamental cycle*, and an *optimal spanning tree* , which will play a crucial role in expressing the result of arbitrary amplitudes. Then we will review the partial gauge fixing procedure to fix the subgroups SU(2) – the internal rotational symmetry on a spanning tree of edges.

In the holomorphic Spin Foam model, the computation of evaluating the partition function essentially amounts to integrations of power series of spinor polynomials. We will introduce *the homogeneity map* – a useful tool which allows us to perform the calculation in a very tractable and compact way. Graphically, integrating the geometrical degrees of freedom from the shared faces of simplices is to integrate loops in the cable diagrams. We will summarize this structure in Section.4.4. In 3D case, the triviality of such loop structures is just another aspect of the fact that 3D gravity is topological and does not have local degrees of freedom. In 4D model, we will see immediately where the nontriviality comes from. The simplicity constraints break certain invariance from a topological theory and integrating along a loop results in non-local couping among different fundamental building blocks. This is a very generic feature which is insensitive to different ways of imposing the simplicity constraints. We expect this carries over to the Lorentzian case.

For coarse graining the Spin Foam model, or trying to evaluate arbitrary amplitudes, identifying relevant degrees of freedom is essential. We will introduce a natural truncation scheme, and the resulting amplitudes are structure preserving, while at the same time encode the non-local degrees of freedom as a non-local coupling function of spins.

Chapter 5 provides examples of applying the techniques developed in the previous chapter. We evaluated all the 3D and 4D Pachner Moves. We are interested in this type of moves because they are the most basic local coarse graining moves on a simplicial decomposition of a manifold [68]: Pachner moves are local changes of triangulation that allow to go from some triangulation

of a manifold to any other triangulation in a finite number of steps. An n–$(2 + d − n)$ Pachner move changes a triangulation composed out of n d-simplices to one with $(2 + d − n)$ d-simplices. Only the n–1 Pachner moves are pure coarse graining moves.

We first reproduce the calculation of Pachner moves in the 3D Ponzano-Regge model in terms of the holomorphic representation. There are two Pachner moves: the 4–1 move and 3–2 move. The results have been long known: the 3–2 move is invariant and 4–1 move is invariant up to a factor of an SU(2) delta function, which results from not fixing the gauge translation symmetry. It is however the first time, that Pachner moves have been calculated explicitly in a simplicity-constrained Spin Foam model of 4–dimensional Quantum Gravity in [105]. We find that the model considered is not invariant under the 5–1 Pachner move, as the configuration of five 4-simplices reduces to a single 4-simplex with an insertion of a nonlocal operator inside. Similar behavior occurs also for the 4–2 move. The truncation scheme allows us to make both the 4–2 and 5–1 moves structure preserving up to a non-local weight depending on the boundary data. The 3–3 move is not invariant, unless very special symmetric boundary data are considered, as expected for a model of 4D quantum gravity.

In Chapter 6 we first start with gaining some preliminary intuition of the structure of amplitudes through understanding coupling of loops and adding edges. We then find a more efficient approach and push the analytical results to arbitrary amplitudes[107]. The goal here is understanding some physical questions, such as what type of geometry has the dominant contribution to the partition function, and what is the exact degree of divergence for the partition function associated with general diagrams. The quantity of interest here is the *bulk amplitude $\mathcal{A}_{bulk}$*, which is the evaluation of partition function on a fully contracted 2-complex, or the evaluation on a connected 2-complex with zero boundary spins.

For certain class of graphs, in which there exist optimal spanning trees, we derive an expression to capture the dominant degrees of freedom in the partition function. Using this expression, one can simply read out the evaluation of truncated bulk amplitude through combinatorial properties of a graph. We will also introduce *simplifed diagrams* to make the structure of the result more transparent. For more general graphs, with a generic choice of spanning trees, we need to evaluate nesting of loop identities which leads to truncation within truncation. However, with the gauge fixing choice along an optimal spanning tree, the error of truncation is minimized. We then show that even though the truncated degrees of freedom depend on the choice of gauge-fixing tree, the dominant contribution is tree-independent and can be captured by a simple expression. A very good approximation to arbitrary 4-d Spin Foam bulk amplitude can be expressed in a compact closed form, which allows us to derive the exact degree of divergence for any amplitude in the next Chapter.

In Chapter 7, using the asymptotic formula of the hypergeometrical functions, we extract

a simple formula for the exact degree of divergence for arbitrary 2-complexes, in which the variables are the number of vertices $|V|$, number of faces $|F|$ and the number of edges $|E|$:

$$D(\Gamma) = \Lambda^{(\eta+2)|F|-6|E|+3|V|-3}, \tag{1.1}$$

where Λ is a large spin cut-off and η is the power of face weight $(2j+1)^\eta$. The dependence on Barbero-Immirzi parameter has dropped out in the asymptotic analysis. The only parameter in the degree of divergence formula is the power of the face weight η. When the face weight is $(2j+1)^3$, i.e. $\eta = 3$, the 5–1 Pachner move has Λ^2 divergence, while 4–2 Pachner move is finite. This is the desired degree of divergence one would expect for recovery of diffeomorphism symmetry in the model [94, 96].

The above expression can also be written in terms of topological invariants. In terms of a topological quantity called the *degree of the graph* $\omega_{4d}(\Gamma)$, we find

$$D(\Gamma) = \Lambda^{(\eta-2)|F|-4\omega_{4d}(\Gamma)/3+13}. \tag{1.2}$$

Hence there are regimes of the face weight η with distinct behaviors and we analyze them in section 7.2. We find that when $\eta = 2$, the divergence solely depends on the degree of the graph as in the colored tensor models [90]. In this case the continuum limit defined by summation of all graphs is described by the branched polymers phase[91]. In the region when 5–1 move is divergent while 4–2 is not, the dominant contribution comes from melonic graphs while maximizing the number of vertices. We finish with discussing the physical implications for different scenarios of defining the continuum limit, and the analytical insights we have gained into the behavior of Spin Foam amplitudes.

9

Chapter 2

Spin Foams and diffeomorphisms

In this chapter, we will review basic ideas and construction of the Spin Foam approach to quantum gravity, especially focusing on the fate of diffeomorphism invariance.

We start with introducing Regge Calculus, a simplicial approximation of General Relativity, which is the desired semi-classical limit of Spin Foam models. Then we will review the relationship between gravity and a topological field theory, known as BF theory, which can be constrained to a first-order formulation of General Relativity at the classical level. This observation has been at the heart of Spin Foam construction. Then we will discuss quantizing BF theory, the constraints at quantum level, and the general structure of Spin Foam amplitudes.

In the discrete approaches towards 4D quantum gravity, a key subtlety is the diffeomorphism invariance. We will review and discuss the state of art regarding this question related to the Spin Foam approach, including the diffeomorphisms in 3D classical and quantum gravity, the divergence from the residual gauge symmetry, identifying gauge symmetry in Regge Calculus, and the challenge for 4D quantum gravity.

2.1   Regge Calculus

Regge Calculus was developed as a powerful tool of analyzing gravitational systems that are not amenable to perturbation approach and are devoid of symmetries. The formalism was introduced by Tullio Regge in 1961 [72]. It is a discrete approximation of the smooth geometrical solutions in General Relativity by piece-wise flat simplicial manifolds.

More precisely, Regge Calculus approximates a smoothly curved n-dmensional manifold

as a collection of n-simplices, joined by codimension-2 hinges on which all the curvature is concentrated. In 4D, the curvature is concentrated on triangles.

The deficit angle ϵ_t associated with a hinge t is defined as summing over the angles for all the simplices $t \subset \sigma$ that meet on the given hinge and subtracting from 2π. If we parallel transported a vector from one simplex to the next around the hinge, it would result in a rotation by an angle

$$\epsilon_t = 2\pi - \sum_{\sigma \supset t} \xi_t^\sigma, \tag{2.1}$$

where ξ_t^σ is the dihedral angle between the two tetrahedra in σ sharing the triangle t. It is the angle between the two 4-vectors $\mathcal{N}_a, \mathcal{N}_b$ which are normal to the two tetrahedra $a, b \subset \sigma$ respectively. In 4 dimension, the action of Regge Calculus reads:

$$S_{Regge} = \sum_t A_t \epsilon_t \tag{2.2}$$

which is the total sum of deficit angles weighted by the area of the hinge. Its continuum limit is the Einstein-Hilbert action. Below we provide a summary of the formalism in different dimensions.

Dimensionality of manifold	2	3	4
Hinge where cycle of simplices meet with a deficit angle ϵ_t	Vertex	Edge	Triangle
"Weight" of such hinge	1	Length l_t	Area A_t
Contribution from all hinges to curvature	$\sum_t \epsilon_t$	$\sum_t l_t \epsilon_t$	$\sum_t A_t \epsilon_t$
Continuum limit of this contribution	$\int \sqrt{-g^{(2)}} R^{(2)} \mathrm{d}^2 x$	$\int \sqrt{-g^{(3)}} R^{(3)} \mathrm{d}^3 x$	$\int \sqrt{-g^{(4)}} R^{(4)} \mathrm{d}^4 x$

Table 2.1: Regge Calculus in different dimensions.

2.2 Basics of Spin Foams

Spin Foam models originated from the insight that classical gravity can be described as a topological field theory, known as BF theory, with a simplicity constraint. As BF theory only has

topological degrees of freedom, it can be quantized very easily. Spin Foam models are then a path integral quantization of BF theory, with simplicity constraints imposed at the quantum level.

2.2.1 From BF theory to Gravity

Classically, BF theory is defined on a principal G-bundle over a d dimensional manifold $\mathcal{M}$, with a group G and connection ω. B field is a d-2 form in the adjoint representation of G. The connection is defined to be a $\mathfrak{g}$-valued one-form on a local trivialization of the principal bundle, and the curvature 2 form associated to ω is $F(\omega) = d\omega + \omega \wedge \omega$. The action is defined as

$$S_{BF} = \int_{\mathcal{M}} \text{Tr}\,[B \wedge F(\omega)]. \tag{2.3}$$

which is invariant under the gauge transformation

$$g^*(\omega) = g^{-1}\omega g + g^{-1}dg, \quad g^*(B) = g^{-1}Bg, \;\; g \in G \tag{2.4}$$

After varying the action, we can get the equations of motion:

$$F = 0, \quad d_\omega B = dB + \omega \wedge B = 0 \tag{2.5}$$

Hence the connection ω is flat and B is closed. It is a topological field theory in the sense that all the solutions of equations of motion are locally gauge equivalent. Hence the theory has no local degrees of freedom.

In 3 dimensions, if we choose the gauge group to be $SU(2)$, the B field is a Lie algebra valued 1 form – same as the triads in 3d gravity. We can see that the BF action is precisely 3d gravity in Euclidean signature without cosmological constant:

$$S_{3d}[e, \omega] = \int_{\mathcal{M}} \text{Tr}\,[e \wedge F(\omega)]. \tag{2.6}$$

We will analyze its gauge symmetry in section 2.3.2.

In 4 dimensions, B field is a bivector that lives at the tangent space of $\mathcal{M}$, in which the tetrad e span the basis. It was proved in [43] [lemma II.1 3] that a bivector B^{IJ} in $\mathbb{R}^4$ or $\mathbb{M}^{1,3}$ is a simple bivector iff there exists a vector n^I such that $n^I B^{IJ} = 0$. When this condition is satisfied, B^{IJ} is constrained to be proportional to $e^I \wedge e^J$ or $*(e^I \wedge e^J)$. Using a parameter γ, known as the *Barbero-Immirzi parameter* to distinguish these two sectors, one gets the Palatini formulation of gravity from S_{BF}:

$$S_{Palatini} = \int_{\mathcal{M}} tr\left[*(e \wedge e) \wedge F(\omega) + \frac{1}{\gamma} e \wedge e \wedge F(\omega) \right] \tag{2.7}$$

12

in which the tetrad and connection are independent variables. Spin Foam models are then a path integral quantization of BF theory, with simplicity constraints imposed at the quantum level such that, semiclassically, the B field is a simple bivector. To well-define the path integral, we discretize the classical BF theory on a simplicial complex first. We will show this in the next section. Using simplicial complexes allows us to have a natural connection with Regge Calculus that we have just introduced, and which is also the critical action for Spin Foam models in the semiclassical limit [126, 127, 63].

2.2.2   BF partition function and diagrammatics

Here we will briefly review the discretized path integral formalism of SU(2) BF theory. We then introduce a convenient graphic notation – the cable diagrams, and discuss their geometrical meaning. We will arrive at two equivalent ways of writing BF partition function: in terms of projectors or vertex amplitudes.

Let Δ be a discretization homeomorphic to a d-dimensional manifold $\mathcal{M}$ and let Γ be its dual 2-complex. The edge e is dual to the (d-1) cell, and the face f is dual to the $d - 2$ cell in the discrete manifold. Now let us discretize the $d - 2$ form B on Δ by smearing it on the $d - 2$ cell,

$$B_f = \int_{(d-2)cell} B, \ \ f \subset \Gamma \tag{2.8}$$

which is an Lie algebra element of the gauge group. There is a group element assigned to each edge e of the dual graph Γ by the path-ordered exponential:

$$g_e = \mathcal{P} \exp(-\int_e \omega) \in SU(2), \ \ e \subset \Gamma \tag{2.9}$$

If we use g_f to represent the product of group elements around a face

$$g_f \equiv \overrightarrow{\prod_{e \subset f}} g_e, \tag{2.10}$$

then the partition function of SU(2) BF theory is simply

$$\mathcal{Z}_{BF}(\mathcal{M}) = \int \prod_{e \in \Gamma} dg_e \prod_{f \in \Gamma} \delta(g_f). \tag{2.11}$$

The delta function for each face ensures the flatness of the connection. It is the discrete analog of vanishing curvature for 3d gravity.

13

We can expand the delta functions in terms of the fundamental representations j_f by using the Peter-Weyl theorem,

$$\delta(g_f) = \sum_{j_f} d_{j_f} \mathrm{tr}\left(\rho(g_f)\right) \tag{2.12}$$

where d_{j_f} is the dimension of the representation space $d_j = 2j+1$, the trace on the RHS is over the representation j_f. Inserting the resolution of identity on the representation space $V^{j_{f_1}} \otimes \cdots \otimes V^{j_{f_d}}$ between each group element in the trace, the partition function of BF theory can be written as

$$\mathcal{Z}_{BF}(\mathcal{M}) = \sum_{j_f} \prod_{f \in \Gamma} (2j_f + 1) \prod_{e \in \Gamma} P^{j_{f_1}, \ldots, j_{f_d}}, \tag{2.13}$$

where $P^{j_{f_1}, \ldots, j_{f_d}}$ is the projector onto the SU(2) invariant subspace of $V^{j_{f_1}} \otimes \cdots \otimes V^{j_{f_d}}$ given by group averaging the tensor product of irreducible representations ρ^j

$$P^{j_{f_1}, \ldots, j_{f_d}} = \int \mathrm{d}g_e \, \rho^{j_{f_1}}(g_e) \otimes \cdots \otimes \rho^{j_{f_d}}(g_e), \tag{2.14}$$

where the basis labels of the representations ρ^{j_f} have been suppressed. The projector is the unique map $P^{j_1, \ldots, j_d} : \rho^{j_1} \otimes \ldots \otimes \rho^{j_d} \to \mathrm{Inv}_{\mathrm{SU}(2)}[\rho^{j_1} \otimes \ldots \otimes \rho^{j_d}]$, and is often called the Haar projector.

Cable diagrams are an intuitive and useful graphic notation for the computations of Spin Foam partition functions (a review of these techniques is given in [100]). Here it is used to represent the structure of partition function on the dual 2-complex Γ. Cable diagrams are basically composed by strands passing through boxes: a strand denotes a representation of a symmetry group living on the edge e of Γ, and a box denotes the group averaging of a set of representations in the projector.

$$\rho^j = \underline{\qquad j \qquad} \qquad \text{and} \qquad P^{j_1, \ldots, j_d} = \begin{array}{c} \underline{j_1} \\ \underline{j_2} \\ \underline{j_3} \\ \underline{j_4} \end{array} \boxed{} \begin{array}{c} \underline{j_1} \\ \underline{j_2} \\ \underline{j_3} \\ \underline{j_4} \end{array} \quad (d = 4) \tag{2.15}$$

Strands form closed loops, which correspond to the faces in the dual 2-complex Γ. Fig.2.1 and Fig.2.2 give an example in 3 dimensions: a 3-simplex, its dual 2-complex and the corresponding cable diagram.

The projector $P^{j_1, \ldots, j_d}$ can be expressed as a sum over a basis of invariant tensors called *intertwiners*, which are elements in the Hilbert space $\bigoplus_{j_i} \mathrm{Inv}_{\mathrm{SU}(2)}\left[V^{j_1} \otimes \cdots \otimes V^{j_4}\right]$

$$P^{j_1, \ldots, j_d} = \sum_{\iota} \begin{array}{c} j_1 \\ j_2 \\ j_3 \\ j_4 \end{array} \!\!\!\searrow \iota \quad \iota \!\!\!\swarrow\!\! \begin{array}{c} j_1 \\ j_2 \\ j_3 \\ j_4 \end{array} \tag{2.16}$$

14
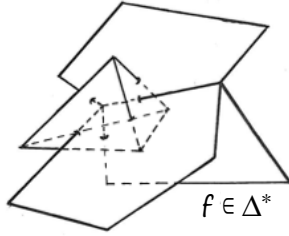
Figure 2.1: A tetrahedron and its dual 2-complex
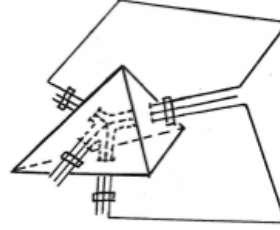
Figure 2.2: A tetrahedron and its cable diagram

where ι labels a basis of normalized intertwiners. We see that the projector factorizes on the edges, while the intertwiners contract at the vertices of Γ expressing the partition function in terms of so called vertex amplitudes $A_v(j_f, \iota_e)$. For example, if $\mathcal{M}$ is 4 dimensional, the BF partition function can be written as

$$\mathcal{Z}_{BF}(\mathcal{M}) = \sum_{j_f} \prod_{f \in \Delta^*} (2j_f + 1) \sum_{\iota_e} \prod_{v \in \Gamma} A_v(j_f, \iota_e) \tag{2.17}$$

where the vertex amplitudes

$$A_v(j_f, \iota_e) := \text{} \; . \tag{2.18}$$

In 4d the vertex amplitudes of the Ooguri model (which is basically quantum 4D BF theory) are 15j symbols labelled by 10 spins and 5 intertwiner labels, which are also spins. In 3d the vertex amplitudes of the Ponzano-Regge model are 6j symbols with no intertwiner labels since the rank three intertwiner space is one dimensional.

2.2.3 Towards 4D quantum gravity – linearized simplicity constraints

We are now ready to discuss the simplicity constraints at the quantum level[10, 43, 46]. In the Riemannian case, the underlying BF theory has the gauge group $\text{Spin}(4) = \text{SU}(2)_L \times \text{SU}(2)_R$,

which is the double cover of SO(4). This means that the Spin(4) BF partition function can be written as the product of two SU(2) BF partition functions. Note that the unitary representations of Spin(4) can be expressed as a direct sum of those of SU(2) by

$$V_{j_L, j_R} = \bigoplus_{j=|j_L - j_R|}^{j_L + j_R} V_j. \tag{2.19}$$

In the following we will see that the simplicity constraints are actually imposed on representation labels, as an isomorphism between the two SU(2) sectors.

Classically, at the discrete level, we can write the constraints imposing that $B^{IJ} = *(e^I \wedge e^J)$ in a simple form if we first define

$$B = \frac{\gamma^2}{\gamma^2 - 1}(J - \frac{1}{\gamma} * J) \tag{2.20}$$

where J is the variable conjugate to the holonomy, and γ is the Barbero-Immirzi parameter we have introduced earlier. Then the linearized simplicity constraints, which impose the existence of a common normal to the B fields, can be written in a compact form as

$$\frac{1}{2}\epsilon^j_{kl}J^{kl} - \frac{1}{\gamma}J^{0j} = 0 \tag{2.21}$$

In the EPRL-FK models, this equation is expressed as an equation constraining the Spin(4) representation labels. This is because J is the rotation generator and the Eq. (2.20) is a condition on the Casimirs of the representations. In the Riemannian case, the solution to the constraints is the restriction on the spins of the two SU(2) sectors

$$j_R = \frac{1 + \gamma}{|1 - \gamma|}j_L, \tag{2.22}$$

together with selecting a projection $\mathcal{Y}$ into one term in direct sum of SU(2) representation spaces in Eq. (2.19). This projection can be written as

$$\mathcal{Y}_j : V_{(1+\gamma)j/2, |1-\gamma|j/2} \to V_j. \tag{2.23}$$

As the Spin(4) Haar projector is a product of two SU(2) Haar projectors, imposing the simplicity constraints results in working with a constrained projector

$$P_{EPRL-FK}(j_1, \ldots, j_4) = P_L^{\frac{|\gamma-1|}{2}j_1 \ldots \frac{|\gamma-1|}{2}j_4} P_R^{\frac{\gamma+1}{2}j_1 \ldots \frac{\gamma+1}{2}j_4}(\mathcal{Y}_{j_1} \otimes \ldots \otimes \mathcal{Y}_{j_4})P_L^{\frac{|\gamma-1|}{2}j_1 \ldots \frac{|\gamma-1|}{2}j_4} P_R^{\frac{\gamma+1}{2}j_1 \ldots \frac{\gamma+1}{2}j_4} \tag{2.24}$$
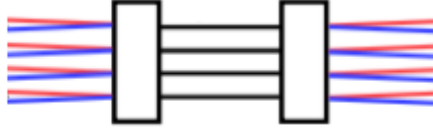
Figure 2.3: Graphic notation of projectors under the $\mathcal{Y}$ map.

Graphically, this can be represented as in Fig.2.3.

The EPRL-FK partition function can be then written as

$$\mathcal{Z}_{EPRL-FK} = \sum_{j_f} \prod_{f \in \Delta^*} d_{(1+\gamma)j_f/2+1} d_{|1-\gamma|j_f+1} \prod_{e \in \Delta^*} P_{EPRL-FK}(j_1, \ldots, j_4), \tag{2.25}$$

where $d_j = 2j + 1$ is the dimension of V_j. As we have discussed in the last section, this product of constrained projectors can be rewritten as a sum over vertex amplitudes.

More generally, a Spin Foam model is defined as a choice of the set of 2-complexes dressed with representations and intertwiners,

$$Z(\Gamma) = \sum_{j_f, \iota_e} \prod_f A_f(j_f) \prod_e A_e(j_f, \iota_e) \prod_v A_v(j_f, \iota_e). \tag{2.26}$$

This expression is also known as the local Spin Foam ansatz [31]. Note that in this general expression, when we write the model in terms of projectors[1], the vertex amplitude A_v is trivial; whereas when we express the model in terms of 15j symbols, like in Eq.(2.17), the edge amplitude A_e will be trivial.

The partition function we have discussed so far has been for a fixed 2-complex. Eventually, to get the full quantum history corresponding to the boundary state $\partial\mathcal{M}$, we need to sum over all the intermediate spinfoams:

$$Z(\partial\mathcal{M}) := \sum_{\Gamma} w(\Gamma)Z(\Gamma), \tag{2.27}$$

where $w(\Gamma)$ is a weight associated to each 2-complex, which has been suggested to be a symmetry factor of the 2-complex. Later in the thesis we will discuss the subtleties of this basic definition.

2.3 Diffeomorphisms

The framework of loop quantum gravity was originally invented by the inspiration of lattice gauge theory, aiming at taking gauge invariant description of gravity as the starting point. The

---

[1]It is only really a projector in BF case, and we will use the term "propagator" for the simplicity constrained models.

spatially diffeomorphic invariant states in LQG are given by equivalence class of knots, which spans the Hilbert space[26, 25]. As this canonical formalism meets an obstacle in terms of dynamics, the path integral formalism was constructed to tackle this issue. Even though the partition function of the model has been well-defined and uses spin networks as boundary states, the precise connection to the canonical formalism and the fate of full spacetime diffeomorphisms is still very unclear.

2.3.1   Gauge symmetry in the lattice gauge theory

Lattice gauge theory was initially developed in the need of a non-perturbative treatment to understand the low energy regime of QCD. In high energy, QCD is an asymptotically free theory, which is intimately connected with the fact that the gauge group is non-abelian. In this strong interacting regime, there were a lot of new questions that required techniques beyond perturbation theory, such as confinement, hadron mass and properties, chiral symmetry breaking etc.

The path integral formalism only has a well-defined meaning for systems with countable number of degrees of freedom. The introduction of a space-time lattice allows a well-defined measure in the path integral since we only have a discrete set of variables to integrate. The finite lattice spacing a also results in a cutoff in momentum space, which serves as a natural regulation of the UV behavior.

In the seminal paper in 1974[71], Wilson introduced the gauge invariant variable $\mathcal{W}_c$ along a closed loop c:

$$\mathcal{W}_c = \mathrm{Tr}[\mathcal{P}\exp i \oint_c A_\mu dx^\mu] \tag{2.28}$$

In the discretization, the gauge field is replaced by a holonomy that lives on the links between lattice points. For example, a lattice Yang-Mills action can be written as

$$S_{YM} = -\sum_c \frac{\beta}{N} Re(\mathcal{W}_c) \tag{2.29}$$

By using the Wilson loops variables, this discretization of the continuum theory has all the local gauge symmetries by construction. The idea of these Wilson loops inspired the loop variables in LQG. It is important to comment here that since the QCD gauge group SU(3) is compact, there is no divergence involved in the path integral due to gauge symmetry. In gravity however, the diffeomorphism invariance is more non-trivial, as we will discuss in the next sections.

2.3.2 Diffeomorphisms in 3D classical and quantum gravity

In this section we will review the analysis of diffeomorphisms of 3D gravity, mostly based on the work [93]. As we known that gravity in lower dimensions is a much simpler theory than the 4D, the gauge symmetry at the quantum level is also a cleaner story. There are however some lessons we can learn, to help us in the models relevant to the real world.

The action of 3D gravity in the natural unit reads

$$S_{3D}[e, \omega] = \int_{\mathcal{M}} Tr\left[e \wedge F(\omega)\right]. \tag{2.30}$$

where e and ω are $\mathfrak{su}(2)$ valued one forms:

$$e = e^i_\mu J_i dx^\mu, \qquad \omega = \omega^i_\mu J_i dx^\mu. \tag{2.31}$$

Here J_i are the $\mathfrak{su}(2)$ generators. The curvature two form of ω is given by $F(\omega) = \mathrm{d}\omega + \omega \wedge \omega$. The trace in the action is given by the contraction of Lie algebra indices by the antisymmetric tensor ϵ_{ijk}. The infinitesimal diffeomorphism transformations parametrized by a vector field ξ^μ are written as

$$\begin{aligned} \delta_\xi e &= \mathcal{L}_\xi e = d(\iota_\xi e) + \iota_\xi(de) \\ \delta_\xi \omega &= \mathcal{L}_\xi \omega = d(\iota_\xi \omega) + \iota_\xi(d\omega) \end{aligned} \tag{2.32}$$

in which the second equal sign is due to the Cartan's identity for Lie derivatives.

In 3D Euclidean gravity, the local Lorentz group is SU(2). If we use X to represent its Lie algebra element, the infinitesimal Lorentz transformation δ^L is

$$\delta^L_X \omega = \mathrm{d}_\omega X, \quad \delta^L_X e = [e, X]. \tag{2.33}$$

There is also another gauge symmetry that acts as a translation of triad field. It is given by

$$\delta^T_X \omega = 0, \qquad \delta^T_X e = \mathrm{d}_\omega \phi, \tag{2.34}$$

where the parameter of the transformations is also an $\mathfrak{su}(2)$ element ϕ. The invariance of the action under this transformation follows from the second Bianchi identity. These symmetries imply that all solutions of the theory are gauge equivalent. One can show [93] that on-shell we have

$$\delta_\xi = \delta^L_{\iota_\xi \omega} + \delta^T_{\iota_\xi e}, \tag{2.35}$$

i.e. the three symmetries are related. Hence the diffeomorphisms in 3D classical gravity can be neatly decomposed into two gauge symmetries – internal rotational "Lorentz" SU(2) gauge symmetry and the *translational* symmetry.

19

Let us now examine these gauge symmetries in the path integral formalism defined on a simplicial lattice. Following the procedure we have introduced in 2.2.2, we consider the partition function on the simplicial decomposition Δ of the manifold. The smearing of triads defines the Lie algebra valued variables E_f corresponding to each face $E_f = \int_b e \in \mathfrak{su}(2)$, where f is the dual face corresponding to the bone b of triangulation. We also denote the Lie algebra valued variable Z_f from the logarithm of the holonomy $Z_f = \ln g_f \in \mathfrak{su}(2)$. The action written in terms of this set of discrete variable reads,

$$S_{\text{3D discrete}} = \sum_f \text{Tr}(E_f Z_f) \tag{2.36}$$

Since both variables Z_f and E_f are valued in the Lie algebra, the local Lorentz transformation at the level of the discrete model is implemented by the action

$$Z_f \to g_v^{-1} Z_f g_v, \quad E_f \to g_v^{-1} E_f g_v, \quad v \in f, \tag{2.37}$$

where v is a vertex in the dual 2-complex where faces meet. For the translation symmetry, we need to study the discretization of the second Bianchi identity,

$$d_\omega F = dF + [\omega, F] = 0. \tag{2.38}$$

Now consider a point p in the triangulation Δ and the surface $\mathcal{S}$ constructed out of faces from the 2-complex which surrounds p. The surface has the topology of a 2-sphere and its interior is denoted as $\mathcal{B}$. Integrating the 3-forms of (2.38) on the 3 dimensional region $\mathcal{B}$ gives us

$$\int_{\mathcal{S}} F + \int_{\mathcal{B}} [\omega, F] = 0. \tag{2.39}$$

To rewrite the above equation in terms of the discrete variables, consider the dual faces f surrounding this vertex $p \in \mathcal{B}$. The curvature in the discrete variables is given by the oriented product of group elements g_f on this collection of faces. The fact that $F = 0$ implies then

$$\overrightarrow{\prod_f} g_f = \mathbb{1} \quad \Rightarrow \quad \ln\left(\overrightarrow{\prod_f} e^{Z_f}\right) = 0 \tag{2.40}$$

Using the Baker-Campbell-Hausdorff formula, in [93] it shows that the Eq.(2.40) can be rewritten as

$$\sum_f (Z_f + [\Omega_f^p, Z_f]) = 0, \tag{2.41}$$

which is the Bianchi identity at the discretized level. The explicit expression for Ω_f^p as a series of commutators in terms of Z_f can be seen in [93].

Recall that the infinitesimal version of the translation symmetry is $\delta_\phi^T e = \mathrm{d}_\omega \phi$, in which ϕ is 0-form. After discretizing this 0-form at the points p of the triangulation as $\Phi_p \in \mathfrak{su}(2)$, the discrete transformation reads,

$$\delta E_f = \Phi_p - [\Omega_f^p, \Phi_p] \tag{2.42}$$

Then we can finally check that the action is invariant under the transformation, by applying the discrete Bianchi identity:

$$\delta S = \sum_f \mathrm{Tr}\left(\Phi_p Z_f - [\Omega_f^p, \Phi_p] Z_f\right) = \mathrm{Tr}\left[\Phi_p \sum_f (Z_f + [\Omega_f^p, Z_f])\right] = 0 \tag{2.43}$$

We have just shown that the discrete action is invariant under the local Lorentz symmetry and a vertex translation symmetry. Since the measure of integration is obviously invariant as well, the partition function is invariant under the full diffeomorphisms. This is as expected because 3D gravity is topological, hence the discrete description captures the full dynamics.

2.3.3   Diffeomorphisms and divergence

Since the partition function is exactly invariant under the local Lorentz symmetry and a vertex tanslation symmetry, if we evaluate it on a closed diagram, the degree of divergence corresponds to the gauge volume:

$$\mathrm{Vol}(SU(2))^V \times \mathrm{Vol}(\mathfrak{su}(2))^P \tag{2.44}$$

where V is the number of vertices in the 2-complex, and P is the number of points in the triangulation. Later in section 5.1, from the aspect of Pachner Moves, we will justify explicitly the gauge invariance of partition function and its degree of divergence.

To perform a precise Fadeev-Popov gauge fixing procedure for the translational symmetry, we need to consider the 1-skeleton of the triangulation Δ, and choose a maximum tree T along the bones of the triangulation. Then we impose that the E_b are zero along $b \in T$. The F-P determinant reads

$$\Delta = \prod_{e \in T}(1 + |\Omega_e|^2) \tag{2.45}$$

One can prove that if Z_e are zero on Δ/T, then the F-P determinant reduces to 1. For all external vertices and corresponding edges of T, $\Omega_e = 0$ and $Z_e = 0$. At the level of partition function, the gauge fixing of E_b to zero for $b \in T$ is translated into a projection on the spins $j_b = 0$ for the edges of the tree T. In section 7.3, we will revisit this gauge fixing again in 3D quantum gravity.

21

2.3.4 The challenge: diffeomorphisms in 4D quantum gravity

As we have discussed, the discrete approaches of quantum gravity were motivated by the attempt of having a well-defined measure. However, the discrete structure in gravity is a double blade. Different with the case in lattice QCD, in which the local gauge symmetry is preserved, in discrete models of gravity, the diffeomorphisms are broken or become approximated generically. This difference comes from the fact that in QCD, spacetime lattice is regular and provides background where the gauge field lives; while in quantum gravity, the lattice itself is inherently dynamical, and the action of diffeomorphisms changes it.

Eventually, to show that a discrete quantum gravity model can recover classical general relativity at low energy is not enough to show the correct semi-classical limit at the level of a single 4-simplex. One has to also study the continuum limit to see whether we have the correct dynamics for smooth manifolds. Any novel predictions from the model, which are to be compared with direct or indirect gravitational observables in the experiments, have to be addressed in the continuum limit of the theory. During the renormalization process to approach this limit, the diffeomorphism invariance has to be restored and fully recovered at the end. Checking whether we have the correct gauge symmetry is a guidance for a correct continuum limit.

We should ask ourselves now what is the situation in the Regge calculus. As the desired semi-classical limit of Spin Foam models, studying the diffeomorphisms in Regge calculus would provide us a first guide. In this topic, systematic analysis has been done in [73, 60, 61, 98].

In Regge calculus, as the solution is a simplicial approximation of a solution of Einstein equation, the notion of diffeomorphisms should be defined on the simplicial decomposition without referencing to the coordinate systems. The geometric data in Regge calculus – area and angles, or length of edges – allows to determine the relative position of the vertices with respect to each other. The appearance of gauge degrees of freedom in Regge calculus was first shown in [73]. Any triangulation of flat spacetime is a solution of the equations of motion from the Regge action. Through a perturbative expansion of the 4D path integral around a flat spacetime, the paper shows that continuum gauge degrees of freedom can be expressed as the freedom of moving an arbitrary vertex within the flat triangulation. Similarly to the 3D case we discussed in the last section, the translation of a vertex in a flat triangulation does not change the solution of the theory. This vertex translation symmetry has been studied precisely in [104].

However, for generic solutions the issue is more involved. For solutions with curvature there do not exist exact gauge symmetries at the discrete level. The authors of [61, 98] developed a systematical criterion to check gauge symmetry in the classical Regge calculus: as we know that the solutions to the equations of motions are extrema of the actions, this means that if there is an exact gauge symmetry, the action is constant in some directions exactly at these extrema. Hence

one criterion to check the gauge symmetry is through the Hessian of the action, which is the matrix of second derivatives evaluated on the solution. If the matrix has null eigenvectors (zero eigenvalues), then it signals that there are exact gauge symmetries.

In this thesis, we will check the vertex translation symmetry in the 4D Spin Foams through computing the 5–1 Pachner Move. We will also study the divergent behavior in general amplitudes, which will help us to gain some insights about residual diffeomorphisms in Spin Foam models.

Chapter 3

Holomorphic Spin Foam Model

In this Chapter, we will introduce the construction of a holomorphic Spin Foam model. It is a 4D Riemannian model with vanishing cosmological constant. We will start from reviewing holomorphic representations and rewrite the BF partition function in this language. Next, we review the holomorphic simplicity constraints. We will introduce a model with an alternative imposition of these constraints, and show that this model still has the same semiclassical limit as the EPRL/FK model.

3.1   The holomorphic representation

We choose to use a spinor representation of SU(2) in the Bargmann-Fock space $L^2_{hol}(\mathbb{C}^2, d\mu)$ of holomorphic polynomials of a spinor [128, 129, 116]. One of the features of this representation that will facilitate our calculations is that the Hermitian inner product is Gaussian:

$$\langle f|g\rangle = \int_{\mathbb{C}^2} \overline{f(z)}g(z)\mathrm{d}\mu(z), \tag{3.1}$$

where $\mathrm{d}\mu(z) = \pi^{-2}e^{-\langle z|z\rangle}\mathrm{d}^4z$ and d^4z is the Lebesgue measure on $\mathbb{C}^2$.

Given $z \in \mathbb{C}^2$ we denote its conjugate by $\check{z}$. We use a bra-ket notation for z and square brackets $\check{z}$ as in

$$|z\rangle = \begin{pmatrix} z_0 \\ z_1 \end{pmatrix}, \qquad |\check{z}\rangle \equiv |z] = \begin{pmatrix} -\bar{z}_1 \\ \bar{z}_0 \end{pmatrix}, \qquad z_0, z_1 \in \mathbb{C}. \tag{3.2}$$

That is $|\check{z}\rangle = |z]$. Notice that while $\langle z|$ is anti-holomorphic, $[z|$ is holomorphic and orthogonal to $|z\rangle$, i.e. $[z|z\rangle = 0$. This non-standard notation for spinors will turn out to be useful, as we

will always work with contractions of spinors, without the need for writing out the indices. Our notation is related to the usual one as follows: $z_A = |z\rangle$, $\bar{z}_{A'} = \langle z|$, and the spinor invariants are $[z|w\rangle = z_{A'} w_A \epsilon^{A'A}$ and $\langle z|w\rangle = \bar{z}_{A'} w_A \delta^{A'A}$. The bracket $[z|w\rangle$ associated with the ϵ tensor is skew-symmetric, holomorphic and $SL(2, \mathbb{C})$ invariant. The bracket $\langle z|w\rangle$ associated with the identity tensor is hermitian, and only $SU(2)$ invariant.

Geometrically, each spinor defines a 3-vector $\vec{V}(z)$. If we use σ to denote Pauli matrix:

$$|z\rangle\langle z| = \frac{1}{2}(\langle z|z\rangle \mathbb{1} + \vec{V}(z) \cdot \vec{\sigma}). \tag{3.3}$$

Let us now study the identity on the Bargmann-Fock space $L^2_{hol}(\mathbb{C}^2, d\mu)$. The delta distribution on this space is given by $\delta_w(z) = e^{\langle z|w\rangle}$, since for any holomorphic function $\int d\mu(z) f(z) e^{\langle z|w\rangle} = f(w)$. Let us use a line to represent the delta graphically by

$$e^{\langle z|w\rangle} = \langle z| \,\text{——————}\, |w\rangle \qquad \text{and} \qquad \frac{\langle z|w\rangle^{2j}}{(2j)!} = \langle z| \,\overset{j}{\text{——————}}\, |w\rangle \,. \tag{3.4}$$

Therefore the Gaussian integral $\int d\mu(w) e^{\langle z|w\rangle + \langle w|z'\rangle} = e^{\langle z|z'\rangle}$ implies the contraction

$$\int d\mu(w) \, \langle z| \,\overset{j}{\text{——————}}\, |w\rangle\langle w| \,\overset{j'}{\text{——————}}\, |z'\rangle = \delta_{j,j'} \, \langle z| \,\overset{j}{\text{——————}}\, |z'\rangle \,. \tag{3.5}$$

For a function of four spinors (with obvious generalization to n spinors) we can thus define the *trivial projector*, which we will denote as

$$\mathbb{1}(z_i; w_i) = e^{\sum_{i=1}^4 [z_i|w_i\rangle} = \begin{array}{l} [z_1| \,\text{——————}\, |w_1\rangle \\ [z_2| \,\text{——————}\, |w_2\rangle \\ [z_3| \,\text{——————}\, |w_3\rangle \\ [z_4| \,\text{——————}\, |w_4\rangle \end{array} \,. \tag{3.6}$$

Next, we will study how $SU(2)$ acts on the elements of the Bargmann-Fock space. For a generic holomorphic function $f \in L^2_{hol}(\mathbb{C}^2, d\mu)$, the group action is given by

$$g \cdot f(z) = f(g^{-1}z). \tag{3.7}$$

The group $SU(2)$ acts irreducibly on the subspaces of holomorphic polynomials homogeneous of degree $2j$. Holomorphic polynomials with different degrees of homogeneity are orthogonal with each other. Indeed,

$$L^2_{hol}(\mathbb{C}^2, d\mu) = \bigoplus_{j \in \mathbb{N}/2} V^j. \tag{3.8}$$

25

and an orthonormal basis of V^j is given by

$$e_m^j(z) \equiv \frac{z_0^{j+m} z_1^{j-m}}{\sqrt{(j+m)!(j-m)!}} \tag{3.9}$$

and it is of dimension $2j + 1$.

In the study of gauge-invariant Spin Foam models, we will be interested in the SU(2) invariant functions on n spinors

$$f(gz_1, gz_2, ..., gz_n) = f(z_1, z_2, ..., z_n), \quad \forall g \in \text{SU}(2). \tag{3.10}$$

We will denote the invariant elements of $L^2(\mathbb{C}^2, d\mu)^{\otimes n}$ to be in $\mathcal{H}_n$, which is the Hilbert space of n-valent intertwiners:

$$\mathcal{H}_n = \bigoplus_{j_i} \mathcal{H}_{j_1,...,j_n} \equiv \bigoplus_{j_i} \text{Inv}_{\text{SU}(2)} \left[V^{j_1} \otimes \cdots \otimes V^{j_n} \right]. \tag{3.11}$$

The n-valent intertwiners are a basis of $SU(2)$ invariant functions of n spinors. One way to construct an element of $\mathcal{H}_n$ is to average a function of n spinors over the group using the Haar measure. In this way we can construct a projector $P : L^2(\mathbb{C}^2, d\mu)^{\otimes n} \to \mathcal{H}_n$ which is called the Haar projector as

$$P(f)(w_i) = \int \prod_i d\mu(z_i) P(\check{z}_i; w_i) f(z_1, z_2, ..., z_n) = \int_{\text{SU}(2)} dg f(gw_1, gw_2, ..., gw_n) \tag{3.12}$$

where the kernel is given by[1]

$$P(z_i; w_i) = \int_{\text{SU}(2)} dg \, e^{\sum_i [z_i|g|w_i\rangle} = \begin{array}{c} [z_1| \\ [z_2| \\ [z_3| \\ [z_4| \end{array} \begin{array}{c} \boxed{} \end{array} \begin{array}{c} |w_1\rangle \\ |w_2\rangle \\ |w_3\rangle \\ |w_4\rangle \end{array}, \tag{3.13}$$

where we use a box to represent group averaging with respect to the Haar measure over SU(2). Hence the projector onto the invariant subspace is simply the group average of $\mathbb{1}(z_i; w_i)$. From the above, we see that a contraction of two spinors on the same strand but belonging to two different projectors is obtained by setting $z_i^1 = \check{w}_i^2$. This implies that the kernel of the projector satisfies the projection property

$$\int \prod_i d\mu(w_i) P(z_i; w_i) P(\check{w}_i; z_i') = P(z_i; z_i'). \tag{3.14}$$

---

[1] For a review of Gaussian integration techniques see Appendix A.1.

We will also refer from now on to the kernel $P(z_i; w_i)$ as a projector for convenience. As shown in [112, 121], we can perform the integration over g in Eq. (3.13) explicitly, which gives a power series in the holomorphic spinor invariants:

$$P(z_i; w_i) = \sum_{[k]} \frac{1}{(J+1)!} \prod_{i<j} \frac{([z_i|z_j\rangle[w_i|w_j\rangle)^{k_{ij}}}{k_{ij}!},$$ (3.15)

where the sum is over a set of $n(n-1)/2$ non-negative integers $[k] \equiv (k_{ij})_{i\neq j=1,\cdots,n}$ with $1 \leq i < j \leq n$ and $k_{ij} = k_{ji}$. A short proof of this statement is given in the Appendix A.3 for the reader's convenience. Thus a basis of n-valent intertwiners is given by

$$(z_i|k_{ij}\rangle \equiv \prod_{i<j} \frac{[z_i|z_j\rangle^{k_{ij}}}{k_{ij}!}.$$ (3.16)

The non-negative integers $(k_{ij})_{i\neq j=1,\cdots,n}$ are satisfying the n homogeneity conditions

$$\sum_{j\neq i} k_{ij} = 2j_i.$$ (3.17)

The sum of spins at the vertex is defined by $J = \sum_i j_i = \sum_{i<j} k_{ij}$ and is required to be a positive integer. We also see from Eq. (3.15) that the identity on $\mathcal{H}_{j_i}$ is resolved as follows

$$\mathbb{1}_{\mathcal{H}_{j_i}} = \sum_{[k]\in K_j} \frac{|k_{ij}\rangle\langle k_{ij}|}{\|k_{ij}\|^2}, \qquad \|k_{ij}\|^2 = \frac{(J+1)!}{\prod_{i<j} k_{ij}!}.$$ (3.18)

with the set K_j defined by integers k_{ij} satisfying Eq.(3.17). For more details on these intertwiners and the coherent states defined by them, see [122] where this basis was introduced for the first time.

Before we go on to the discussion of simplicity constraints, let us notice that using a multinomial expansion Eq.(3.15) can be written in terms of total spin:

$$P(z_i; w_i) = \sum_{J=0}^{\infty} \frac{\left(\sum_{i<j}[z_i|z_j\rangle[w_i|w_j\rangle\right)^J}{J!(J+1)!},$$ (3.19)

which will turn out to be a quite useful expression for the projector for computation purposes. Note that this is an expansion in U(N) coherent intertwiners of total area J.

Finally, now we can write down the SU(2) BF partition function in terms of projectors written in the holomorphic representation:

$$\mathcal{Z}_{BF}(\Gamma) = \prod_{f\in F} \sum_{j_f} (2j_f + 1) \int \left\{ \prod_{all} d\mu(z)d\mu(w) \right\} \prod_{e\in\Gamma} P_\rho(z_i^e; w_i^e),$$ (3.20)

27

3.2 Holomorphic simplicity constraints

Holomorphic simplicity constraints for spinorial Spin Foam models were first introduced in [115] for Riemannian gravity. Here we give a short summary, but refer the reader to the original paper for their full derivation.

For the Riemannian 4d Spin Foam models, we use the gauge group $\mathrm{Spin}(4) = \mathrm{SU}(2)_L \times \mathrm{SU}(2)_R$, which is the double cover of $\mathrm{SO}(4)$. The holomorphic simplicity constraints are isomorphisms between the two representation spaces of $\mathrm{SU}(2)$: for any two edges i, j that are a part of the same vertex a, they are defined by

$$[z_{iL}^a | z_{jL}^a \rangle = \rho^2 [z_{iR}^a | z_{jR}^a \rangle, \tag{3.21}$$

where ρ is a function of the real-valued Immirzi parameter γ given by

$$\rho^2 = \begin{cases} (1-\gamma)/(1+\gamma), & |\gamma| < 1 \\ (\gamma-1)/(1+\gamma), & |\gamma| > 1 \end{cases} \tag{3.22}$$

The holomorphic simplicity constraints Eq.(3.21) essentially tell us that there exists a unique group element $g_a \in \mathrm{SL}(2,\mathbb{C})$ for each vertex a, such that

$$\forall i, \quad g_a | z_{iL}^a \rangle = \rho \, | z_{iR}^a \rangle. \tag{3.23}$$

A general element of $\mathrm{SL}(2,\mathbb{C})$ can be decomposed into the product of an hermitian matrix times an element of $\mathrm{SU}(2)$, so that $g_a = h_a u_a$ with $h_a^\dagger = h_a$. It is only when $h_a = \mathbb{1}$ that the holomorphic simplicity constraints imply the usual geometrical simplicity constraints. In the FK formulation of the spin foam model which is only partially holomorphic this is implied since the norm of the spinors is fixed. The fully holomorphic formulation of DL therefore relaxes at the quantum level the simplicity constraints. Fortunately, one one can check following [122] that in the semi-classical limit of Holomorphic amplitudes the Gauss constraints due to the gauge invariance of the amplitude can be realized in the form

$$\sum_i |z_{iL}^a \rangle \langle z_{iL}^a| = A_L \mathbb{1}, \quad \sum_i |z_{iR}^a \rangle \langle z_{iR}^a| = A_R \mathbb{1}. \tag{3.24}$$

This imposes that in the classical limit $h_a = \mathbb{1}$ and the geometrical simplicity constraints $u_a | z_{iL}^a \rangle = \rho \, | z_{iR}^a \rangle$ with $u_a \in \mathrm{SU}(2)$ are satisfied.

Let us recall the geometrical meaning of these: Each spinor defines a three vector $\vec{V}(z) \in \mathbf{R}^3$ through the equation

$$|z\rangle\langle z| = \frac{1}{2}\left(\mathbb{1}\langle z|z\rangle + \vec{V}(z)\cdot\vec{\sigma}\right), \qquad |z][z| = \frac{1}{2}\left(\mathbb{1}[z|z] - \vec{V}(z)\cdot\vec{\sigma}\right) \tag{3.25}$$

where $\vec{\sigma}$ is the vector made by Pauli matrices. Thus around a vertex in a spin-network, each link dual to a triangle in the simplicial manifold, is associated with two 3-vectors $\vec{V}_L(z)$ and $\vec{V}_R(z)$ given by the left and right spinors. Classically, they correspond to the selfdual b_+ and anti-selfdual b_- components of the B field respectively :

$$V_L^i(z) = b_+^i := B^{0i} + \frac{1}{2}\epsilon_{kl}^i B^{kl}, \quad V_R^i(z) = b_-^i := -B^{0i} + \frac{1}{2}\epsilon_{kl}^i B^{kl}. \tag{3.26}$$

Note here that the time norm is chosen to be $N_I = (1, 0, 0, 0)^T$. For the Hodge dual of the B field, we find $(*b)_+ = b_+ = \vec{V}_L(z)$, and $(*b)_- = -b_- = -\vec{V}_R(z)$.

For the vectors $\vec{V}_L(z)$ and $\vec{V}_R(z)$ defined by the spinors of the two copies of SU(2) this means that the holomorphic simplicity constraints imply

$$g_a \rhd \vec{V}_L(z_i^a) = \rho^2 \vec{V}_R(z_i^a), \quad \forall i \in a \tag{3.27}$$

which leads to the constraint that the norm of the selfdual and anti-selfdual components of the bivector $(g_a, \mathbb{1}) \rhd (B + \gamma * B)$ have to be equal to each other:

$$|(1 + \gamma)g_a \rhd b_+| = |(1 - \gamma) \rhd b_-|. \tag{3.28}$$

Thus B and $*B$ are simple bivectors, and for the spin network vertex a, there exists a common time norm to all the bivectors:

$$\mathcal{N}_a = (g_a, \mathbb{1})^{-1} \rhd (1, 0, 0, 0). \tag{3.29}$$

The existence of this shared time norm implies the linear simplicity constraints introduced by the EPRL and FK models [43, 44, 45, 46].

It is interesting to note that g_a can be expressed purely in terms of spinors as

$$g_a = \frac{|z_{iR}^a\rangle\langle z_{iL}^a| + |z_{iR}^a][z_{iL}^a|}{\sqrt{\langle z_{iL}^a|z_{iL}^a\rangle\langle z_{iR}^a|z_{iR}^a\rangle}}, \quad \forall i \in a. \tag{3.30}$$

It is easy to check that this satisfies Eq. (3.23). Note here that g_a is a unique group element for all strands belonging to the same vertex.

3.3 Imposing constraints

We will now impose the holomorphic simplicity constraints on the Spin(4) BF theory in order to obtain a model of 4d Riemannian Quantum Gravity. There are two natural ways of imposing

these constraints - either on the boundary spin network defined by contraction of coherent states [115], or on the whole projector (3.13). We will first summarize the usual approach, which we will refer to as the DL prescription. Then we will introduce an alternative model in which the constraint is imposed on the whole projector. It is very surprising that the alternative model actually has the same asymptotic behavior as the DL prescription and EPRL/FK model (with $|\gamma| < 1$)[126, 127, 63], i.e. the amplitude is weighted by a cosine of the Regge [72] action. It leads however to a much simpler calculation when we evaluate the Pachner moves than the DL case. Even though there is no technical obstacle to use the DL prescription, we will study it in a subsequent article, and focus on the constrained projector model in this thesis.

DL prescription

In [115, 118] Dupuis and Livine introduced a Spin Foam model similar to the EPRL/FK models, but written in terms of spinorial coherent states with the holomorphic simplicity constraints. Since BF amplitudes can be seen as evaluations of spin network functions, the simplicity constraints in this model are imposed in the usual way – on the boundary spin network given by the amplitude. The amplitude for a single 4-simplex σ is given by a product of contraction of coherent states for left and right sectors, with the simplicity constraints imposed on the boundary spinors as follows

$$\mathcal{A}_\sigma(\{z_\Delta^\tau\}) = \int \left[\mathrm{d}g_\tau^L\right]^5 \left[\mathrm{d}g_\tau^R\right]^5 e^{\sum_{\Delta\in\sigma} \rho^2 [z_\Delta^{s(\Delta)}| g_{s(\Delta)}^L \,^{-1} g_{t(\Delta)}^L |z_\Delta^{t(\Delta)}\rangle + [z_\Delta^{s(\Delta)}| g_{s(\Delta)}^R \,^{-1} g_{t(\Delta)}^R |z_\Delta^{t(\Delta)}\rangle} \tag{3.31}$$

where Δ label different triangles/strands and $\tau, s(\Delta), t(\Delta)$ label tetrahedra/projectors. Graphically this is presented in Fig. 3.1. This amplitude corresponds to two copies of 20j symbols from BF theory constrained by $[z_L^{s(\Delta)}|z_L^{t(\Delta)}\rangle = \rho^2 [z_R^{s(\Delta)}|z_R^{t(\Delta)}\rangle$ on the boundary.

Imposing the constraints on the projector

Since spin foam amplitudes for BF theory are constructed by glueing together projectors (3.19) into graphs corresponding to 4d quantum geometries, we find it natural to instead impose the constraints on the arguments of the projectors themselves. Let us consider the Spin(4) projector obtained by taking a product of two SU(2) projectors

$$P(z_i; w_i)P(z_i'; w_i') = \sum_J \frac{\left(\sum_{i<j}[z_i|z_j\rangle[w_i|w_j\rangle\right)^J}{J!(J+1)!} \sum_{J'} \frac{\left(\sum_{i<j}[z_i'|z_j'\rangle[w_i'|w_j'\rangle\right)^{J'}}{J'!(J'+1)!}, \tag{3.32}$$
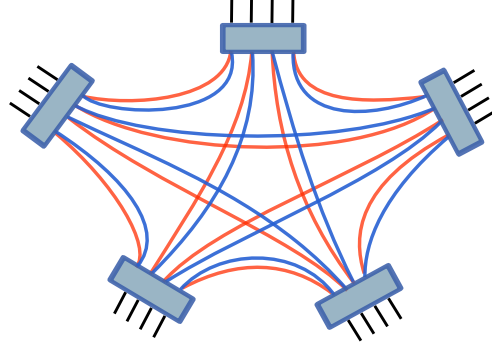
Figure 3.1: Graph for the 4-simplex amplitude in the DL model. The contractions inside correspond to two copies of BF 20j symbols, constrained on the boundary.

where we use a prime to distinguish the left and right SU(2) sectors. We will now impose the holomorphic simplicity constraints on both incoming and outgoing strands in the Spin(4) projector

$$[z_i'|z_j'\rangle = \rho^2[z_i|z_j\rangle \qquad [w_i'|w_j'\rangle = \rho^2[w_i|w_j\rangle.$$

This will make the two products of spinors in the two projectors proportional to each other, with the proportionality constant being ρ^4. Note that the imposition of simplicity constraints on all of the spinors also forces the measure of integration on $\mathbb{C}^2$ to change to

$$\mathrm{d}\mu_\rho(z) := \frac{(1 + \rho^2)^2}{\pi^2} e^{-(1+\rho^2)\langle z|z\rangle} \mathrm{d}^2 z. \tag{3.33}$$

The factor of $(1 + \rho^2)^2$ is added for normalization. It insures that

$$\int \mathrm{d}\mu_\rho(z) = 1. \tag{3.34}$$

Moreover this choice of normalization is confirmed by the study of asymptotics of both this and the DL model, as we will see later in the next section. It is exactly this choice that insures that both models have the same semi-classical limit. We are now ready to define a new *constrained propagator* P_ρ by applying the simplicity constraints on the Spin(4) projector

$$P_\rho(z_i; w_i) \equiv P(z_i; w_i)P(\rho z_i; \rho w_i) = \sum_J \sum_{J'} \frac{\rho^{4J'}}{J!(J + 1)!J'!(J' + 1)!} \left(\sum_{i<j} [z_i|z_j\rangle[w_i|w_j\rangle \right)^{J+J'}. \tag{3.35}$$

The two sums over integers J and J' are independent, so we can simplify this expression for the constrained propagator into a single sum by letting $J + J' \to J$. This allows us to arrive at a more

compact form of the constrained propagator, given by

$$P_\rho(z_i; w_i) = \sum_J F_\rho(J) \frac{\left(\sum_{i<j} [z_i|z_j\rangle [w_i|w_j\rangle\right)^J}{J!(J+1)!}, \tag{3.36}$$

where we have recognized that the numerical factor in front of the spinors is actually the power series expansion of the hypergeometric function

$$F_\rho(J) := {}_2F_1(-J-1, -J; 2; \rho^4)$$
$$= \sum_{J'=0}^{J} \frac{J!(J+1)!\rho^{4J'}}{(J-J')!(J-J'+1)!J'!(J'+1)!} = \sum_{J'=0}^{J} \binom{J}{J'}\binom{J+1}{J'}\frac{\rho^{4J'}}{(J'+1)} \tag{3.37}$$

Now let us get some intuition of the hypergeometric function:
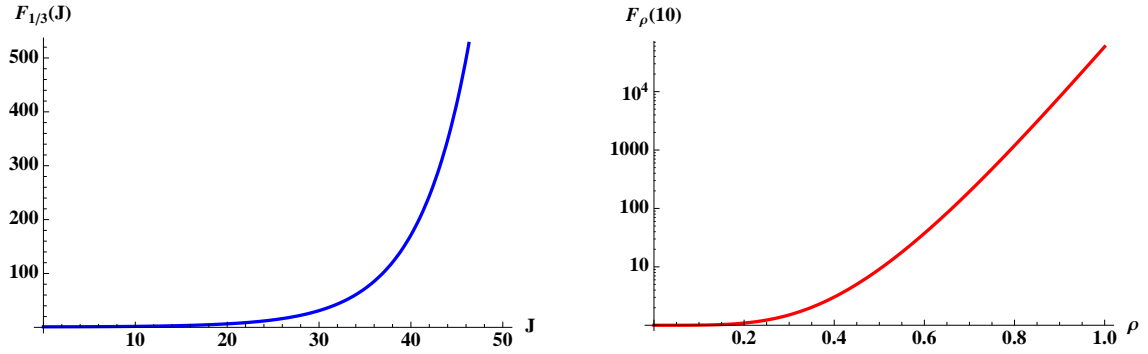
Figure 3.2: Left: The value of hypergeometric function $F_\rho(J)$ with different spins and fixed $\rho = 1/3$ as an example. Right: The value of hypergeometric function $F_\rho(J)$ with different ρ and fixed spin $J = 10$.

.

Notice that the constrained Spin(4) propagator is just an SU(2) projector with non-trivial weights (greater than 1) for each term that depends on the Barbero-Immirzi parameter. In general, this hypergeometric function is a complicated function of ρ, but let us look at two interesting limiting cases. For $\rho = 0$, which corresponds to $\gamma \to 1$, we have

$$_2F_1(-J-1, -J; 2; 0) = 1, \tag{3.38}$$

so we end up with pure SU(2) BF theory. This is obvious, as $\rho = 0$ forces all the left spinors to be 0. Another limit often considered is $\rho = 1$, which in this construction surprisingly corresponds

to both of the limits $\gamma \to 0$ and $\gamma \to \infty$. In this limit we get also a relatively simple expression

$$_2F_1(-J-1,-J;2;1) = \frac{(2J+2)!}{(J+2)!(J+1)!}.$$ (3.39)

This limit does not have an obvious interpretation apart from its simplicity.

3.4   The partition function

The partition function of the holomorphic spin foam model is defined on a 2-complex $\Gamma(V, E, F)$, which is dual to a simplicial decomposition of a 4-d manifold. To make the geometrical relationship transparent, for each 2-complex we can also draw the corresponding cable diagram to label the degrees of freedom [10]. For an example of two 4-simplices sharing one tetrahedron, the dual 2-complex and its cable diagram, see Fig. 3.3. In the cable diagram notation, a propagator is represented as

$$P_\rho(z_i; w_i) \equiv \begin{array}{c} [z_1| \\ [z_2| \\ [z_3| \\ [z_4| \end{array} \begin{array}{c} \\ \framebox[1cm]{} \end{array} \begin{array}{c} |w_1\rangle \\ |w_2\rangle \\ |w_3\rangle \\ |w_4\rangle \end{array},$$ (3.40)

where a strand represents a spinor, and a box represents group averaging with respect to the Haar measure over SU(2), which is reduced from the projector of $\mathrm{Spin}(4) = \mathrm{SU}(2)_L \times \mathrm{SU}(2)_R$ by simplicity constraints.

The faces F in the dual 2-complex correspond to $d-2$ faces shared by tetrahedra. In the cable diagram, they correspond to loops formed by single strands. The structure of the partition function is essentially the contraction of the constrained propagators with non-trivial face weight:

$$\mathcal{Z}(\Gamma) = \prod_{f \in F} \sum_{j_f} \mathcal{A}_f(j_f) \int \left\{ \prod_{all} d\mu_\rho(z) d\mu_\rho(w) \right\} \prod_{e \in \Gamma} P_\rho(z_i^e; w_i^e),$$ (3.41)

where $\mathcal{A}_f(j_f)$ is the face weight, which is a function of spin $(2j_f + 1)^\eta$. With $\rho = 0$ and $\eta = 1$, the theory reduces to SU(2) BF theory. The partition function in principle can be defined for any type of discretization of the manifold: simplicial lattice, hypercubic lattice etc. The rest of the paper is focusing on the discussion on simplicial lattice, but the result can be easily generalized to other cases. At the leading order, for a single simplex, the holomorphic spin foam model has the same semiclassical limit as EPRL/FK model [106].

33
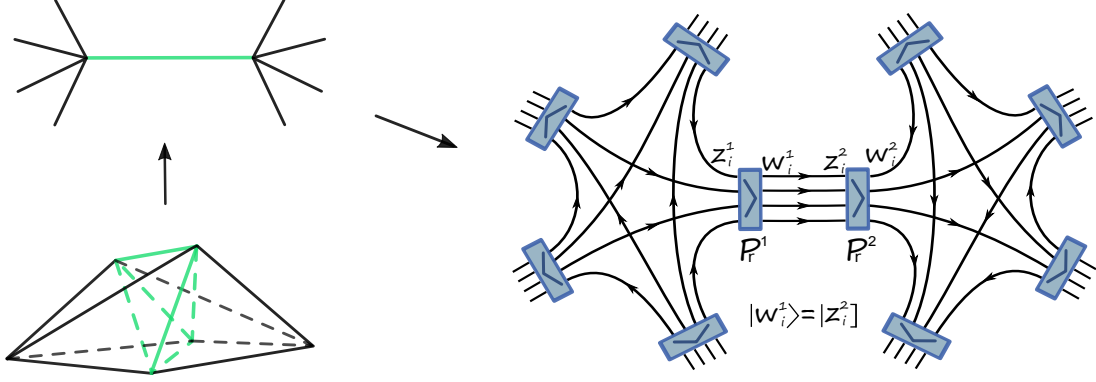
Figure 3.3: The triangulation of two 4-simplices sharing one tetrahedron, the dual 2-complex and its cable diagram. The shared tetrahedron is dual to an edge propagator in the 2-complex. P^1_ρ and P^2_ρ belong to the same edge but two different 4-simplices. The spinors belonging on the same strand but belonging to different propagators are contracted according to the strand orientation. For example, spinors $w^1_i = \check{z}^2_i$.

Each constrained propagator comes with an orientation, with spinors z incoming into the box and spinors w outgoing in this paper's convention. A change of this edge orientation results in overall minus sign for the amplitude. Additionally we also put an orientation on each strand, which dictates how spinors on different propagators are contracted. An example is shown in Fig. 3.3. When we glue 4-simplices, we have two propagators contracted on the dual edge along which they are glued.

If we want to write the partition function in terms of intertwiner basis:

$$\mathcal{Z}^{\Delta^*}_G = \sum_{j_f} \prod_{f \in \Delta^*} \mathcal{A}_f(j_f) \int \left\{ \prod_{all} \mathrm{d}\mu_\rho(z)\mathrm{d}\mu_\rho(w) \right\} \sum_{k^e_{ff'} \in K_j} \prod_e P^{k^e_{ij}}_\rho(z^e_i; w^e_i), \qquad (3.42)$$

where the set K_j was defined previously in Eq. (3.17) to be the set of integers k_{ij} satisfying $\sum_{i \neq j} k_{ij} = 2j_i$ and contraction of spinors according to the 2-complex Δ^* on different edges is implied. The constrained propagator at fixed spins is given by

$$P^{k^e_{ij}}_\rho(z^e_i; w^e_i) := \frac{F_\rho(J_e)}{(J_e + 1)!} \prod_{i<j} \frac{([z^e_i|z^e_j\rangle[w^e_i|w^e_j\rangle)^{k^e_{ij}}}{k^e_{ij}!}. \qquad (3.43)$$

It is interesting to note here that, unlike in the usual Spin Foam models, this definition in terms of propagators does not necessarily constrain the partition function to be a product of vertex amplitudes, thus allowing for more general non-geometrical structures.

34

3.5 Asymptotics

In this section we will calculate the asymptotics of the two models with different imposition of simplicity constraints. First we show that the Dupuis-Livine model indeed has the same asymptotic behavior as the EPRL-FK models. We then show that there are non-trivial cancellations in the asymptotic expansion of the constrained propagator model that lead to the same semiclassical limit as the DL model.

3.5.1 The dihedral angle

Before we calculate the asymptotic expansion of the Spin Foam amplitudes, we have to understand how to reconstruct from our data the angle appearing in the classical area-angle Regge action [120]:

$$S = \sum_{a<b} A_{ab}\xi_{ab}, \tag{3.44}$$

where A_{ab} is the area of face shared by tetrahedra a and b, which share a common face with each other, and ξ_{ab} is the 4-d dihedral angle, which is the angle between the two 4-vectors $\mathcal{N}_a, \mathcal{N}_b$ normal to the two tetrahedra a, b.

We can find the expression for the 4-d dihedral angle using Eq. (3.29) from the section on simplicity constraints:

$$\cos(\xi_{ab}) = \mathcal{N}_a \cdot \mathcal{N}_b$$
$$= \frac{1}{2}tr\left[g_a^{-1} \cdot g_b\right] = \frac{1}{2}tr\left[g_b^{-1} \cdot g_a\right] \tag{3.45}$$

Using the expression of eq.(7.3), we can write the cosine of dihedral angle in terms of spinors,

$$\cos(\xi_{ab}) = \frac{[z_{iR}^a|z_{jR}^b\rangle\langle z_{jL}^b|z_{iL}^a] + \langle z_{iL}^a|z_{jL}^b\rangle\langle z_{jR}^b|z_{iR}^a\rangle + c.c.}{2\,|z_{iL}^a||z_{iR}^a||z_{jL}^b||z_{jR}^b|} \tag{3.46}$$

From the above two expressions, we can see that to decide the cosine of the dihedral angle ξ_{ab}, we need the data of two group elements associated with two nodes (tetrahedra), or the data of both left and right spinors of any one strand from each of the two tetrahedra. In summary,

$$\{g_a, g_b\} \to \cos(\xi_{ab}), \text{ or } \{z_{iR}^a, z_{iL}^a, z_{jR}^b, z_{jL}^b\} \to \cos(\xi_{ab}) \;\; \forall i \in a, \forall j \in b$$

Let us recall additionally, that the models we consider have Spin(4) symmetry, so we can rotate these results by a Spin(4) transformation $G = (g_L, g_R)$.

3.5.2 The asymptotics of DL model

An apparent difference between the holomorphic simplicity constraints and the ones in Euclidean EPRL/FK models is that they are constraints on spinors. However, they lead to the same constraint between spins,

$$\langle z_L | z_L \rangle = j_L = \rho^2 j_R = \rho^2 \langle z_R | z_R \rangle \tag{3.47}$$

for the coherent intertwiners in the large $|z|$ limit [115]. In this section, we briefly show that for the amplitude of a 4-simplex, the DL model has the same action at critical points as EPRL/FK models for Barbero-Immirzi parameter $\gamma < 1$.

We can rewrite the amplitude (3.31) of a 4-simplex σ by expanding it in power series as

$$\mathcal{A}_\sigma = \int \prod_{a<b} dg_{a,b}^{L,R} \, \mathbf{e}^{\rho^2 [z_b^a | g_a^{L-1} g_b^L | z_a^b \rangle + [z_b^a | g_a^{R-1} g_b^R | z_a^b \rangle}$$

$$= \int \prod_{a<b} dg_{a,b}^{L,R} \sum_{j_{ab}^{L,R}} \frac{\left(\rho^2 [z_b^a | g_a^{L-1} g_b^L | z_a^b \rangle \right)^{2j_{ab}^L} \left([z_b^a | g_a^{R-1} g_b^R | z_a^b \rangle \right)^{2j_{ab}^R}}{(2j_{ab}^L)!(2j_{ab}^R)!}. \tag{3.48}$$

Now that we have made the summation over spins explicit, we can re-exponentiate this expression to get the effective action of a 4-simplex amplitude $\mathcal{A}_\sigma = \sum_{j_{ab}^{L,R}} \int \prod_a dg_a^{L,R} \, \mathbf{e}^{S_{eff}(j_{ab}^{L,R})}$ with

$$S_{eff}(j_{ab}^{L,R}) = \sum_{a,b\in\sigma} 2j_{ab}^L \ln[z_b^a | g_a^{L-1} g_b^L | z_a^b \rangle + 2j_{ab}^R \ln[z_b^a | g_a^{R-1} g_b^R | z_a^b \rangle + N. \tag{3.49}$$

where the numerical factor N is given by

$$N = \sum_{a,b\in\sigma} 4j_{ab}^L \ln\rho - \ln(2j_{ab}^L)! - \ln(2j_{ab}^R)! \tag{3.50}$$

It is important to note that this action is complex-valued. To study the asymptotic behavior of the amplitude, we have to separate the real and imaginary parts. The real part of the action is

$$\mathbf{Re}S_{eff}(j_{ab}^{L,R}) = \sum_{a,b\in\sigma} j_{ab}^L \ln \frac{1}{2}(|z_b^a|^2 |z_a^b|^2 - (g_a^L \triangleright \vec{V}_b^a) \cdot (g_b^L \triangleright \vec{V}_a^b)) +$$

$$+ j_{ab}^R \ln \frac{1}{2}(|z_b^a|^2 |z_a^b|^2 - (g_a^R \triangleright \vec{V}_b^a) \cdot (g_b^R \triangleright \vec{V}_a^b)) + N. \tag{3.51}$$

In the asymptotic analysis of complex functions the main contribution to the integral comes from critical points, which are stationary points of the action for which the real part is maximized. The critical point equations we get from variation of spinors $|z\rangle$ are the closure constraints

$$\sum_{b\neq a} |z_b^a\rangle\langle z_b^a| = \sum_{b\neq a} j_{ab}^R \mathbb{1} \tag{3.52}$$

36

and the orientation condition requiring certain vectors to be anti-parallel, which we get from the maximization of the real part of the action:

$$g_a^L \triangleright \hat{v}_b^a = -g_b^L \triangleright \hat{v}_a^b, \quad g_a^R \triangleright \hat{v}_b^a = -g_b^R \triangleright \hat{v}_a^b, \quad \text{where} \quad \hat{v} = \vec{V}/|\vec{V}|. \tag{3.53}$$

Using the relation between vectors and spinors, we find that these conditions imply that the action of group elements on a spinor z_a^b rotates it up to a phase into $\hat{z}_b^a$:

$$g_a^{L-1}g_b^L|z_a^b\rangle = e^{i\phi_L^{ab}}|z_b^a], \quad g_a^{R-1}g_b^R|z_a^b\rangle = e^{i\phi_R^{ab}}|z_b^a]. \tag{3.54}$$

This implies that the following identity holds

$$g_b^{R-1}g_a^R g_a^{L-1}g_b^L|z_a^b\rangle = e^{i\phi_L^{ab}-\phi_R^{ab}}|z_a^b\rangle. \tag{3.55}$$

The reconstruction theorem from [127] tells us now that given non-degenerate boundary data satisfying the closure constraint (3.52) and a set of group elements $g_a^{L,R} \in \mathrm{SU}(2), a = 1,\ldots,5$ solving the orientation condition (6.19), we can reconstruct a geometric 4-simplex with the B field given by

$$B_{ab} = \pm(j_{ab}^R + j_{ab}^L)(g_a^L, g_a^R) \triangleright (v_b^a, v_b^a), \tag{3.56}$$

with the outward-pointing normal $\mathcal{N}_a$ obtained by acting with the Spin(4) element (g_a^L, g_a^R) on the vector $N_a = (1, 0, 0, 0)$.

At this point, it is clear that the critical action of DL model is exactly the same as the one calculated in the asymptotic analysis of the EPRL model in [127], and the imaginary part of the action reads

$$\mathbf{Im}S_{eff}(j_{ab}^{L,R}) = \sum_{a,b\in\sigma} 2j_{ab}^L\phi_L^{ab} + 2j_{ab}^R\phi_R^{ab} = \sum_{a,b\in\sigma} k_{ab}(\phi_L^{ab} + \phi_R^{ab}) + \gamma k_{ab}(\phi_R^{ab} - \phi_L^{ab}), \tag{3.57}$$

where $k_{ab} = j_{ab}^L + j_{ab}^R$. To relate this to the area-angle Regge action, we have to relate the ϕ's to the dihedral angle. We cannot directly use our expression in Eq. (3.46) for the dihedral angle, since we no longer have the information about both the left and right spinors. We can however use the result of the reconstruction theorem from the Eq.(3.56) to construct the dihedral angle by the data $\{g_a^R g_a^{L-1}, g_b^R g_b^{L-1}\}$ as follows

$$\begin{aligned}\cos(\xi_{ab}) &= \mathcal{N}_a \cdot \mathcal{N}_b \\ &= \frac{1}{2}\mathrm{Tr}\left[g_a^R g_a^{L-1} \cdot g_b^L g_b^{R-1}\right]\end{aligned} \tag{3.58}$$

37

Notice however that we can obtain the same trace from the Eq. (3.55), which tells us that we can identify the cosine between the phase $(\phi_L^{ab} - \phi_R^{ab})$ and the dihedral angle ξ_{ab}

$$\cos(\phi_L^{ab} - \phi_R^{ab}) = \cos(\xi_{ab}). \tag{3.59}$$

In [127] it has been shown explicitly that the phase difference $(\phi_R^{ab} - \phi_L^{ab})$ and the dihedral angle ξ_{ab} can be identified up to a $\pm$ sign, which is due to the relative orientation of the bivector and 4-simplex. The angle $(\phi_L^{ab} + \phi_R^{ab})$ can be shown to be proportional to 2π [127].

Hence the semi-classical limit of the Dupuis-Livine model is the same as the EPRL-FK models and is given by the action

$$S = \sum_{a,b \in \sigma} \gamma k_{ab} \xi_{ab}. \tag{3.60}$$

Since in Loop Quantum Gravity the spectrum of the area operator is given by $A_j = \gamma \sqrt{j(j+1)}$, in the large spin limit we have obtained exactly the area-angle Regge action [72, 120].

3.5.3 The asymptotics of constrained propagator model

Let us now finally show that the constrained propagator model also leads to the same semi-classical limit as the EPRL-FK models. We first have to rewrite the amplitude in terms of group variables. Recall that we can write an SU(2) propagator as

$$P(z_i; w_i) = \int_{SU(2)} dg \, e^{\sum_i [z_i | g | w_i \rangle} \tag{3.61}$$

Thus taking two copies of such projectors and constraining them both in the $|w\rangle$ and in the $|z\rangle$ spinors, we get that the constrained propagator (3.36) can be written as

$$P_\rho(z_i; w_i) = \int_{SU(2)_L \times SU(2)_R} dg^L dg^R \mathbf{e}^{\sum_i [z_i | g^R + \rho^2 g^L | w_i \rangle}. \tag{3.62}$$

The 4-simplex amplitude is now just a simple contraction of 5 such propagators. To compare it however to the amplitude in the DL model, we have to perform the integrate out the $|w_i\rangle$ spinors in order to have the same number of variables. After the $|w_i\rangle$ integration, the amplitude becomes

$$\tilde{\mathcal{A}}_\sigma = \int \prod_a dg_a^{L,R} \, \mathbf{e}^{(1+\rho^2)^{-1}[z_b^a|(g_a^{R^{-1}} + \rho^2 g_a^{L^{-1}})(g_b^R + \rho^2 g_b^L)|z_a^b \rangle}. \tag{3.63}$$

We can see that there is a mixing between left and right sectors – while in the DL model the left and right group elements g^L, g^R are multiplied separately as in Eq.(3.48), here the relevant

group elements become a combination $(g^R + \rho^2 g^L)$. Expanding this in a power series it would seem we would get four independent terms. However, since in the large z limit the holomorphic simplicity constraints imply that we have $j^L = \rho^2 j^R$, one can show that only three summations are independent, so the amplitude can be written as

$$\tilde{\mathcal{A}}_\sigma = \int \prod_a dg_a^{L,R} \sum_{j_{ab}^{L,R}, J_{ab}} \frac{([z_b^a|g_a^{R-1}g_b^R|z_a^b\rangle)^{2j_{ab}^R - 2J_{ab}}}{(2j_{ab}^R - 2J_{ab})!} \frac{(\rho^4[z_b^a|g_a^{L-1}g_b^L|z_a^b\rangle)^{2j_{ab}^L - 2J_{ab}}}{(2j_{ab}^L - 2J_{ab})!} \times$$
$$\times \frac{(\rho^2[z_b^a|g_a^{R-1}g_b^L|z_a^b\rangle)^{2J_{ab}}}{(2J_{ab})!} \frac{(\rho^2[z_b^a|g_a^{L-1}g_b^R|z_a^b\rangle)^{2J_{ab}}}{(2J_{ab})!}(1+\rho^2)^{-2(j_{ab}^L + j_{ab}^R)}, \tag{3.64}$$

with the the spins satisfying

$$j_{ab}^R \geq J_{ab}, \qquad j_{ab}^L \geq J_{ab}. \tag{3.65}$$

This means that the mixed left-right terms never overtake the pure left and right sectors. For the details of this calculation, see the Appendix.

We thus get that the effective action of the constrained propagator model for a single 4-simplex is simply

$$\tilde{S}_{eff}(j_{ab}^{L,R}, J_{ab}) = \sum_{a,b\in\sigma} 2(j_{ab}^R - J_{ab}) \ln[z_b^a|g_a^{R-1}g_b^R|z_a^b\rangle + 2(j_{ab}^L - J_{ab}) \ln[z_b^a|g_a^{L-1}g_b^L|z_a^b\rangle$$
$$\underbrace{+2J_{ab} \ln[z_b^a|g_a^{R-1}g_b^L|z_a^b\rangle + 2J_{ab} \ln[z_b^a|g_a^{L-1}g_b^R|z_a^b\rangle}_{\text{mixed}} + \tilde{N}, \tag{3.66}$$

where the numerical factor $\tilde{N}$ carries all the normalization factors and is a function of the different spins and ρ given by

$$\tilde{N} = \sum_{a,b\in\sigma} 8j_{ab}^L \ln\rho - 2(j_{ab}^L + j_{ab}^R)\ln(1+\rho^2) - \ln(2j_{ab}^L - 2J_{ab})! - \ln(2j_{ab}^R - 2J_{ab})! - 2\ln(2J_{ab})! \tag{3.67}$$

We can see that compared with the DL model, the effective action of the constrained propagator model has two additional terms which are underbraced and an additional spin J_{ab}. Nonetheless, we again obtain the closure equation from the variation of spinor $|z\rangle$,

$$\sum_{b\neq a} |z_b^a\rangle\langle z_b^a| = \sum_{b\neq a} j_{ab}^R \mathbb{1}. \tag{3.68}$$

To see how these additional terms change the asymptotics, let us examine the terms in the real part of this action

$$(j_{ab}^L - J_{ab})\ln\frac{1}{2}\left(|z_b^a|^2|z_a^b|^2 - (g_a^L \triangleright \vec{V}_b^a)\cdot(g_b^L \triangleright \vec{V}_a^b)\right) + (j_{ab}^R - J_{ab})\ln\frac{1}{2}\left(|z_b^a|^2|z_a^b|^2 - (g_a^R \triangleright \vec{V}_b^a)\cdot(g_b^R \triangleright \vec{V}_a^b)\right)$$
$$+ J_{ab}\ln\frac{1}{2}\left(|z_b^a|^2\,|z_a^b|^2 - (g_a^R \triangleright \vec{V}_b^a)\cdot(g_b^L \triangleright \vec{V}_a^b)\right) + J_{ab}\ln\frac{1}{2}\left(|z_b^a|^2\,|z_a^b|^2 - (g_a^L \triangleright \vec{V}_b^a)\cdot(g_b^R \triangleright \vec{V}_a^b)\right) + \tilde{N}. \tag{3.69}$$

39

At the critical points, we also require the real part of the effective action to be maximized. Since the real part of the action can be written as $\mathbf{Re}\tilde{S}_{eff} = S_{LL} + S_{RR} + S_{RL} + S_{LR}$ and all the coefficients in front of the logarithms are positive, the maximization condition implies that all the four terms have to be maximized independently. Thus the following critical equations substitute the Eq.(6.19) in DL model,

$$g_a^L \triangleright \hat{v}_b^a = -g_b^L \triangleright \hat{v}_a^b = g_a^R \triangleright \hat{v}_b^a = -g_b^R \triangleright \hat{v}_a^b, \quad \text{where} \quad \hat{v} = \vec{V}/|\vec{V}|. \tag{3.70}$$

When written in terms of spinors $|z\rangle$ and $|z]$, this means that apart from the spinorial orientation condition in Eq.(3.54),

$$g_a^{L-1} g_b^L |z_a^b\rangle = e^{i\phi_L^{ab}} |z_b^a], \quad g_a^{R-1} g_b^R |z_a^b\rangle = e^{i\phi_R^{ab}} |z_b^a],$$

relating $|z_a^b\rangle$ to $|z_b^a]$ up to a phase, we also have two additional phases ψ and θ appearing between the mixed left-right terms

$$g_a^{L-1} g_b^R |z_a^b\rangle = e^{i\psi^{ab}} |z_b^a], \quad g_a^{R-1} g_b^L |z_a^b\rangle = e^{i\theta^{ab}} |z_b^a]. \tag{3.71}$$

Let us now plug in the critical point equations (3.54) and (3.71) into the the effective action to find the semi-classical behavior of the amplitude. The imaginary part of the effective action becomes a function of three spins and four angles, given by

$$\mathbf{Im}\tilde{S}_{eff}(j_{ab}^{L,R}, J_{ab}) = \sum_{a,b \in \sigma} 2(j_{ab}^L - J_{ab})\phi_L^{ab} + 2(j_{ab}^R - J_{ab})\phi_R^{ab} + 2J_{ab}(\psi^{ab} + \theta^{ab}) \tag{3.72}$$

At first sight this is quite different from the effective action of the DL model, with two extra angles and an additional spin label to sum over. Let us notice however, that using the critical point equations (3.54) and (3.71), we can get the relation

$$g_b^{L-1} g_b^R |z_a^b\rangle = e^{i(\psi^{ab} - \phi_L^{ab})} |z_b^a] = e^{i(\phi_R^{ab} - \theta^{ab})} |z_b^a]. \tag{3.73}$$

This condition implies that the additional angles ψ and θ we had to introduce are actually related to the angles ϕ_L and ϕ_R by

$$\psi^{ab} + \theta^{ab} = \phi_L^{ab} + \phi_R^{ab} \mod 2\pi. \tag{3.74}$$

This is exactly the combination of angles that allows us to drop the terms proportional to J_{ab} in the action. Hence we have that the imaginary part of the effective action is exactly the same as the one in DL model,

$$\mathbf{Im}\tilde{S}_{eff}(j_{ab}^{L,R}, J_{ab}) = \sum_{a,b \in \sigma} 2j_{ab}^L \phi_L^{ab} + 2j_{ab}^R \phi_R^{ab} = \mathbf{Im}S_{eff}(j_{ab}^{L,R}) \tag{3.75}$$

The rest of the asymptotic analysis of this action carries over in exactly the same way, as in the EPRL-FK models. Thus we have proved that the constrained propagator model has in the asymptotic expansion the same effective action as the DL model, which in turn has the same semi-classical limit as the EPRL-FK models.

It is important to note here that in the case of both of the models we have not performed the full asymptotic analysis, which would require the calculation of the Hessian, as it is not necessary for establishing that the models are described by Regge Calculus in the semi-classical limit. We expect that where the two models show differences is exactly in the Hessian and the overall normalization as well as possibly in the higher order terms in the asymptotic expansion.

We have studied the asymptotic expansion of 4-simplex amplitudes for the DL Spin Foam model and the newly introduced constrained propagator model. In the large $|z|$ limit (corresponding to the usual large-j limit in the spin representation) we have found that the DL model has the same first order expansion as the EPRL-FK Riemannian model. We have also shown that the constrained propagator model has a different amplitude for a 4-simplex, which however agrees with the DL model's one on-shell. We expect the differences to show up in the Hessian matrix and in the higher order terms. Hence both models lead to Regge Calculus in the semi-classical limit.

Chapter 4

Techniques of Evaluating arbitrary amplitude

4.1   Graph structure

In the 4-d spin foam model, the partition function is defined on a 2-complex $\Gamma(V, E, F)$, which is dual to a simplicial discretization of a 4-dimensional manifold. The vertices $v \in V$ are dual to 4-simplices, edges $e \in E$ are dual to tetrahedra, and the faces F of the 2-complex are dual to common triangles which are shared by 4-simplices. Given a (connected) 2-complex $\Gamma(V, E, F)$, there exist at least one *spanning tree* [130] $T_\Gamma(E_T)$ in the 1-skeleton of $\Gamma(V, E, F)$ and each of the trees contains $|V| - 1$ branches E_T.

Now if we add one edge to the spanning tree, it will create a cycle. This type of cycle is called a *fundamental cycle* in graph theory [130]. Let us denote the set of fundamental cycles which are correlated with the spanning tree $T_\Gamma(E_T)$ as C_T. For a given spanning tree, there is one to one correspondence between the edges not in the tree and the fundamental cycles in C_T [130]. The number of fundamental cycles $|C_T|$ is a tree-independent quantity:

$$|C_T| = |E \setminus E_T| = |E| - |V| + 1 \tag{4.1}$$

For certain graphs, for example the diagrams of Pachner moves and melons, we can always choose a spanning tree such that all the corresponding fundamental cycles are also faces of the 2-complex (in cable diagram notation, this would be loops formed by the strands). Let us call such type of spanning tree an *optimal tree* and define Ω_Γ as a set of graphs which contain optimal spanning trees:

$$\Omega_\Gamma \equiv \{\Gamma \mid \exists\, T_\Gamma(E_T),\ s.t.\ C_T \subset F\}. \tag{4.2}$$
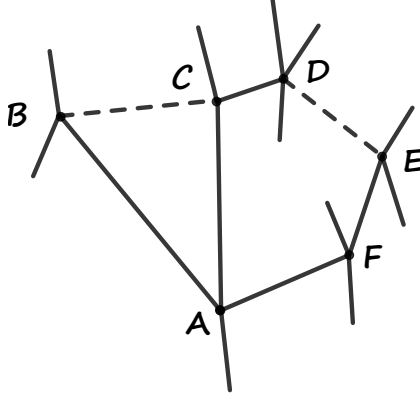
Figure 4.1: The solid lines represent spanning tree $T_\Gamma = AB \cup AC \cup CD \cup EF \cup AF$. Edge $BC \in E \setminus E_T$ corresponds to fundamental cycle $ABC \in C_T$. Edge DE corresponds to $ACDEF \in C_T$.

In section 6, we will see that the existence of optimal spanning trees in a graph is a very convenient property. We will show that the truncated bulk amplitude in such a graph can be written down just from reading out the combinatorics.

4.2 Partial gauge fixing

In this section we briefly review a gauge fixing procedure which was first introduced and proved in [131]. Let us now understand how to fix the "Lorentz" gauge on a spin network. Since the volume of the group SU(2) is finite, the gauge fixing amounts to only a change of variables along a maximal tree. We follow [131] in defining the gauge fixing procedure. Consider a graph Γ with E edges and V vertices. Each edge is oriented so that it starts at a source vertex $s(e)$ and ends at target $t(e)$. Consider now a spin network function such that

$$\psi^\Gamma(g_{e_1}, \ldots, g_{e_E}) = \psi^\Gamma(h_{s(e_1)}^{-1} g_{e_1} h_{t(e_1)}, \ldots, h_{s(e_E)}^{-1} g_{e_E} h_{t(e_E)}). \tag{4.3}$$

Now choose a maximal tree T in Γ, i.e. a collection of $V - 1$ edges which passes through every vertex, without forming loops. Choose a vertex A to be the root[1] of the tree T and label g_{vA}^T the product of group elements g_{e_i} along T that connect vertex v and A. Next we will use Eq. (4.3) with $h_v = g_{vA}^T$, so that $\psi^\Gamma = \psi^\Gamma(G_1^T, \ldots, G_E^T)$ with $G_e^T = g_{As(e)}^T g_e g_{t(e)A}^T$.

Now, for any edge $e \in T$, there is a unique path along the tree connecting A and $s(e)$ or $t(e)$. Let us choose this to be $t(e)$, since the other case works in the same way. It follows

---

[1] One can show that the gauge fixing procedure is independent of this choice.
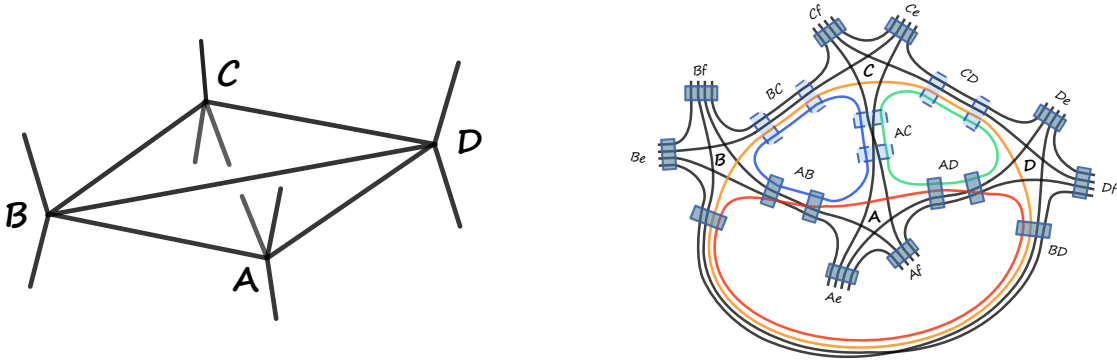
Figure 4.2: Take the graph of 4–2 Pachner move as an example: all the fundamental cycles of spanning tree $CA \cup CB \cup CD$ are faces of the 2-complex (single loops formed by strands in the right cable diagram): $ABC, ACD, BCD \in F$. However, for another choice of tree $CA \cup CB \cup AD$, one of the cycles $BCAD \notin F$.

that $g^T_{s(e)A} = g_e g^T_{t(e)A}$ and so $G^T_e = \mathbb{1}$ for $e \in T$. Hence the procedure for gauge fixing is to set all the group elements on the maximum tree to $\mathbb{1}$ and change all the other to $g_{e_i} = G^T_{e_i}$. Since $\int_{SU(2)} \mathrm{d}g = 1$, ending up with empty integrations does not lead to any divergences. In the language of amplitudes written in terms of projectors, this corresponds to replacing the projectors $P(z_i; w_i) = \int_{\mathrm{SU(2)}} \mathrm{d}g\, e^{\sum_i [z_i|g|w_i\rangle}$ on the maximal tree by the trivial propagators $\mathbb{1}(z_i; w_i) \equiv e^{\sum_i [z_i|w_i\rangle}$. This procedure carries over to the 4-dimensional case trivially, since Spin(4) is just a product $SU(2) \times SU(2)$. Given a (connected) 2-complex $\Gamma(V, E, F)$ on which a partition function $Z(\Gamma)$ is defined, one can choose any spanning tree $T_\Gamma(E_T) \subset \Gamma$ and gauge fix all the propagators on its edge $P^e_\rho, e \in E_T$ into

$$P_\rho(z_i; w_i) \rightarrow \mathbb{1}_\rho(\tilde{z}_i; \tilde{w}_i) \equiv \sum_{j_i}^{\infty} F_\rho(J) \prod_{i=1}^{4} \frac{[z_i|\mathbb{1}|w_i\rangle^{2j_i}}{2j_i!}, \tag{4.4}$$

leaving the partition function $Z(\Gamma)$ invariant. Note that $J = \sum_i j_i$.

The invariance of the partition function can be proved through a systematic change of variables in the SU(2) integrations of propagators. Note that for the convenience of notation later, we will always add a tilde on the spinors which belong to the partially gauge fixed propagator. Each spanning tree contains $|V| - 1$ branches, thus we can gauge fix $|V| - 1$ propagators based on Eq.(4.4) in a given 2-complex.

4.3   The homogeneity map

As evaluating the partition function essentially amounts to integrations of power series of spinor polynomials, in [105] we introduced a useful tool - the homogeneity map - which allows us to perform the calculation in a more tractable and compact way.

The basic idea of homogeneity map comes from the property that the holomorphic monomials of different degrees of homogeneity are orthogonal to each other. When we perform integration of a spinor, terms with different homogeneity do not mix:

$$\int d\mu(w)[z_i|w\rangle^j \langle w|z_2]^l = j! \, [z_1|z_2]^j \, \delta_{j,l}. \tag{4.5}$$

It would be convenient if instead of computing term by term in the power series, we could perform the integration in a compact form, with some book-keeping parameter to keep track of each term with different homogeneity degree. In this spirit, we define a general propagator G_τ in terms of an exponential form

$$G_\tau(z_i; w_i) = \sum_J \tau^J \frac{\left(\sum_{i<j}[z_i|z_j\rangle[w_i|w_j\rangle\right)^J}{J!} = e^{\tau \sum_{i<j}[z_i|z_j\rangle[w_i|w_j\rangle} \tag{4.6}$$

and denote it graphically by

$$G_\tau(z_i; w_i) = \begin{array}{c} [z_1| \\ [z_2| \\ [z_3| \\ [z_4| \end{array} \boxed{\tau} \begin{array}{c} |w_1\rangle \\ |w_2\rangle \\ |w_3\rangle \\ |w_4\rangle \end{array} . \tag{4.7}$$

in which τ keeps track of the homogeneity of the polynomial in spinors. If we transform each of these τ^J into a function of J, the integrals of the polynomials stay the same. In this way we can perform complicated calculations with G_τ and in the end we can use the following map, defined by a functional H_f mapping G_τ to the desired function f:

$$H_\rho : G_\tau \to P_\rho \quad \text{with} \quad H_\rho : \tau^J \to \frac{F_\rho(J)}{(J+1)!} \quad \text{(Simplicity Constraints)} \tag{4.8}$$

$$H_P : G_\tau \to P \quad \text{with} \quad H_P : \tau^J \to \frac{1}{(J+1)!} \quad \text{(BF Theory)} \tag{4.9}$$

in order to recover the propagators of the BF theory or the one of the gravity model with simplicity constraints imposed. Not that $P_0 = P$ so the BF model is included in our more general

description. We are of course not limited to only these choices and could in principle study a much wider class of spin foam models built by non-trivial propagators.

By considering how BF projectors compose in Eq. (3.14), it is quite easy to find the homogeneity map for composing the propagator P_ρ n times: $P_\rho \circ \cdots \circ P_\rho$. To do this, we just realize that if one reintroduces back the factor of $1/(J+1)!$ into the definition of G_τ, it then defines just the BF projector P with the spinors z rescaled to $\sqrt{\tau} z$. The homogeneity map for the composition is therefore given by[2]

$$\tau^J \to \frac{F_\rho(J)^n}{(J+1)!(1+\rho^2)^{2(n-1)J}} \qquad \text{for} \qquad G_\tau \to P_\rho^n \qquad (n \text{ Propagators}). \qquad (4.10)$$

Using τ to keep track of homogeneity of each term, we first perform spinor integration with the exponential form G_τ, then expand the result in terms of power series, and use the homogeneity map H to restore the desired coefficients to get the final answer.

Here is a simple example. To evaluate any amplitudes in which the triangulation has shared faces, we will need to consider contracted loops of spinors. In BF theory, such a loop should correspond to an SU(2) delta function. Using the spinorial language however, we get

$$\bigcirc \quad = \quad \int d\mu(z) e^{\langle z|z \rangle} = \sum_j \int d\mu(z) \frac{\langle z|z \rangle^{2j}}{(2j)!} = \sum_j \chi^j(\mathbb{1}) = \sum_j (2j+1), \qquad (4.11)$$

whereas a delta function is $\delta_{SU(2)}(\mathbb{1}) = \sum_j (2j+1)^2$. One way of going around this is to change measure of integration for this loop to $d\tilde{\mu}(z) = (\langle z|z \rangle - 1) d\mu(z)$, as was suggested in [118]. This provides the additional factor of $(2j+1)$. An alternative way is to follow in the spirit of the homogeneity map and introduce a τ' that tracks the homogeneity in this loop. For clarity, we add a symbol for this face weight into the graph:

$$\bigcirc_f \quad = \quad \int d\mu(z) e^{\tau' \langle z|z \rangle} = \sum_j \tau'^{2j}(2j+1). \qquad (4.12)$$

The replacement of $\tau'^{2j} \to (2j+1)$ now defines a homogeneity map for a BF loop. Of course, we now do not have to restrict ourselves to this simple face weight and can choose an arbitrary function of spin.

---

[2]Note that the factor of $(1+\rho^2)^{2J}$ in (4.8) comes from the fact that the measure has changed under the simplicity constraints to $d\mu_\rho(z) = (1+\rho^2)^2 \pi^{-2} e^{-(1+\rho^2)\langle z|z \rangle}$. Hence every contraction produces a factor $(1+\rho^2)^{-2j}$ where j is the representation of the line. There is one such contraction for each j where $J = \sum j$ for each τ.

The homogeneity map we have developed in this section will be very useful in computing the 4-dimensional Pachner moves. In later sections we will define additional homogeneity maps as we go on, to simplify the calculations.

4.4   Loop Identity

4.4.1   3D case

The BF theory partition function is independent of the triangulation Δ. This can be shown by demonstrating its invariance (up to an overall factor) with respect to a finite set of coarse graining moves, constructed out of Pachner moves. The Pachner moves can all be derived from one identity which we will call the loop identity. This identity follows from the coherent state representation of the SU(2) delta function

$$\delta(g) = \int d\tilde{\mu}(z) e^{\langle z|g|z \rangle}, \tag{4.13}$$

where $d\tilde{\mu}(z) = d\mu(z)(\langle z|z \rangle - 1)$. Therefore

$$
\begin{aligned}
\int d\tilde{\mu}(z_n) P(z_1, ..., z_n; w_1, ..., \check{z}_n) &= \int dg e^{\sum_{i=1}^{n-1} [z_i|g|w_i\rangle} \int d\tilde{\mu}(z_n) e^{[z_n|g|z_n]} \\
&= \int dg e^{\sum_{i=1}^{n-1} [z_i|g|w_i\rangle} \delta(g) \\
&= e^{\sum_{i=1}^{n-1} [z_i|w_i\rangle} \\
&= \mathbb{1}(z_1, ..., z_{n-1}; w_1, ..., w_{n-1}),
\end{aligned}
\tag{4.14}
$$

which is represented graphically by

$$\tag{4.15}$$

Since each closed loop of the BF partition function (2.17) has a factor of $2j_f + 1$ we will use the convention that two lines are contracted with $d\mu(z)$ as in (3.5), however, the contraction of a

line with itself, i.e. a loop, is contracted with the measure $d\tilde{\mu}(z)$ as in (4.15). An alternative way would be to use the homogeneity map to keep track of this face weight.

The expression for the loop identity we have just derived, while compact, does not generalize straightforwardly to the case of 4-dimensional QG models with simplicity constraints (due to the presence of the group integrals). We will thus redo the above calculation with the projector written in terms of only spinors without group integration.

We expect that the loop identity (4.14) applied to the projector (3.19) implies that

$$\sum_{j_n}(2j_n + 1)\int d\mu(z_n)\frac{\left(\sum_{i<j}[z_i|z_j\rangle[w_i|w_j\rangle\right)^J}{J!(J + 1)!} = \prod_{i=1}^{n-1}\frac{[z_i|w_i\rangle^{2j_i}}{(2j_i)!},\tag{4.16}$$

where the integration is performed with $w_n = \check{z}_n$. Below we will directly show this. Let us perform the integration on the LHS explicitly by using the homogeneity map to keep track of the $1/(J + 1)!$ and the face weight $(2j_n + 1)$ and then summing over j_i. Namely, let us use the homogeneity maps $\tau^J \to 1/(J + 1)!$ and $\tau'^{2j_n} \to (2j_n + 1)$. The result is then

$$\int d\mu(z_n)\exp\left(\tau\sum_{i<j<n}[z_i|z_j\rangle[w_i|w_j\rangle - \tau\tau'\sum_{i<n}\langle z_n|z_i\rangle[w_i|z_n\rangle\right) = \frac{e^{\tau\sum_{i<j<n}[z_i|z_j\rangle[w_i|w_j\rangle}}{\det\left(\mathbb{1} - \tau\tau'\sum_{i<n}|w_i\rangle[z_i|\right)}.\tag{4.17}$$

To continue, we have to be able to evaluate the determinant in the denominator. This is thankfully not too difficult, as the matrix in question is just a 2×2 matrix made up by spinors. Indeed, the following lemma comes in handy

Lemma 4.4.1. *Let* $M = \mathbb{1} - \sum_i C_i|A_i\rangle[B_i|$ *then*

$$\det M = 1 - \sum_i C_i[B_i|A_i\rangle + \sum_{i<j}C_iC_j[A_i|A_j\rangle[B_i|B_j\rangle.$$

The proof is given in Appendix A.4.

Using this result, we can immediately find the determinant in (4.17). In our case, all $C_i = \tau\tau'$, hence we get that the loop identity for the homogenized projector P_τ becomes

$$\frac{e^{\sum_{1\leq i<j<n}\tau\tau'[z_i|z_j\rangle[w_i|w_j\rangle}}{1 - \sum_{i\neq n}\tau\tau'[z_i|w_i\rangle + \sum_{1\leq i<j<n}\tau^2\tau'^2[z_i|z_j\rangle[w_i|w_j\rangle}.\tag{4.18}$$

Now we can expand both the numerator and the denominator in a power series and then use the homogeneity map to restore the $1/(J + 1)!$ terms and the face weight. This allows us to get the

48

loop identity for the projector (3.19)

$$\sum_{J,J'} C_{BF}(J, J') \left(\sum_{i<n} [z_i|w_i\rangle \right)^J \left(\sum_{i<j<n} [z_i|z_j\rangle[w_i|w_j\rangle \right)^{J'} , \qquad (4.19)$$

where we have defined the coefficient $C_{BF}(J, J')$ to be given by

$$C_{BF}(J, J') = \sum_K (-1)^{J'-K} \frac{(J + J' - K)!(J + 2J' - 2K + 1)}{J!(J' - K)!K!(J + 2J' - K + 1)!}. \qquad (4.20)$$

At first glance, this is a worrisome result, as we do not only get the trivial projection (raised to power J), but also an unwanted *mixing* term (raised to power J'). Notice though, that we have an additional free sum over the variable K in the definition of the coefficient. We can actually explicitly evaluate this sum over K to find the expected result

$$C_{BF}(J, J') = \frac{\delta_{J',0}}{J!}. \qquad (4.21)$$

Hence only the $J' = 0$ term is non-vanishing, so the mixing terms always drop out in BF theory. We thus recover the result (4.16) that we set out to prove. This calculation readily is generalized in the following section to the case with simplicity constraints. The major difference in this case is the lack of the cancellation of the mixing terms.

4.4.2 4D case

Toy Loop

To capture the essence of the computation without too much complexity, let us start with repeating the calculation of the BF loop identity, but with the constrained propagator $P_\rho(z_i; w_i)$ (3.36) rather than the SU(2) projector. We will follow the treatment of the loop identity from the previous section. We will thus find the loop identity for the generating functional

$$G_\tau(z_i; w_i) = e^{\tau \sum_{i<j} [z_i|z_j\rangle[w_i|w_j\rangle}$$

and at the end of the calculation use the homogeneity map to get the loop identity for $P_\rho(z_i; w_i)$ by changing $\tau^J \to F_\rho(J)/(J + 1)!$. We also want to be able to insert a face weight, which is a
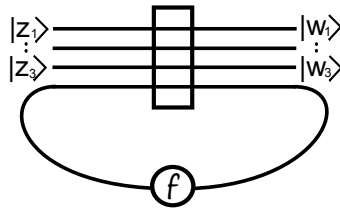
function of the spin we will sum over. This face weight could be *a priori* arbitrary, but for the sake of definiteness, let us choose it to be $(2j + 1)^\eta$ with $\eta \in \mathbb{R}$ being a free parameter, which keeps track of divergence properties of the Spin Foam model. The method we use allows us of course to modify the face weight to an arbitrary function of spin. To insert the face weight, we follow the calculation in BF theory and rescale the spinor in the loop by an additional factor of τ', which will keep track of homogeneity of that specific spinor. At the end of the calculation we can restore the face weight by replacing $\tau'^{2j} \to (2j + 1)^\eta$ in the series expansion. Let us now calculate the constrained loop identity:

$$\int d\mu_\rho(z_4) e^{\tau \sum_{i<j<4}[z_i|z_j\rangle[w_i|w_j\rangle - \tau\tau' \sum_{i<4}\langle z_4|z_i\rangle[w_i|z_4\rangle} = \frac{e^{\tau \sum_{i<j<4}[z_i|z_j\rangle[w_i|w_j\rangle}}{\det\left(\mathbb{1} - \frac{\tau\tau'}{1+\rho^2} \sum_{i<4} |w_i\rangle[z_i|\right)}. \tag{4.22}$$

Unsurprisingly, we get nearly the same result as in the previous section, the difference being the additional factor of $1/(1 + \rho^2)$, which arises from the modified integration measure $d\mu_\rho(z)$. Of course, the τ also carries a hypergeometric function of ρ. We can again use the lemma 4.4.1 to evaluate the determinant. We arrive thus at the result

$$\int d\mu_\rho(z_4) G_\tau(z_1, \ldots, \tau' z_4; w_1, \ldots, \check{z}_4) = \frac{e^{\tau \sum_{i<j<4}[z_i|z_j\rangle[w_i|w_j\rangle}}{1 - \frac{\tau\tau'}{1+\rho^2} \sum_{i<4}[z_i|w_i\rangle + \sum_{i<j<4} \frac{\tau^2\tau'^2}{(1+\rho^2)^2}[z_i|z_j\rangle[w_i|w_j\rangle}$$

$$= e^{\tau \sum_{i<j<4}[z_i|z_j\rangle[w_i|w_j\rangle} \sum_{N,M} \frac{(N + M)!}{N!M!} \left(\frac{\tau\tau'}{1+\rho^2}\right)^{N+2M} \left(\sum_{i<4}[z_i|w_i\rangle\right)^N \left(-\sum_{i<j<4}[z_i|z_j\rangle[w_i|w_j\rangle\right)^M. \tag{4.23}$$

We can now expand the exponential, combine the mixing terms and use the homogeneity map to reintroduce the face weight and the hypergeometric function of ρ. We hence find that the constrained loop identity for $P_\rho(z_i; w_i)$ is given by
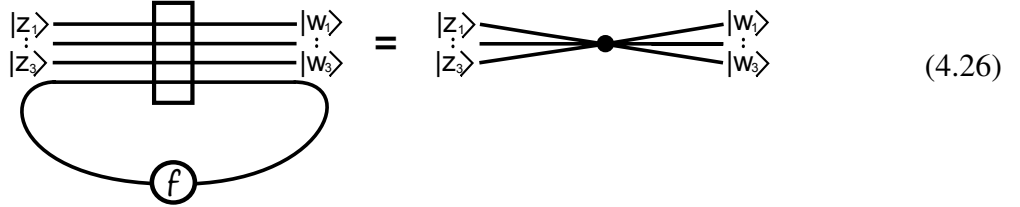
 $$= \sum_{J,J'} C_\rho(J, J') \left(\sum_{i<n}[z_i|w_i\rangle\right)^J \left(\sum_{i<j<n}[z_i|z_j\rangle[w_i|w_j\rangle\right)^{J'}, \tag{4.24}$$

with the coefficient $C_\rho(J, J')$ given by

$$C_\rho(J, J') = \sum_K (-1)^{J'-K} \frac{(J+J'-K)!(J+2J'-2K+1)^\eta}{J!(J'-K)!K!(J+2J'-K+1)!} \frac{F_\rho(J + 2J' - 2K)}{(1 + \rho^2)^{J+2J'-2K}}, \tag{4.25}$$

where $F_\rho(J) = {}_2F_1(-J - 1, -J; 2; \rho^4)$. We have hence arrived at an expression very similar to the one in BF theory – we again got the trivial propagation terms $\sum_{i<4}[z_i|w_i\rangle$ together with

additional mixing terms like $\sum_{i<j<4}[z_i|z_j\rangle[w_i|w_j\rangle$. Unlike in the BF loop identity however, there is no miraculous cancellation of the $J' \neq 0$ terms, unless we choose $\rho = 0$ and $\eta = 1$, i.e. we reduce this to SU(2) BF theory. Hence the way in which simplicity constraints break the topological symmetry is by introducing additional mixing terms in the loop identity. We can represent this graphically as

$$ (4.26) $$

The Constrained Loop Identity

We are now going to see that the loop identity we need for Pachner moves is somewhat different with the one we considered in the previous section. When we glue together 4-simplices, we need to glue them along their boundaries, necessitating the glueing of two propagators, i.e. we should work with $P_\rho \circ P_\rho$, rather than a single P_ρ. The reason for this being that in our model the propagator P_ρ is inserted around each vertex and we get the composition of them along an edge. Since P_ρ is not a projector unless $\rho = 0$ we have $P_\rho \circ P_\rho \neq P_\rho$. Additionally, the loops arising in all the Pachner moves always are composed of three groups of propagators $P_\rho \circ P_\rho$, rather than the single one we have considered. Fortunately, two of these can be always gauge fixed by a proper choice of a maximal tree, so that we have to consider the loop identity shown in Fig.4.3. In BF theory the gauge-fixing reduces the projectors to trivial propagators $\mathbb{1}(z_i; w_i)$, so we did not have to worry about this issue.

We thus have to first find the equivalent of the trivial propagator in the constrained case, i.e. the analog of setting $g = \mathbb{1}$ in (3.13) to get (3.6) but for the propagator (3.36). We thus have to restore the group integration. Fortunately, by tracking homogeneity for each term, we know that

$$ \frac{\left(\sum_{i<j}[z_i|z_j\rangle[w_i|w_j\rangle\right)^J}{J!(J+1)!} = \sum_{\sum j_i = J} \int \mathrm{d}g \prod_{i=1}^{4} \frac{[z_i|g|w_i\rangle^{2j_i}}{(2j_i)!}. \tag{4.27} $$

Setting this SU(2) group element to identity and summing over all J allows us to get the partially gauge fixed propagator, which we denote $\mathbb{1}_\rho$

$$ \mathbb{1}_\rho(\tilde{z}_i; \tilde{w}_i) = \sum_J {}_2F_1\left(-\frac{J}{2} - 1, -\frac{J}{2}; 2; \rho^4\right) \frac{(\sum_i[\tilde{z}_i|\tilde{w}_i\rangle)^J}{J!}. \tag{4.28} $$

51
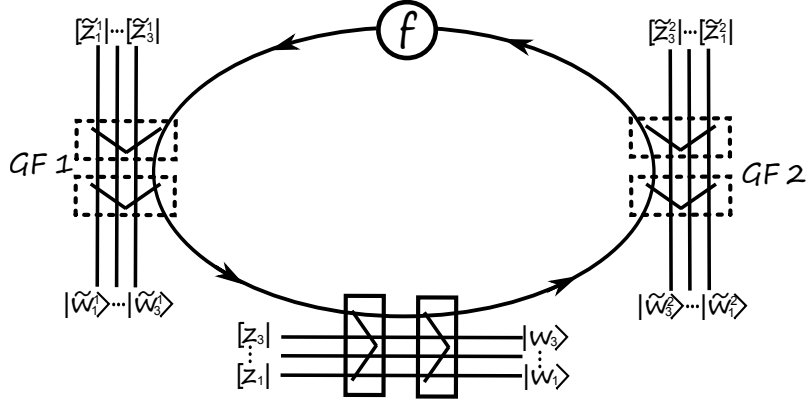
Figure 4.3: Loop identity with for the constrained projector with two extra gauge fixed projectors

Note that for the convenience of notation later, we will always add a tilde on the spinors which belong to the partially gauge fixed propagator. As in the case of the propagator, we find that setting $\rho = 0$ we recover the BF trivial propagator $\mathbb{1}(z_i; w_i)$, as we would expect. We can now use the homogeneity map to define a homogenized trivial propagator $\mathbb{1}_{\tilde\tau}$ as

$$\mathbb{1}_{\tilde\tau} = e^{\tilde\tau \sum_i [\tilde z_i | \tilde w_i \rangle} \qquad \text{with} \qquad \tilde\tau^J \to F_\rho(J/2) \qquad \text{for} \qquad \mathbb{1}_{\tilde\tau} \to \mathbb{1}_\rho. \tag{4.29}$$

We thus have arrived at the expression for the gauge fixed propagators that are necessary for the loop identity. We will have to consider however $P_\rho \circ P_\rho$ and $\mathbb{1}_\rho \circ \mathbb{1}_\rho$, rather than single propagators, as we have mentioned above. We will thus use the following homogeneity maps: for the pair of gauge-fixed propagators we will have

$$\mathbb{1}_{\tilde\tau} \circ \mathbb{1}_{\tilde\tau} = e^{\tilde\tau \sum_i [\tilde z_i | \tilde w_i \rangle} \quad \text{with} \quad \tilde\tau^J \to \frac{F_\rho(J/2)^2}{(1+\rho^2)^J} \quad \text{for} \quad \mathbb{1}_{\tilde\tau} \circ \mathbb{1}_{\tilde\tau} \to \mathbb{1}_\rho \circ \mathbb{1}_\rho, \tag{4.30}$$

while for the pair of propagators P_ρ we get

$$G_\tau \circ G_\tau = e^{\tau \sum_{i<j} [z_i | z_j \rangle [w_i | w_j \rangle} \quad \text{with} \quad \tau^J \to \frac{F_\rho(J)^2}{(1+\rho^2)^{2J}(J+1)!} \quad \text{for} \quad G_\tau \circ G_\tau \to P_\rho \circ P_\rho. \tag{4.31}$$

With this, we are ready to perform the calculation of this loop identity. The addition of the extra two pairs of gauge-fixed propagators leads to very simple contractions, using our results of spinor Gaussian integrals in the Appendix. Integrating over the three strands inside the loop leads to nearly the same calculation as in the previous section, with the difference being the addition of the trivial propagation in the extra strands connected to the gauge-fixed propagators. Using the

homogeneity map, we finally find that the constrained loop identity is given by

$$= \sum_{A,B,J,J'=0}^{\infty} \frac{N(A,B,J,J',\rho)}{A!B!J!J'!} \times$$

(4.32)

$$\times \underbrace{\left(\sum_{i=1}^{3} [\tilde{z}_i^1 | \tilde{w}_i^1 \rangle \right)^A}_{GF1} \underbrace{\left(\sum_{i=1}^{3} [\tilde{z}_i^2 | \tilde{w}_i^2 \rangle \right)^B}_{GF2} \underbrace{\left(\sum_{i=1}^{3} [z_i | w_i \rangle \right)^J}_{\text{Trival projection}} \underbrace{\left(\sum_{i<j<4} [z_i | z_j \rangle [w_i | w_j \rangle \right)^{J'}}_{\text{Mixing terms}},$$

with the coefficient $N(A,B,J,J',\rho)$ given by

$$N(A,B,J,J',\rho) \equiv \sum_{K=0}^{J'} \frac{J'!(J+K)!(J+2K+1)^\eta}{K!(J'-K)!(J+J'+K+1)!} \frac{(-1)^K}{(1+\rho^2)^{(A+B+12K+7J+2J')}} \times$$
$$\times F_\rho^2(J+J'+K) F_\rho^2((A+J)/2+K) F_\rho^2((B+J)/2+K),$$

where we have defined $F_\rho(J) \equiv {}_2F_1(-J-1,-J;2;\rho^4)$. The variables $|\tilde{z}_i^1\rangle, |\tilde{w}_i^1\rangle$ appear in the strands attached to the first gauge fixing term, similarly $|\tilde{z}_i^2\rangle, |\tilde{w}_i^2\rangle$ appear in the second gauge fixing, while $|z_i\rangle, |w_i\rangle$ are are labelled for the strands we haven't gauge fixed. The face weight coupling constant η should be fixed by requirements of divergence, which we will discuss in a later section. A more detailed calculation of this loop identity can be found in the Appendix.

Even though the expression in Eq.(4.32) has a few layers of summations like a Russian nesting doll and the coefficients look complicated, the physical meaning behind the expression is quite clean – up to a weight, we get the trivial propagation, like in BF theory, but we also get additional mixing terms for $J' \neq 0$.

For the purpose of calculating the 4-dimensional Pachner moves, it will be convenient to again define an exponentiated expression for this loop identity, which can then be transformed into the proper expression by the homogeneity map. Before using the homogeneity map in Eq. (4.32), we would have an expression purely in terms of τ's that can be exponentiated. We hence define the exponentiated loop identity to have the following very simple form:

$$L_\tau(z_i, w_i; \tilde{z}_i^1, \tilde{w}_i^1; \tilde{z}_i^2, \tilde{w}_i^2) = \exp\left(\sum_{i=1}^{3} \tilde{\tau}_1 [\tilde{z}_i^1 | \tilde{w}_i^1 \rangle + \tilde{\tau}_2 [\tilde{z}_i^2 | \tilde{w}_i^2 \rangle + \tau_N [z_i | w_i \rangle + \tau_M \sum_{i<j<4} [z_i | z_j \rangle [w_i | w_j \rangle \right). \quad (4.33)$$
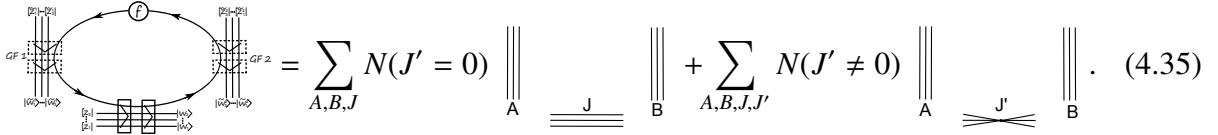
The full loop identity can then be recovered through the following homogeneity map:

$$\tau_N^J \tau_M^{J'} \to \sum_{K=0}^{J'} \frac{(-1)^K (J+K)! J'!}{K!(J'-K)!} (J+2K+1)^\eta \tau^{J'-K} \left(\frac{\tilde{\tau}_1 \tilde{\tau}_2 \tau}{(1+\rho^2)^3} \right)^{J+2K}$$

(4.34)

and the $\tilde{\tau}$'s and τ keep track of the F_ρ factors according to the rules given in Eq. (4.30) and Eq. (4.31).

4.5 Truncation

To evaluate a partition function $Z(\Gamma)$ is to integrate out all the loops in its cable diagram. In [105], we have calculated an identity for a partially gauge fixed loop with only one propagator not gauge fixed (see Appendix). It is crucial for evaluating Pachner moves in both 3-d and 4-d. The special feature that differentiates BF theory and the spin foam model with simplicity constraints, is that integrating out loops results in mixing of strands:

$$\text{(diagram)} = \sum_{A,B,J} N(J' = 0) \; \begin{Vmatrix} \\ A \quad\underline{\underline{J}}\quad B \end{Vmatrix} + \sum_{A,B,J,J'} N(J' \neq 0) \; \begin{Vmatrix} \\ A \quad\underline{J'}\quad B \end{Vmatrix}. \tag{4.35}$$

In [105], it was shown that the mixing terms are sub-leading. We introduced a natural truncation scheme, in which we keep only the non-mixing term in Eq.(4.35). The resulting amplitudes are structure preserving, and at the same time encode the non-local degrees of freedom as a non-local function of spins. To see this, let us define an error function as:

$$\text{Error}(A, B, J, \rho) := \frac{\sum_{J'=1}^{\infty} N(A, B, J, J', \rho)}{\sum_{J'=0}^{\infty} N(A, B, J, J', \rho)} \tag{4.36}$$

For large spins, the truncation scheme leads to very small errors compared with the full amplitude. Examples are shown in Fig.4.4

After truncation, the simplest and the most useful way of expressing the loop identity is in terms of an exponentiated form L using the homogeneity map trick. In general, for a partially gauge fixed loop with one original propagator and $\tilde{n}$ gauge fixed propagators labeled by $k = 1...\tilde{n}$, the truncated loop identity is given by

$$L_\tau(z_i, w_i; \tilde{z}_i^k, \tilde{w}_i^k) = \exp \sum_{i=1}^{3} \left(\sum_{k=1}^{\tilde{n}} \tilde{\tau}_k [\tilde{z}_i^k | \tilde{w}_i^k \rangle + T[z_i | w_i \rangle \right). \tag{4.37}$$

We can see that this is essentially a product of $\tilde{n} + 1$ trivial propagators with different book-keeping parameters $\tilde{\tau}_k$ and T. The truncated loop identity can be recovered through applying the homogeneity map:

$$T^J \rightarrow \frac{J!(J+1)^\eta \tau^J}{(1+\rho^2)^{J \cdot (\tilde{n}+1)}} \left(\prod_k^{\tilde{n}} \tilde{\tau}_k \right)^J \tag{4.38}$$
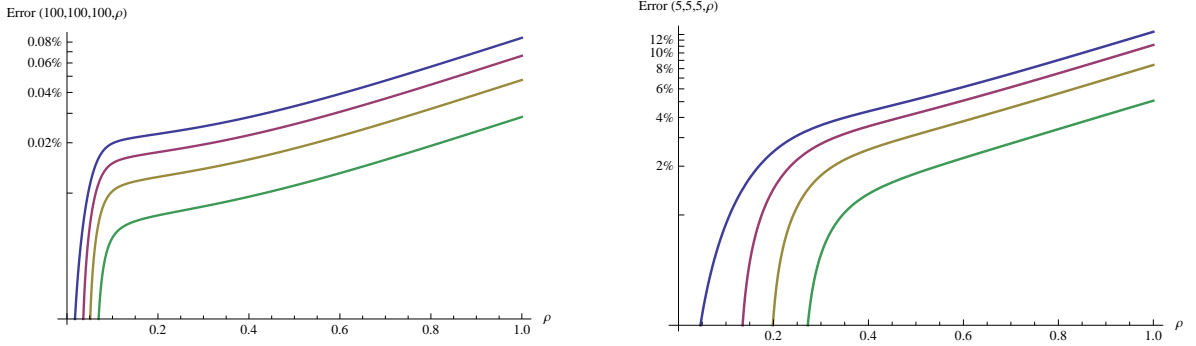
Figure 4.4: Plots of the error from truncation for a single loop identity. The left plot is for large spin. The total spin on each propagator is 100 ($A = B = J = 100$). The right plot is for small spin, in which the total spin on each propagator is 5 ($A = B = J = 5$). Blue, red, yellow and green lines correspond to face weight η equal to 1,2,3,4 respectively. The truncation is a better approximation for larger spins and larger face weights.

in which the propagators are tracked by

$$\tau^J \to \frac{F_\rho(J)^2}{(1+\rho^2)^{2J}(1+J)!}, \quad \tilde{\tau}_k^J \to \frac{F_\rho(J/2)^2}{(1+\rho^2)^J}. \tag{4.39}$$

From Eq.(4.38), we can see that the homogeneity map associated with the original propagator contains the information ($\tilde{\tau}_k$) from the gauge fixed propagators. Thus integrating out loops creates non-local spin couplings in 4-d spin foam amplitudes. We graphically represent this non-local coupling as in Fig.4.5.
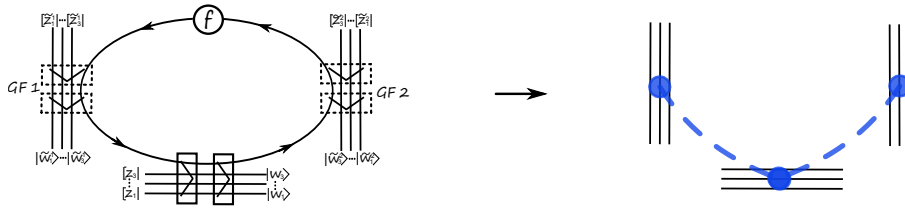
Figure 4.5: We use blue dashed lines to represent the resulting non-local spin coupling from integrating out the loop.

Chapter 5

Computing Pachner Moves

5.1   Pachner moves in 3D topological theory

In this section we review the notion of Pachner moves and their calculation in 3d SU(2) BF theory, to set up the stage for comparison to the 4-dimensional models. To show that a theory defined on a triangulated manifold is topologically invariant, we need a way to relate different triangulations. This is provided by the Pachner moves, which are local replacements of a set of connected simplices by another set of connected simplices. They are a special class of moves because one can prove any simplicial piecewise linear manifold $\mathcal{M}$ can be transformed into any other simplicial piecewise linear manifold $\mathcal{M}'$ homeomorphic to $\mathcal{M}$ by a finite sequence of Pachner moves. [68].

Pachner moves are constructed by adding (or removing) vertices, edges, triangles etc. to (from) the existing triangulation. They can be also obtained in d dimensions by glueing a (d+1)-simplex onto the d-dimensional triangulation. There are several Pachner moves in each dimension and they correspond to changing a configuration of n basic building blocks (d-simplices) into a configuration of m building blocks - we call them n–m Pachner moves. In two dimensions we hence have the moves 2–2, 1–3 moves and their reverse. The 2–2 move corresponds to changing the edge along which two triangles are glued, while the 1–3 move corresponds to adding a vertex inside a triangle and connecting it to the other vertices by three edges, arriving in a configuration with three triangles. Fig. 5.1 shows the inverse. In three dimensions we have 3–2, 4–1 moves and their reverse, see Fig. 5.2. The 3–2 move corresponds to removing an edge, along which three tetrahedra were glued and changing it into a configuration of two tetrahedra. The 4–1 move is combining four tetrahedra into one tetrahedron through removing a common vertex.
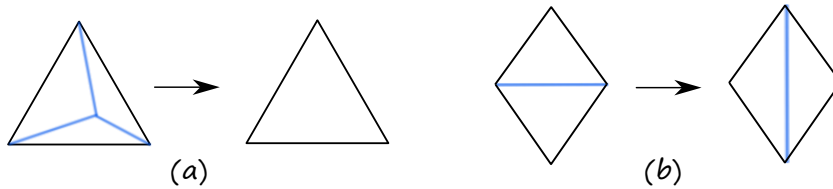
Figure 5.1: Two dimensional Pachner moves: a) 3–1 move, in which three triangles are merged into one by removing a vertex inside; b) 2–2 move, in which two triangles exchange the edge, along which they are glued.
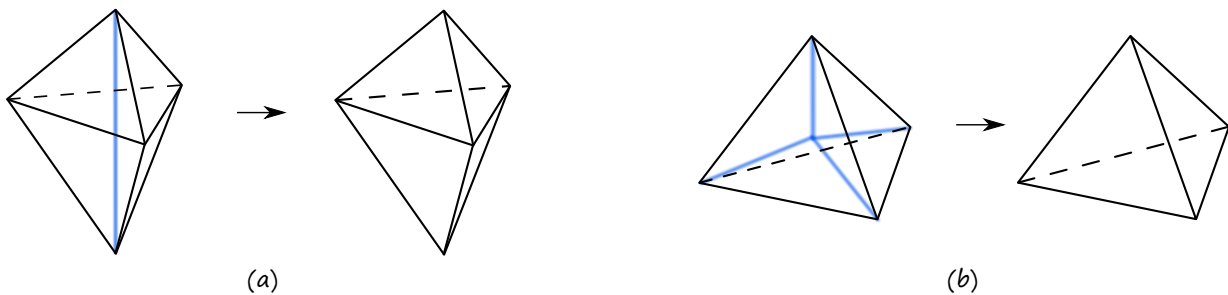
Figure 5.2: Three dimensional Pachner moves: a) 3–2 move, in which three tetrahedra are changed into two tetrahedra by removing a common edge; b) 4–1 move, in which four tetrahedra are combined into one by removing a common vertex.

We will now proceed to show the invariance of the 3-dimensional SU(2) BF theory under 3–2 and 4–1 Pachner moves using the language of spinors. In the case of 4-1 move we find a divergence directly related to the translational symmetry.

3–2 move

As can be seen in the Fig. 5.2 a), the configuration of three tetrahedra in the 3–2 move is glued along one edge. This corresponds to a loop of a single strand in the cable diagram, see Fig.5.3.

By choosing a maximum tree (with a root at the projector 1) in the diagram, we can gauge fix the projectors number 7 and 9. This allows us to apply the loop identity (4.14) to integrate out the strand number 10 by performing the group integral in projector number 8. We can identify now that the resulting cable diagram is exactly that of the two tetrahedra glued together, see Fig. 5.2 b). Hence it is immediate that the SU(2) BF theory is invariant under the 3–2 Pachner move, as the two configurations are gauge equivalent.
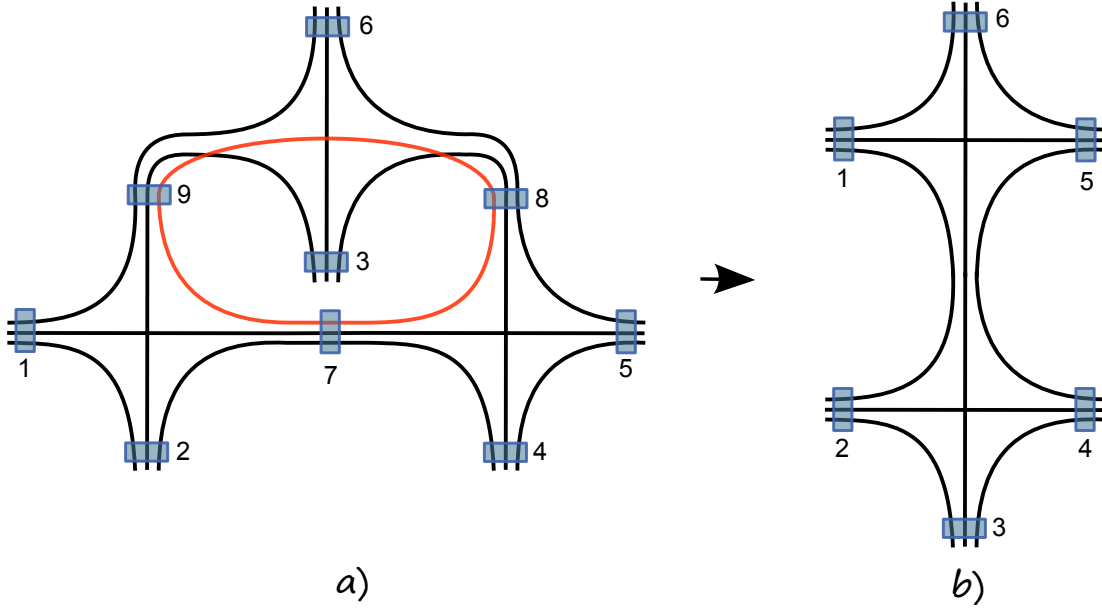
Figure 5.3: a) Cable diagram for the 3-2 move. The internal loop is colored. b) After gauge-fixing projectors 7 and 9 and performing loop identity on projector 8, the diagram reduces to gluing of two tetrahedral graphs.

4–1 move

The configuration of four tetrahedra in the 4–1 move shares in total four edges, which corresponds to four loops in a cable diagram, see Fig. 5.4 a).

We choose a maximum tree with a root at vertex 1, which allows us to gauge fix the projectors number 5, 6 and 9. We can now apply the loop identity (4.14) to the projector 10 to remove the blue loop. Similarly we can apply the loop identities to projectors 7 and 8 to remove the yellow and green loops respectively. This leaves us with the last loop and no projectors left inside the graph, as in Fig. 5.4 b). This final loop corresponds to the following integral

$$\int d\tilde{\mu}(z)e^{\langle z|z\rangle} = \sum_j \int d\tilde{\mu}(z)\frac{\langle z|z\rangle^{2j}}{(2j)!} = \sum_j(2j+1)\int d\mu(z)\frac{\langle z|z\rangle^{2j}}{(2j)!}$$
$$= \sum_j(2j+1)\chi^j(\mathbb{1}) = \delta_{SU(2)}(\mathbb{1}).$$

(5.1)

Hence, we have shown that the BF partition function is invariant under the 4–1 move up to an overall divergent factor. The divergence we obtain in SU(2) BF theory is exactly a SU(2) delta
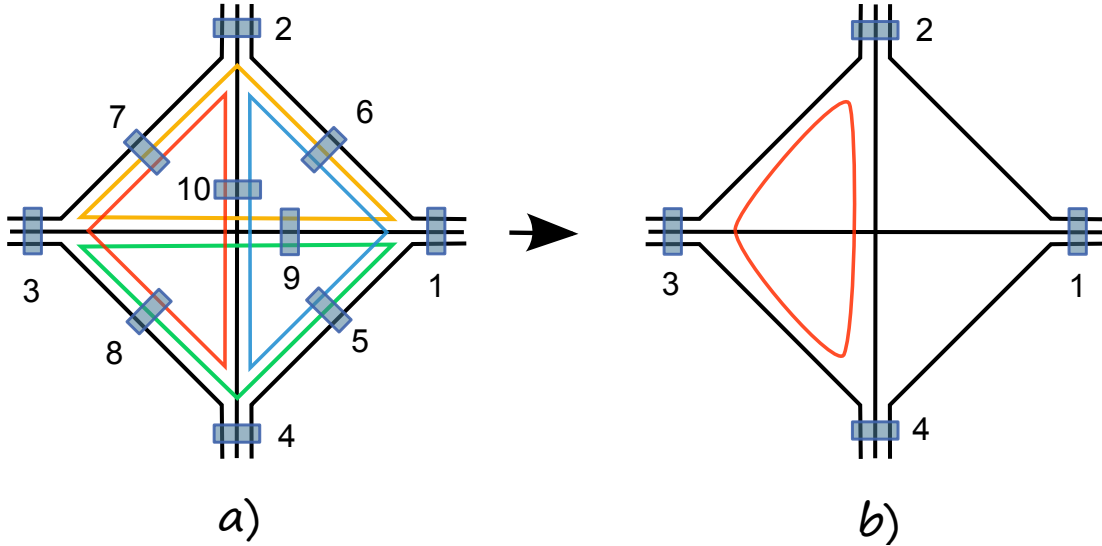
Figure 5.4: a) Cable diagram for the 4–1 move. The 4 different loops are colored. b) After applying three loop identities we are left with a tetrahedral cable graph with an insertion of one loop.

function $\delta_{SU(2)}(\mathbb{1}) = \sum_j (2j+1)^2$. In [93] it was shown that this is the same as the volume of the $\mathfrak{su}(2)$ Lie algebra. If we put on a cut-off Λ on spins, then the divergence scales as $\sum_j (2j+1)^2 \sim \Lambda^3$. Since in 3d spin is proportional to length, we get a divergence that corresponds to the translation symmetry of placing the extra vertex inside the tetrahedron. A correct Fadeev-Popov procedure [93] divides the amplitude by exactly this divergence, so the Ponzano-Regge model is invariant after gauge fixing under both the 3–2 and 4–1 Pachner moves. This gauge fixing procedure was subsequently refined in [77, 78, 79, 80] to lead to a complete definition of 3 dimensional manifold invariant.

5.2 Pachner moves in 4D quantum gravity

In this section we compute all the Pachner moves in the 4-d holomorphic Spin Foam model based on the techniques we have developed in the previous sections. All these moves are based on the configurations of 6 vertices ($ABCDEF$). In the following we adopt the following notation: a simplex A indicates the 4-simplex opposite to the vertex A, i.e. it is composed by $[BCDEF]$. AE indicates the tetrahedron $A \cap E$ composed of the vertices $[BCDF]$, with vertex A and E removed from the triangulation. Triangle ABD indicates the one composed by $[CEF]$. Also in order to

keep track of which vertex is "active", i-e dual to a 4-simplex and which vertex is "inactive", i-e not dual to a 4-simplex, we introduce a distinction in our notation: an upper case letter $A, B \cdots$ denotes an active vertex, while a lower case letter $c, d \cdots$ denotes an inactive vertex.

5.2.1 3–3 move

According to these conventions the move 3–3 corresponds to

$$ABCdef \rightarrow abcDEF.$$

The 3–3 move is shown as Fig.5.5. In the first figure the 4-simplices A, B, C are sharing the blue triangle. After the move the configuration is changed into three 4-simplices D, E, F which share the green triangle.
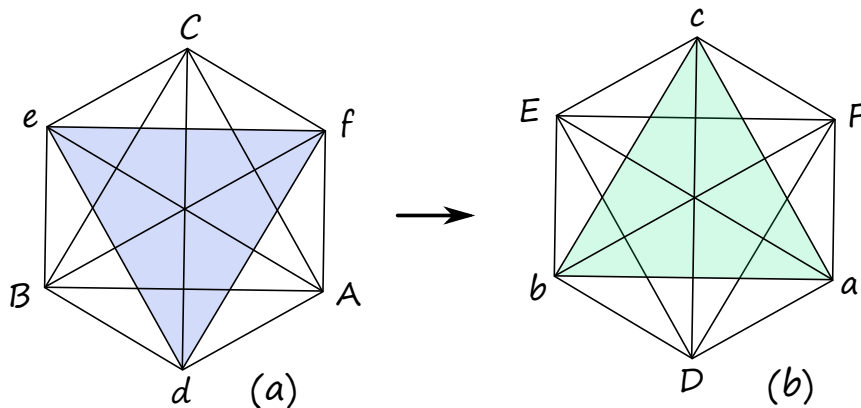
Figure 5.5: Triangulations for the 3–3 move.

The corresponding cable diagram is shown in Fig.5.6. The various colours of strands in the graph are used to indicate the different positions of triangles. The blue loop to be integrated out corresponds to the triangle ABC. The purple strands in (a) for example are dual to the triangles $Adf \subset A$, $Bde \subset B$, $Cef \subset C$ and they run from the tetrahedra $Af \rightarrow Ad$, $Bd \rightarrow Be$, $Ce \rightarrow Cf$. After performing the 3–3 Pachner move, the same triangles (still indicated by the purple strands) are no longer shared by two tetrahedra within a given 4-simplex. They become commonly shared by tetrahedra belonging to the three different 4-simplices: $aDF \subset (D \bigcap F)$, $bDE \subset (D \bigcap E)$, $cEF \subset (E \bigcap F)$. The same happens to the black strands, whereas the opposite happens for the red and light blue strands. In summary, on one hand, due to the 3–3 move from (a) to (b), the red and light blue strands, shared between different simplices in (a) become unshared strands which belong to one simplex in (b). On the other hand, the unshared

strands (the black and purple strands) in *a* become the commonly shared ones in (*b*). The dark blue loop and the green loop correspond to faces which are dual to the internal triangles *ABC* and *DEF* respectively.
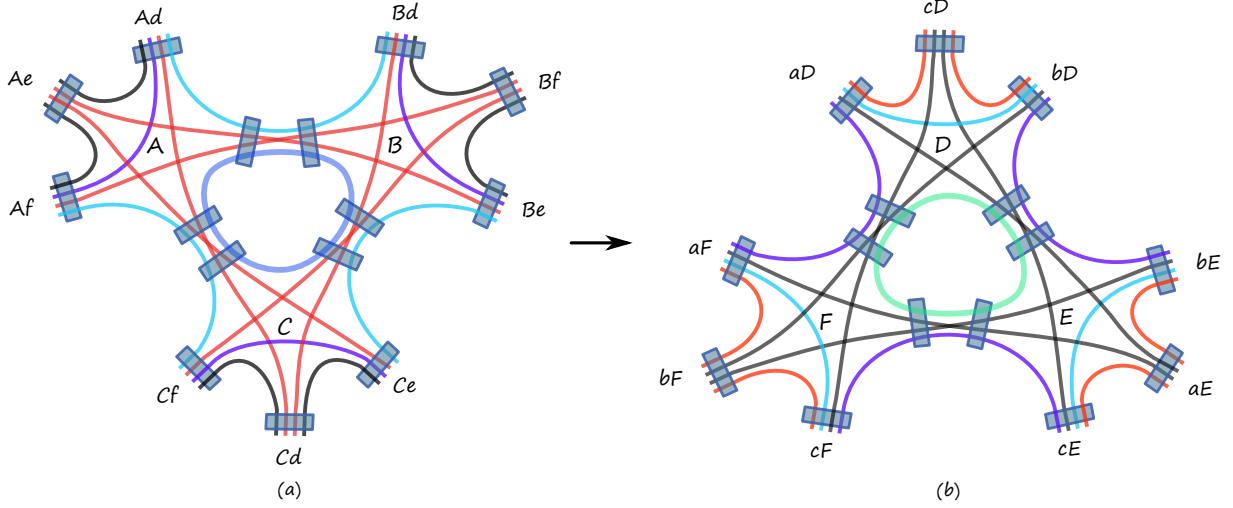
Figure 5.6: Cable diagram for the 3–3 move $ABCdef \rightarrow abcDEF$.

To compare the partition function/amplitudes between the configurations (a) and (b), we need to integrate out the shared loop on both sides. We can gauge fix two out of three pairs of the constrained propagators around the loop by a choice of a maximal tree in a way that leaves the amplitude invariant. We then need to apply only once the constrained loop identity which we obtained in the previous section to complete the 3–3 Pachner move. In order to do so, it is important to introduce some notation for the spinors. Let us describe the parametrization of $(a) = (ABCdef)$. For each 4-simplex $\alpha \in \{A, B, C\}$ we need to introduce a collection of spinors associated with each strand within that 4-simplex. Each strand carries a label which corresponds to a pair of tetrahedra $\alpha\beta$ sharing a face. Within A we have two types of tetrahedra: three external ones Ad, Ae, Af and two internal ones AB, AC. The strands run either between two internal tetrahedra or from one internal to one external tetrahedron. Accordingly, we label the external strands by boundary spinors $z_\gamma^{\alpha\beta}$ where $\alpha \in \{A, B, C\}$, $\beta \in \{d, e, f\}$, $\gamma \in \{A, B, C, d, e, f\}$ for (*a*) in Fig.5.6 , and $\alpha \in \{D, E, F\}$, $\beta \in \{a, b, c\}$, , $\gamma \in \{a, b, c, D, E, F\}$ for (*b*). $\alpha\beta$ are the indices labeling boundary tetrahedra, and $z_\gamma^{\alpha\beta}$ indicate boundary spinors. The boundary propagators are then labeled as $P_\rho(z_\gamma^{\alpha\beta}; w_\gamma^{\alpha\beta})$.

Let us label the internal pairs of propagators by $P_\rho \circ P_\rho(v_\gamma^{\alpha\alpha'}, w_\gamma^{\alpha'\alpha})$, where $\alpha, \alpha' \in \{A, B, C\}$ for (*a*) and $\alpha, \alpha' \in \{D, E, F\}$ for (*b*). We need to contract these spinors with the spinors $w_\gamma^{\alpha\beta}$ of the external propagators. An example of this is shown in Fig. 5.7 with all the labels and orientations
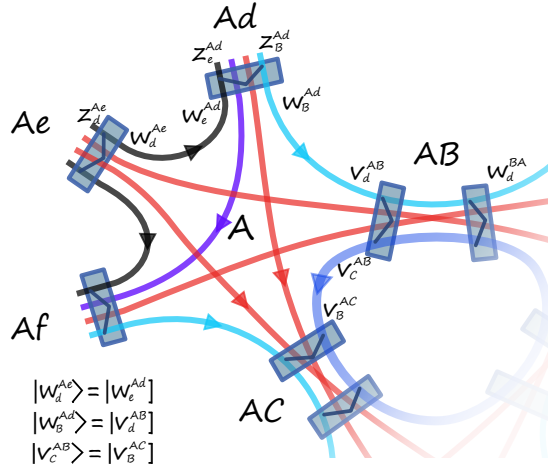
Figure 5.7: Zoomed in part of the cable diagram for the 3–3 move with some of the labels and contractions of spinors explicitly written down.

written explicitly of a part of (a). The contractions are done according to the orientations of strands, and for example we have $|w_B^{Ad}\rangle = |v_d^{AB}]$. In summary, the amplitude is constructed from $z_\gamma^{\alpha\beta}$ and $w_\gamma^{\alpha\beta}$ for the external propagators and on $w_\gamma^{\alpha\alpha'}$, $v_{\gamma'}^{\alpha\alpha'}$ for the internal ones. The amplitude is obtained then after integration over the internal spinors after imposing the contractions, thus becomes a function of $z_\gamma^{\alpha\beta}$ only.

We thus find that the amplitude for three 4-simplices combined as in Fig.5.6 can be written as

$$\mathcal{A}_3(z_\gamma^{\alpha\beta}) = \int \prod_{all} d\mu_\rho(v) d\mu_\rho(w) \prod_{\alpha\beta} P_\rho(z_\gamma^{\alpha\beta}; w_\gamma^{\alpha\beta}) \cdot \quad \text{} . \tag{5.2}$$

The spinors of the three internal propagators which share a loop are labeled by v and w and each of them is contracted with different boundary constrained propagators, with the gluing depending on the orientation of the graph.

The crucial difference between amplitude (a) and (b) is that the non-trivial coefficient $N(J, J', A, B, \rho)$ of Eq.(4.32) encodes the spin information of different strands. In (a), the coefficient N encodes the spin information of the blue and red strands in one configuration, while in (b) it encodes the spin of the black and purple strands. Unless the corresponding boundary spins are chosen to be the same, the 3–3 move cannot be invariant.

It is thus very easy to see where the topological invariance of BF theory is broken. Let us

come back to BF theory and look at the 3–3 move. The BF loop identity (4.15) does not have any factor depending on spins and hence gives a trivial equality, as the diagrams in Fig. 5.8 are combinatorially equivalent. Thus for BF theory, the partition function/amplitudes are invariant under 3–3 move.
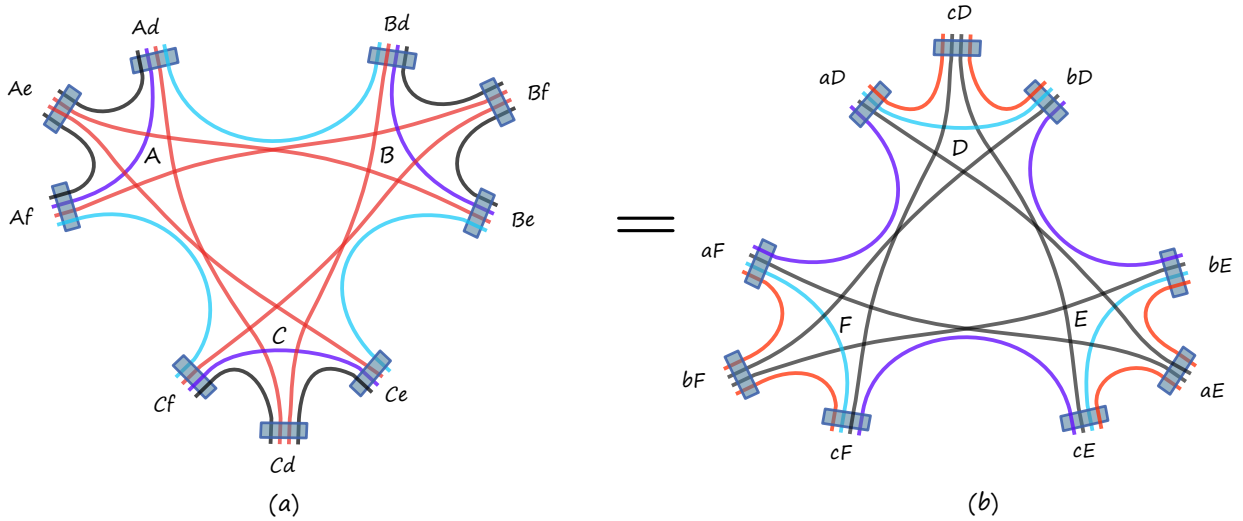
Figure 5.8: For 4-d BF theory, after integrating out the middle loops in the 3–3 move, the rest of the strands are combinatorially equivalent.

5.2.2 4–2 move

The 4–2 move $ABCDef \mapsto abcdEF$ is shown in Fig.5.9. In (*a*), four 4-simplices A, B, C, D are sharing 6 tetrahedra. After removing four triangles (or four loops in the dual cable graph) and changing the combinatorial structure, the four 4-simplices are rearranged in two 4-simplices E, F glued by one tetrahedron. The corresponding cable diagram of the four 4-simplices is shown in Fig.5.10.

We can perform gauge fixing of this graph by choosing vertex C as the root of the maximal tree in such a way that we can gauge fix 3 couples of propagators BC, AC, CD. This allows us to apply the constrained loop identities Eq.(4.32) to three of the four loops. More specifically, we can apply the constrained loop identity to the propagators (AB, BC, CA) to drop the blue loop, then apply it to the propagators (AC, CD, DA) to integrate the green loop and propagators (BC, CD, DB) to remove the big yellow loop. This results in integrating out all couples of constrained propagators, and hence we are left with one last (red) loop, which is mixed with the external strands, as can be seen in Fig.5.11.
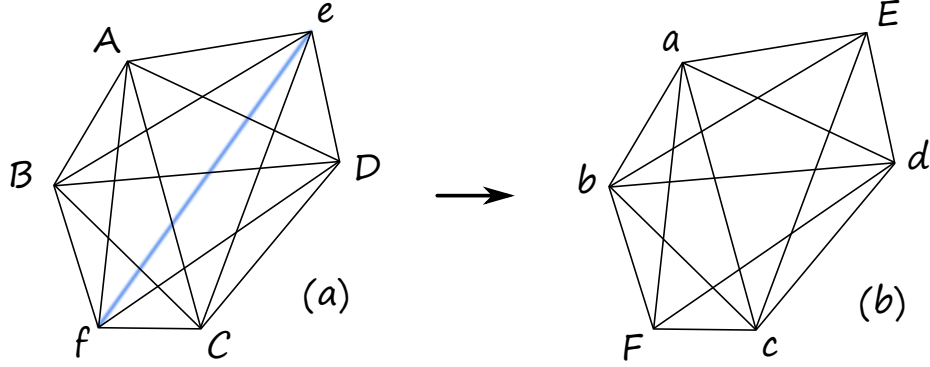
Figure 5.9: Triangulations for the 4–2 move.

Note, that we have applied the three loop identities, but the last loop is left without any extra group averaging. Similar to the case of the loop identity, we have to add in a face weight for this last loop. We will do so again by inserting a factor of τ' on one of the strands of the left-over loop (say the red strand for edge AD), so that we can use homogeneity map $\tau'^{2j} \to (2j+1)^\eta$.

Similar as in the previous section, we will denote the spinors on the boundary as z, and spinors in the bulk as w and v with indices labeling the propagator and the strand they belong to. Each spinor carries three indices: $z_\gamma^{\alpha\beta}$ with indices α labeling the 4-simplex, $\alpha\beta$ labelling the tetrahedron they belong to, γ labelling which strands they represent. With assuming a specific orientation of the graph as $C \to A, C \to B, C \to D, A \to B, D \to A, D \to B$ [1], the amplitude in terms of the exponentiated loop identity Eq.(4.37) is given then by

$$\mathcal{A}_{4-2}^\tau(z_\gamma^{\alpha\beta}) = \int \left\{ \prod_{\text{all}} d\mu_\rho(v) d\mu_\rho(w) \right\} \prod_{\alpha\beta} P_\rho(z_\gamma^{\alpha\beta}; w_\gamma^{\alpha\beta}) \cdot \exp\left[\sum_{\sigma i} \tilde{\tau}_{\sigma C} [\tilde{v}_i^{C\sigma} | \tilde{w}_i^{\sigma C}\rangle \right]$$

$$\times \exp\left[\sum_{\mu\nu} (\tau_N^{\mu\nu} \sum_j \alpha_j^{\mu\nu} [v_j^{\mu\nu}|w_j^{\nu\mu}\rangle + \tau_M^{\mu\nu} \sum_{j<k} \alpha_j^{\mu\nu} [w_j^{\nu\mu}|w_k^{\nu\mu}\rangle [v_j^{\mu\nu}|v_k^{\mu\nu}\rangle) \right]. \tag{5.3}$$

For the external propagators $\alpha \in \{A, B, C, D\}$ and $\beta \in \{e, f\}$ label the tetrahedron, while $\gamma \in \{A, B, C, D, e, f\}$ labels the strands in each tetrahedron. For internal gauge fixed propagators, $\sigma \in \{A, B, D\}$, $i \in \{e, f\}$, and for the non-gauge fixed propagators, $\mu\nu \in \{AB, AD, BD\}$, $j, k \in \{e, f, r\}$, where r indicates the red strand of the left-over loop. We define $\alpha_j^{\mu\nu}$ as

$$\alpha_j^{\mu\nu} = 1 + \delta_{AD}^{\mu\nu} \delta_j^r (\tau' - 1) \tag{5.4}$$

for keeping track of the homogeneity factor for the face weight of the last loop.

---

[1] When one reverses the orientation of one propagator, the corresponding $[v|w\rangle \to [w|v\rangle = -[v|w\rangle$
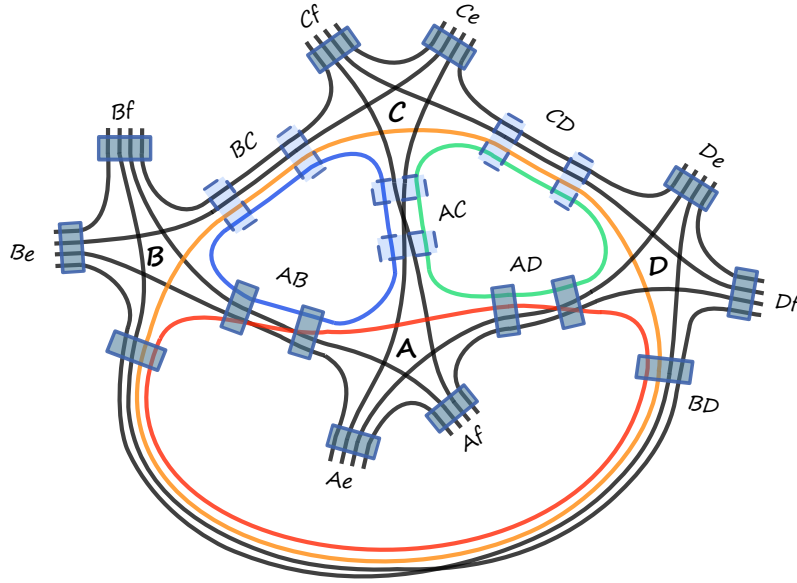
Figure 5.10: Cable diagram for the 4–2 move with gauge fixing along BC, AC, CD.

The equation (5.3) gives a compact and explicit expression for the amplitude associated with the 4–2. It is obtained by using the exponentiated loop identity Eq.(4.37), which then can be transformed using the homogeneity map to obtain the full expression after performing all of the contractions of spinors and all the Gaussian integrals. The homogeneity maps we need to apply to this expression to get the full result were defined in Eq. (4.30) for the $\tilde{\tau}$, in Eq.(4.34) for τ_N and τ_M and the homogeneity map for τ' is $\tau'^{2j} \to (2j+1)^\eta$. The calculation can be straightforwardly done, but the resulting expression itself is a complicated, one with lots of mixed strands that is difficult to manipulate. The integrals also contain potential divergences that have to be taken care of. We will delay the discussion of the resulting expression and the significance of the mixing terms until the next section, as we first encounter a similar behavior for the 5–1 Pachner move as well.

5.2.3   5–1 move

We now calculate the 5–1 Pachner move. The 5–1 move corresponds to a change of a configuration of five 4-simplices sharing an internal vertex into a single 4-simplex by removing the common vertex, see Fig. 5.12.

The cable diagram for this move can be seen in Fig. 5.13. We have a total of 10 loops and 10 pairs of constrained propagators inside the bulk of the graph. Even though there is an increase
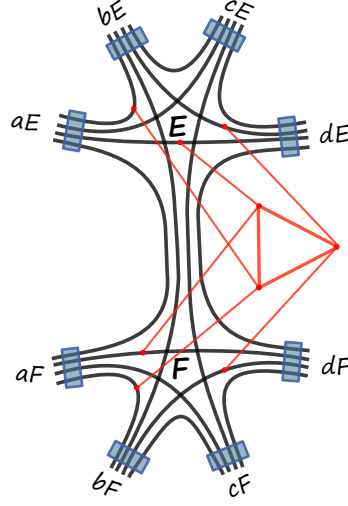
Figure 5.11: Performing the calculation we get a configuration of two 4-simplices with a nonlocal gluing.

in complexity, compared to the 4–2 move, the calculation will go over in nearly the same way. We start by choosing a maximal tree in the diagram, which allows us to gauge fix 4 of the pairs of propagators. A careful choice of this tree corresponds to a root at one of the 4-simplices and allows us to apply loop identities to 6 of the loops, leaving us with 4, as can be seen in Fig. 5.14.

We can write the amplitude for the 5–1 move using the exponentiated loop identity Eq.(4.37) as in the case of the 4–2 move. We will again have to add the face weights for the last four loops by adding factors of τ'. The expression for the full Pachner move then would be obtained by applying the homogeneity map to the resulting power series. We keep to the notation of inside spinors being w and v labeled by the strands and propagators they belonged to. With assuming the orientation of the graph as $E \to A, E \to B, E \to C, E \to D$, the amplitude in terms of boundary spinors z is formally given then as

$$\mathcal{A}_{5-1}^{\tau}(z_{\gamma}^{\alpha f}) = \int \left\{ \prod_{\text{all}} d\mu_{\rho}(v) d\mu_{\rho}(w) \right\} \prod_{\alpha} P_{\rho}(z_{\gamma}^{\alpha f}; w_{\gamma}^{\alpha f}) \cdot \exp\left[\sum_{\beta} \tilde{\tau}_{E\sigma}[\tilde{v}^{E\sigma}|\tilde{w}^{\sigma E}\rangle \right]$$

$$\times \exp\left[\sum_{\mu\nu} (\tau_N^{\mu\nu} \sum_i \beta_i^{\mu\nu}[v_i^{\mu\nu}|w_i^{\nu\mu}\rangle + \tau_M^{\mu\nu} \sum_{i<j} \beta_i^{\mu\nu}[w_i^{\nu\mu}|w_j^{\nu\mu}\rangle[v_i^{\mu\nu}|v_j^{\mu\nu}\rangle) \right],$$

$$(5.5)$$

where the the indices run over the following ranges: $\sigma \in \{A, B, C, D\}$, $\mu\nu \in \{AB, AC, AD, BD, BC, CD\}$, $i, j \in \{f, b, r, y, g\}$, where b, r, y, g indicates the blue (ABD), red (BCD), yellow (ACD), green (ABC) strands of the left-over loops respectively, and f indicates the black strands which compose the simplex F after the move. The external propagators $P_{\rho}(z_{\gamma}^{\alpha f}; w_{\gamma}^{\alpha f})$ are defined

66
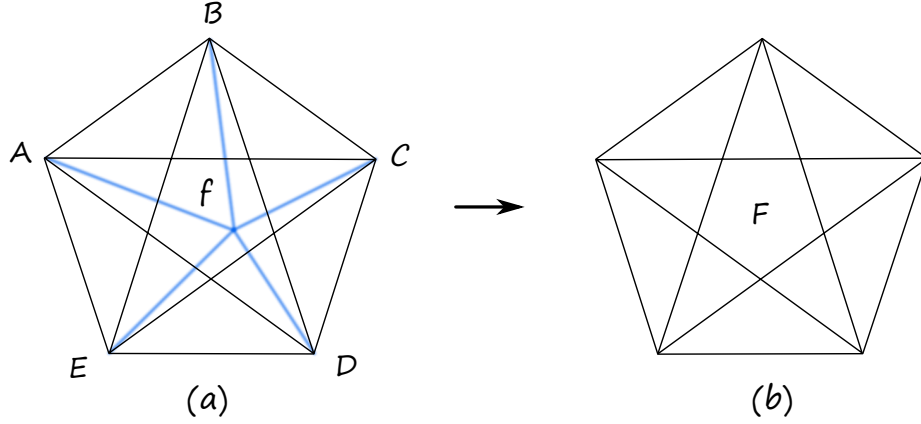
Figure 5.12: Triangulations for the 5–1 Pachner move.

the same way as in previous sections, namely $\alpha \in \{A, B, C, D, E\}$ labels the simplices in which the boundary tetrahedra belong to, and γ labels the strands in each tetrahedra. The coefficients $\beta_i^{\mu\nu}$ that keep track of homogeneity of the face weights are defined this time as

$$\beta_i^{\mu\nu} = 1 + \delta_{AD}^{\mu\nu}\delta_i^y \left(\tau_y' - 1\right) + \delta_{AC}^{\mu\nu}\delta_i^g \left(\tau_g' - 1\right) + \delta_{AB}^{\mu\nu}\delta_i^b \left(\tau_b' - 1\right) + \delta_{BC}^{\mu\nu}\delta_i^r \left(\tau_r' - 1\right). \tag{5.6}$$

The formal expression of 5–1 is of similar structure as the 4–2 move, with the difference being the range of the indices due to bigger number of loops and propagators. The expression (5.5) is relatively compact for such a complicated calculation and it contains all the information necessary to evaluate the amplitude after the Gaussian integrations are performed. In order to do so we just need to specify is the homogeneity map

$$H_{5-1}[\mathcal{A}_{5-1}^\tau] = \mathcal{A}_{5-1}. \tag{5.7}$$

The 5–1 homogeneity map H_{5-1} is given by the composition of :

$$\tau_N^{\mu\nu J}\tau_M^{\mu\nu J'} \rightarrow \sum_K \frac{(-1)^{J'-K}(J+J'-K)!J'!}{K!(J'-K)!}(J+2J'-2K+1)^\eta \tau_{\mu\nu}^K \left(\frac{\tilde{\tau}_{E\mu}\tilde{\tau}_{E\nu}\tau_{\mu\nu}}{(1+\rho^2)^3}\right)^{J+2J'-2K}$$

$$\tau_{\mu\nu}^J \rightarrow \frac{F_\rho(J)^2}{(1+\rho^2)^{2J}(J+1)!}, \qquad \tilde{\tau}_{E\sigma}^J \rightarrow \frac{F_\rho(J/2)^2}{(1+\rho^2)^J}, \qquad \tau_i'^{2j} \rightarrow (2j+1)^\eta, \tag{5.8}$$

with $F_\rho(J)$ previously defined as the hypergeometric function $F_\rho(J) = {}_2F_1(-J-1, -J; 2; \rho^4)$. The same map can be used to find the full expression for the 4–2 Pachner move as well. The Gaussian integrals for the last four loops can be performed explicitly. Using the results from
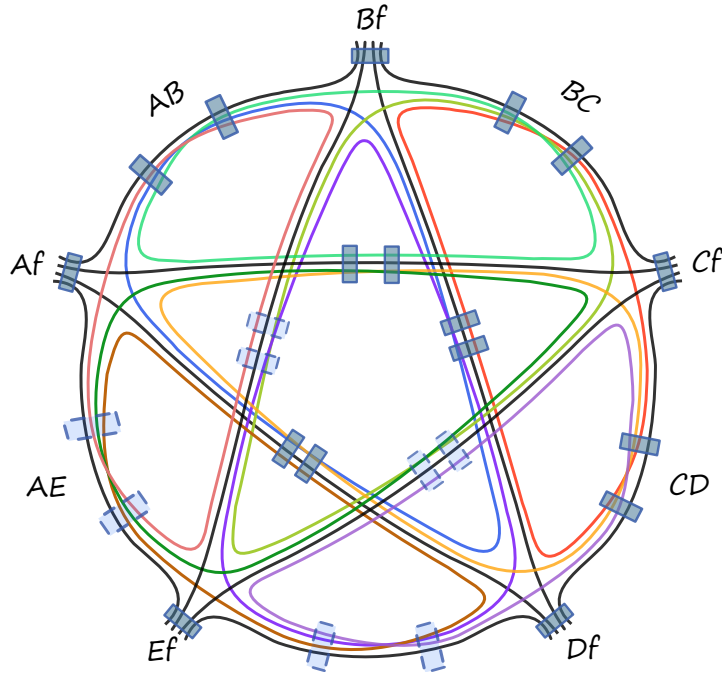
Figure 5.13: Cable diagram for the 5–1 move. The loops inside are colored.

[121], we can write this as an inverse of a determinant of a large matrix. We leave these integrals undone however to make the trucation procedure in the next section more clear.

Let us now try to understand our result. In BF theory the 5–1 Pachner move would lead to 4 decoupled loops, each giving a factor of a SU(2) delta function evaluated at identity. This would correspond to setting all the τ_Ms to 0 and all the other τs to 1 in our expression. For the constrained propagator, as in the previous case of the 4-2 move, the loops inside are coupled to each other and to the strands of the boundary spinors. This means that as expected the spin foam model we consider is not invariant under both the 4–2 and 5–1 Pachner moves. It is natural to conjecture here, that this would be the case for the other spin foam models as well.

The new feature of the model is the mixing between internal loops and external edges that creates a coupling between all the different strands not present in the original form of the vertex amplitude. Let us try to study this mixing in some more detail. By splitting the 6-valent vertices in the loops, as in Fig. 5.15, it is obvious that we can try to interpret these coupled loops as an insertion of an operator[112].

The connections between loops and the boundary spinors correspond to gauge invariant operators inserted inside the 4-simplex amplitude. It is well known that such operators can be
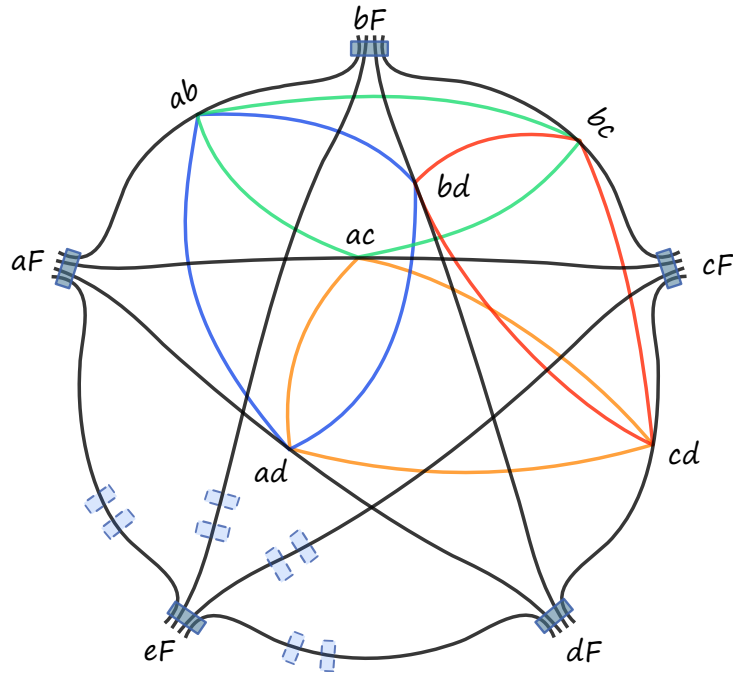
Figure 5.14: Gauge-fixing 4 strands allows to apply loop identities 6 times, leaving the 4 colored loops.

expressed as a sum of grasping operators.

In the holomorphic context these operators are due to the insertions of the SU(N) operators [112], from which all geometrical operators are made. The insertion of Wilson loops and the action of SU(N) operators are two sides of the same coin [69] – they are constructed from the same type of gauge-invariant observables, which in our language are the products $[z|w\rangle$ and $\langle z|w\rangle$. The operators we get for the 4–2 and 5–1 moves can be thus thought as an exponentiated combination of SU(N) grasping operators and Wilson loops. Iteration of 5-1 moves leads to a new kind of loop expansion, reminiscent of higher order diagrams in perturbative quantum field theory. It might be interesting to flesh out more this correspondence and understand if this series converges to some interesting object. We leave this question for future work since this requires to first disentangle the divergent part from the part that purely acts as grasping and leads to mixing of strands. We will now try a different approach to understanding these operators.

Now let us perform the truncation that we have introduced in the last chapter. Truncating the loop identities in the 5–1 move allows us to perform the Gaussian integrals easily. After truncation, the amplitude in Eq. (5.5) becomes
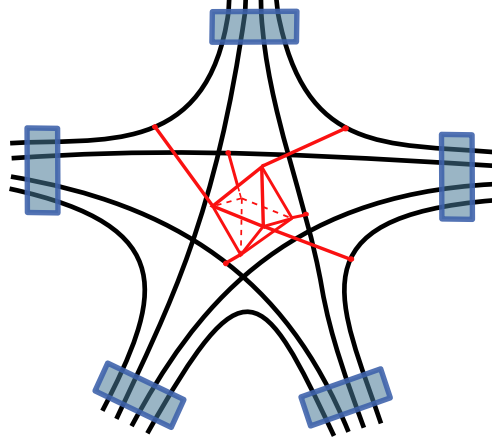
Figure 5.15: Performing the calculation we get a 4-simplex with an insertion of a nonlocal operator.

$$
\begin{aligned}
\mathcal{A}^{5-1}_{\tau \text{ truncated}}(z^{\alpha f}_\gamma) &= \int \prod_{\text{all}} d\mu_\rho(v,w) \prod_\alpha P_\rho(z^{\alpha f}_\gamma; w^{\alpha f}_\gamma) \cdot e^{\sum_\sigma \tilde{\tau}_{E\sigma}[\tilde{v}^{E\sigma}|\tilde{w}^{E\sigma}\rangle + \sum_{\mu\kappa i} \tau_N^{\mu\nu} \beta_i^{\mu\nu}[v_i^{\mu\nu}|w_i^{\gamma\mu}\rangle} \\
&= \int \prod_{\text{left over}} d\mu_\rho(v,w) \prod_\alpha P_\rho(z^{\alpha f}_\gamma; w^{\alpha f}_\gamma) \cdot e^{\sum_\sigma \tilde{\tau}_{E\sigma}[\tilde{v}^{E\sigma}|\tilde{w}^{E\sigma}\rangle + \sum_{\mu\nu} \tau_N^{\mu\nu}[v_f^{\mu\nu}|w_f^{\gamma\mu}\rangle} \mathcal{A}^{5-1}_{\tau \text{ truncated}}(0),
\end{aligned}
\tag{5.9}
$$

where recall that indices run over $\sigma \in \{A, B, C, D\}$, $\mu\nu \in \{AB, AC, AD, BD, BC, CD\}$, $i \in \{f, b, r, y, g\}$, $\alpha, \gamma \in \{A, B, C, D, E\}$. We have also defined the amplitude with boundary spins set to zero, $\mathcal{A}^{5-1}_{\tau \text{ truncated}}(0)$ to be given by

$$
\mathcal{A}^{5-1}_{\tau \text{ truncated}}(0) = \frac{1}{\left(1 + \frac{\tau_N^{AC} \tau_N^{AD} \tau_N^{CD} \tau'_y}{(1+\rho^2)^3}\right)^2 \left(1 + \frac{\tau_N^{AB} \tau_N^{AD} \tau_N^{BD} \tau'_b}{(1+\rho^2)^3}\right)^2 \left(1 + \frac{\tau_N^{AB} \tau_N^{AC} \tau_N^{BC} \tau'_g}{(1+\rho^2)^3}\right)^2 \left(1 + \frac{\tau_N^{BC} \tau_N^{BD} \tau_N^{CD} \tau'_r}{(1+\rho^2)^3}\right)^2}.
$$

where, similarly as in the 4–2 move, the six loops that we have integrated out were labeled by the set $\{AB, AC, AD, BC, BD, CD\}$ and the left over four loops are labeled by $\{y, g, b, r\}$.

It is imperative now to notice that this does not trivially factorize, as we still have to apply the homogeneity map to obtain the final expression. The map defined in Eq. (5.8) tells us that the τ_Ns are actually functions of the $\tilde{\tau}$s from the partially gauge-fixed propagators. The homogeneity map for the truncated 5–1 Pachner move is $H_{5-1}[\mathcal{A}^{5-1}_{\tau \text{ truncated}}] = \mathcal{A}^{5-1}_{\text{truncated}}$ and is given by

$$
H_{5-1} : \tau_N^{\mu\nu J} \to F_\rho(J)^2 (J+1)^{\eta-1} \left(\frac{\tilde{\tau}_{E\mu} \tilde{\tau}_{E\nu}}{(1+\rho^2)^5}\right)^J, \qquad \tilde{\tau}_{E\sigma}^J \to \frac{F_\rho(J/2)^2}{(1+\rho^2)^J}, \qquad \tau_i'^{2j} \to (2j+1)^\eta. \tag{5.10}
$$

Comparing this to the 4–2 move expression, we see that clearly we have 4 loops, that are not connected by any strands, but which are nonetheless coupled by sharing the τs, and hence functions of spin and ρ. We can now expand this in a power series for the fours spins j_y, j_g, j_b, j_r and reintroduce the factors of the hypergeometric functions and face weights by using the homogeneity map from Eq. (5.8). Letting $a, b, c \in \{y, g, b, r\}$ we can write the full expression for the degree of divergence as

$$D_{5-1} = \sum_{j_y, j_p, j_b, j_r} \frac{\prod_a (2j_a+1)^{\eta+1}}{(1+\rho^2)^{24 \sum_a 2j_a}} \left(\prod_{a<b} F_\rho(2j_a+2j_b)^2 (2j_a+2j_b+1)^{\eta-1} \right) \left(\prod_{a<b<c} F_\rho(2j_a+2j_b+2j_c)^2 \right), \quad (5.11)$$

where, recall, we have previously defined $F_\rho(J) = {}_2F_1(-J-1, -J; 2; \rho^4)$ for simplification. We will provide a through analysis of the degree of divergence in Chapter 7

In summary, this is the first time that Pachner moves have been calculated explicitly in a simplicity-constrained Spin Foam model of 4–dimensional Quantum Gravity. We found that 4d gravity Spin Foam models are not invariant under 3–3 move unless very specific and symmetric boundary configurations are chosen. This is expected of a model for 4 dimensional gravity. A naive expectation, at least at the level of the classical action, is that the model should be invariant under the 4–2 and 5–1 Pachner moves. We found however this to be not the case for the exact evaluation. For both the 4–2 and 5–1 moves, there is an insertion of a non-local combination of SU(N) grasping operators in the final coarse grained simplices, with a mixing of strands leading to non-geometrical and non-local configuration.

From the viewpoint of real-space renormalization group however, such non-local operators are expected to appear in each step of coarse graining, and have to be truncated to local ones in a controlled manner. Our proposed truncation scheme removes the mixing of strands in the coarse-grained simplices, thus allowing them to remain geometrical, and hence making the 5–1 Pachner move structure preserving. After the truncation, the 4–2 and 5–1 Pachner moves are invariant up to a weight depending on the boundary spins. We should not expect an exact invariance, until a properly gauge-fixed model at a fixed point of renormalization flow corresponding to the continuum limit is found. However, the vertex translation symmetry, which is the residual diffeomorphisms, is not presented in the model yet.

Chapter 6

Bulk amplitude

In this section, we will study the *bulk amplitude* - the evaluation of the partition function on a fully contracted 2-complex, or the evaluation on a connected 2-complex with zero boundary spins. This quantity is of interest because it isolates the degrees of freedom in the model which could lead to divergence. In spin foam amplitudes, the divergence comes from unbounded summations of spins, hence any finite boundary data is irrelevant for evaluating the degrees of divergence.

First we will perform some numerical analysis of how different diagrammatic structures influence the bulk amplitude $\mathcal{A}_{bulk}$ to obtain some intuition. The basic approach is isolating the factors from loops and edges, then varying those factors on each spin channel of $\mathcal{A}_{bulk}$. However, we will find that the degree to which the coupling of loops influences the value of the amplitude depends on the diagrammatic structure, hence this leads us to a more efficient and general method to study $\mathcal{A}_{bulk}$.

In the previous section 4.1 we have defined a certain set Ω_Γ of 2-complexes, which contain optimal spanning trees. Here we will first derive a formula of the truncated bulk amplitude for such type of graphs in this section. The formula will allow us to simply write down the truncated bulk amplitude by reading out the combinatorial properties of the graph. We then generalize the result to the arbitrarily connected 2-complex. The results we obtain in this section will pave our way towards evaluating the divergence for arbitrary amplitude.

6.1 Preliminary analysis

Effect of coupling loops

Evaluating amplitudes for large triangulations essentially comes to integrating loops in the cable diagrams. Loops correspond to internal common faces in the triangulation that are shared by a few tetrahedra in the simplicial decomposition. At the same time, once a tetrahedron has more than one common faces with others, it is graphically represented as loops coupled with each other through a common edge in the cable diagram.

With a fixed number of loops in a cable diagram, in general the coupling structures would increase the amplitude compared with the isolated structures, and this effect can be simply characterized by the following inequality of hypergeometrical functions:

$$F_\rho(J_1 + J_2) \geq F_\rho(J_1) \cdot F_\rho(J_2) \tag{6.1}$$

in which we recall that

$$F_\rho(J) := {}_2F_1(-J - 1, -J; 2; \rho^4) = \sum_{J'=0}^{J} \binom{J}{J'}\binom{J+1}{J'}\frac{\rho^{4J'}}{(J'+1)}$$

It becomes an equality only when $\rho = 0$, which corresponds to the BF theory .

More precisely, the cases we are comparing here correspond to Fig.6.1 [1]. Supposing two partially gauge fixed loops are not coupled, after applying the homogeneity map, the amplitude contributed to $\mathcal{A}_{bulk}$ by the partial gauge fixed propagators A, B on each loop respectively can be factorized for each spin channel:

$$\tilde{\tau}_A^{2j_{f_1}} \tilde{\tau}_B^{2j_{f_2}} \rightarrow \frac{F_\rho(j_{f_1})^2 F_\rho(j_{f_2})^2}{(1 + \rho^2)^{2j_{f_1} + 2j_{f_2}}} \tag{6.2}$$

For the case in the top graph of Fig. 6.1, we have $j_{f_1} = j_{f_2} = j_f$, which is what happens in the Fig. 5.10 of 4–2 move. However, if the two loops are coupled by a common tetrahedron A, when we apply the homogeneity map to get the amplitude, the coupling effect results in:

$$\tilde{\tau}_A^{2j_{f_1} + 2j_{f_2}} \rightarrow \frac{F_\rho(j_{f_1} + j_{f_2})^2}{(1 + \rho^2)^{2j_{f_1} + 2j_{f_2}}} \tag{6.3}$$

---

[1] An example would be the tetrahedra AC, BC, CD in Fig.5.10 of the 4-2 move.
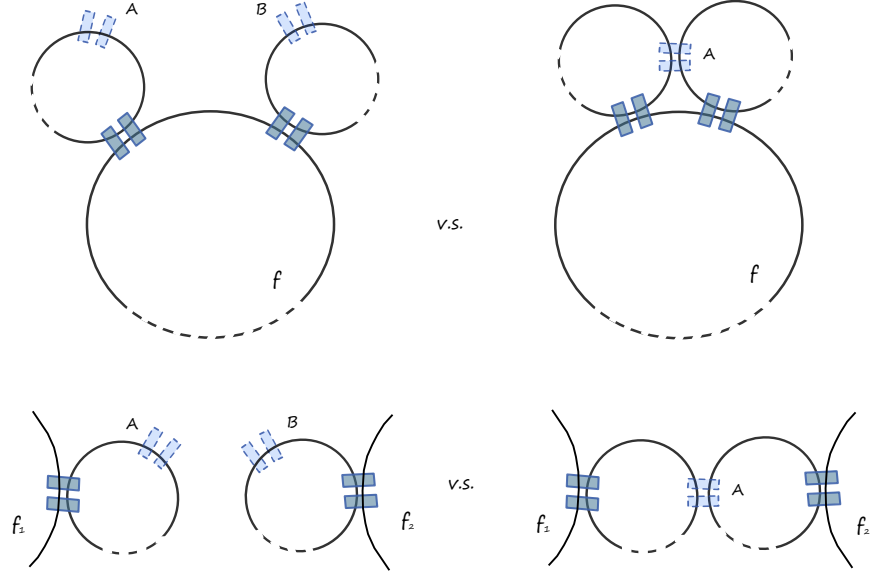
Figure 6.1: Loops coupling effect. (The cables which connect to boundary with zero spins are omitted.)

which leads to a larger contribution to the amplitude compared with the isolated loops, due to Eq.(6.1). If other structures in the cable diagram are the same after setting boundary spins to zero:

$$\tilde{\mathscr{A}}_{coupled} = \sum_{\{j_f\}} ...F_\rho(j_{f_1} + j_{f_2})^2... \geq \tilde{\mathscr{A}}_{separated} = \sum_{\{j_f\}} ...F_\rho(j_{f_1})^2 F_\rho(j_{f_2})^2... \qquad (6.4)$$

where the dots indicate the same expression on both sides. Under the condition that we fix the number of loops and number of tetrahedra per loop, the coupling structures increase the amplitude compared with the isolated structures.

Varying numbers of tetrahedra

As we have learned in section 5.2, in a partially gauge fixed loop, each edge (a pair of gauge-fixed propagators) has the following contribution for each spin J channel in the loop:

$$C_{edge}(J) = \frac{F\rho(J/2)^2}{(1 + \rho^2)^{2J}}, \qquad (6.5)$$

Note that $(1+\rho^2)$ has power of $2J$, in which one J comes from the pair of gauge-fixed propagators, while the other J comes from the spinor integration of contracting with the other propagator in

the loop. Eventually, when we expand the bulk amplitude in terms of spin channels, we have

$$\mathcal{A}_{bulk} = \sum_{\{j_f\}} ...C_{edge}(j_f)... \tag{6.6}$$

If $C_{edge}(j) \leq 1$ for any spin, then purely adding an edge into the cable diagram would decrease the total amplitude. The following plots Fig.[6.2,6.3] show that it is indeed the case:
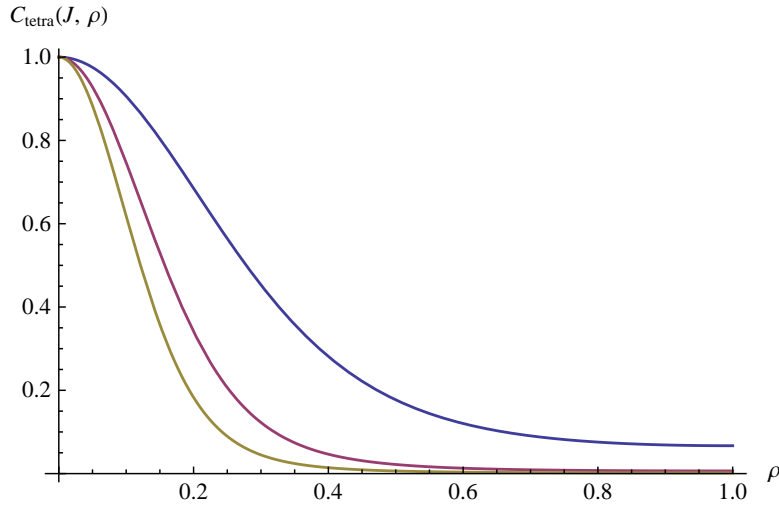
Figure 6.2: Blue, red and yellow line correspond to $J = 5, 15, 25$ respectively, as examples. In the whole range of ρ, $C_{edge} \leq 1$.

Thus with total number of loops fixed in the whole cable diagram, adding tetrahedra to loops (but not causing loop coupling) would decrease $\mathcal{A}(0)$. The bigger ρ is, the stronger the effect would be. In BF theory, i.e. $\rho = 0$, varying the number of tetrahedra around loops does not change the amplitude.

Varing number of loops

First let us have a brief discussion of the simple case – isolated loops. When a loop is completely isolated with other loops, i,e, the strands in the constrained propagators around the loop are all connected to the boundary, then this loop itself contributes nothing to the bulk amplitude $\mathcal{A}_{bulk}$. We can easily see this from the coefficient function $N(0, 0, 0, 0, \rho) = 1$ in the loop identity Eq.(4.32). Adding more isolated loops in the cable diagrams does not increase the bulk amplitude. The diagram of 3–3 Pachner Move belongs to this case.
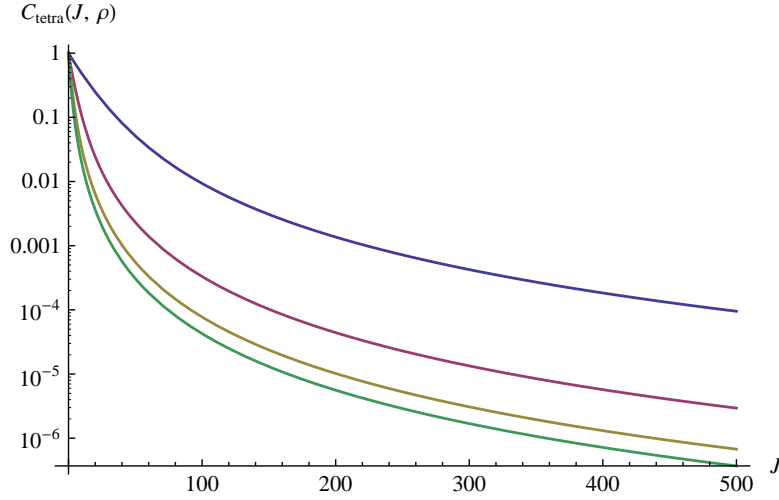
Figure 6.3: The logarithmic plot of $C_{tetra}(J,\rho)$. Blue, red, yellow, green line correspond to $\rho = 1/5, 2/5, 3/5, 4/5$ respectively. $C_{tetra}(J,\rho)$ monotonously decrease with both spin and ρ.

However, when we try to analyze coupled loops, we cannot just look at their number in isolation, because the result will depend on the diagrammatic structure of their coupling. Hence we need a more efficient and general approach to study this question. This leads us to the approach in the next subsection.

6.2   Simple cases

Now we will derive a formula for the truncated bulk amplitude of the 2-complexes in Ω_Γ. The graphs in Ω_Γ are convenient to consider, because they possess optimal spanning trees such that all the corresponding fundamental cycles are faces of the 2-complex (loops formed by strands in the cable diagram notation). The strategy to evaluate the amplitude of such a graph is as follows: first we gauge fix the propagators (4.4) along a chosen optimal tree $T_\Gamma(E_T)$. We denote the corresponding set of fundamental cycles as C_T. These cycles are loops formed by single strands in the cable diagram notation. After gauge fixing, there are two types of propagators: the gauge-fixed propagators on the branches E_T of the tree and the original propagators on the edges of the tree's complement $E \setminus E_T$. The bijection between C_T and $E \setminus E_T$ is justified by the fact that there is a unique original propagator per fundamental cycle, and on the other hand any original propagator belongs to a fundamental cycle. We can apply truncated loop identity Eq.(4.38) on elements of C_T. The truncated loop identity annihilates all the fundamental cycles, as well as

76

$|V| - 1$ number of gauge fixed propagators and $|E| - |V| + 1$ number of original propagators on the loops. At this stage there are $|F| - |C_T|$ loops remaining with non-local functions coupling them through the homogeneity map (4.38). Let us refer to these loops as *residual loops L.*

Integrating out all the spinors in the residual loops and then applying homogeneity maps give us the truncated bulk amplitude. Without loss of generality, we use T_α to track the homogeneity of each original propagator α after applying the loop identity, use l to label the residual loops, and use n_l to denote the number of propagators in each of these residual loops. The structure of the exponentiated bulk amplitude $\mathcal{A}^\tau_{bulk}$ is a product of $|F| - |C_T|$ spinor Gaussian integrations corresponding to the residual loops:

$$
\begin{aligned}
\mathcal{A}^\tau_{bulk} &= \prod_{l=1}^{|F|-|C_T|} \int d\mu_\rho(z_l) \ \exp\left[\frac{\tau'_l \cdot \prod_{\alpha=1}^{n_l} T_\alpha}{(1+\rho^2)^{n_l-1}}\langle z_l|z_l\rangle\right] \\
&= \prod_{l=1}^{|F|-|C_T|} \sum_{j_l\in\mathbb{Z}/2} (2j_l + 1)\left(\frac{\tau'_l \cdot \prod_{\alpha=1}^{n_l} T_\alpha}{(1+\rho^2)^{n_l}}\right)^{2j_l},
\end{aligned}
\tag{6.7}
$$

in which τ'_l keeps track of the face weight. The equality from the first to second line comes from series expansion of the integration result. Applying the homogeneity maps (4.38), (4.39) and $\tau'^J_l \rightarrow (J_l + 1)^\eta$ to $\mathcal{A}^\tau_{bulk}$ leads to the desired truncated bulk amplitude $\mathcal{A}_{bulk}$.

In each term of the series expansion, T_α is raised to a power of spins $\sum_{l\in\Phi_\alpha} 2j_l$, which is a summation of spins from the residual loops coupled with the original propagator α. In other words, Φ_α is the set of residual loops $L = F \setminus C_T$ which contain $\alpha \in E \setminus E_T$ as an edge. Hence the set Φ_α associated with the original propagator α is defined as:

$$
\Phi_\alpha \equiv \{ l \in L \mid \alpha \subset l \}.
\tag{6.8}
$$

The homogeneity map corresponding to the T_α comes from (4.38) and (4.39). It is given by

$$
T^J_\alpha \rightarrow \frac{(J+1)^{\eta-1} F_\rho(J)^2}{(1+\rho^2)^{J(3+\tilde{n}_\alpha)}} \left(\prod_i^{\tilde{n}_\alpha} \tilde{\tau}_i\right)^J, \quad \text{in which } J = \sum_{l\in\Phi_\alpha} 2j_l,
\tag{6.9}
$$

in which $\tilde{\tau}$ tracks the homogeneity of gauge-fixed propagators. Let us use index k to label the gauge-fixed propagators. In Eq.(6.7), each $\tilde{\tau}_k$ is raised up to a power of spins $\sum_{l\in\Theta_k} 2j_l$. The set of summation contains spins from the residual loops which are connected with propagator $k \in E_T$ through a fundamental cycle $c_k \in C_T$ ($k \subset c_k$). Therefore we can define the set Θ_k associated with the gauge-fixed propagator k as:

$$
\Theta_k \equiv \{f \in L \mid \exists c_k, \ f \cap c_k \neq \emptyset\}.
\tag{6.10}
$$

The homogeneity map corresponding to the gauge-fixed propagator k in (6.7) can be summarised as:

$$\tilde{\tau}_k^J \rightarrow \frac{F_\rho(J/2)^2}{(1+\rho^2)^J}, \quad \text{in which } J = \sum_{l \in \Theta_k} 2j_l. \tag{6.11}$$

Before we write down the final result, let us however pause for a moment to introduce *simplified diagrams* notation to make the structure simpler and more transparent. The simplified diagrams are reduced from the full cable diagrams by removing fundamental cycles, and only keep the combinatorial data we need for the final expression. They are very useful for us to write down the evaluation of $\mathcal{A}_{bulk}$ in a compact way.
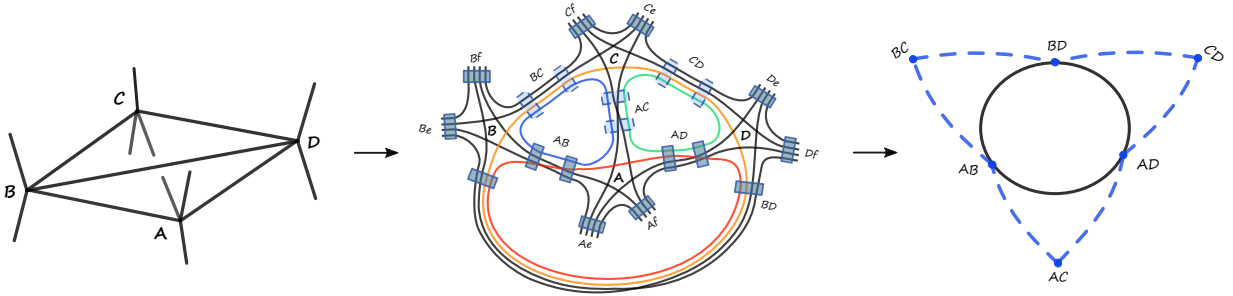
Figure 6.4: We take 4–2 Pachner move as a simple example of showing how to reduce the cable diagram to the simplified diagram. Figures from left to right are the dual 2-complex, the cable diagram, and the simplified diagram respectively. With an optimal tree $CB \cup CA \cup CD$, the fundamental cycles are precisely the green, blue, yellow loops. Each gauge-fixed propagator is represented as a blue node in the simplified diagram, connected with two shared nodes on the residual loop ABD due to two loop identities. Thus evaluating the bulk amplitude for 4–2 Pachner move reduces to a single loop integration with non-local spin couplings, which are represented by the dashed lines.

In a simplified diagram, the residual loops L are represented by circles and propagators are represented by nodes. The gauge-fixed ones, which are on the branches E_T of the chosen spanning tree, have index k and are denoted by the nodes outside of the circles. The original propagators, which are on the edges of the spanning tree's complement $E \setminus E_T$, have index α and are denoted by the nodes on the circles in the simplified diagram. We then use dashed lines (as in Fig.4.5) connecting nodes to represent the non-local coupling among propagators resulting from the loop identities, as we have discussed in the last section. Each dashed lines can be specified by a pair of indices αk. We show two examples of reducing the cable diagram to the simplified diagram in Fig.6.4 and Fig.6.5 . When we have $|F| - |C_T| \geq 1$, there is more than one residual

loop. In this case a few circles might share a same node, which corresponds to loops coupled at the same propagator, as in Fig.6.5.

In the language of the simplified diagrams, the set Φ_α contains the residual loops intersecting at node α. Θ_k contains the residual loops which have connection through dashed lines αk with node k. Hence the definition of Θ_k (6.10) can be written equivalently as:

$$\Theta_k \equiv \{ f \in L \,|\, \exists \alpha, \; \alpha k \cap f \neq \emptyset \}. \tag{6.12}$$

With all the above preparation, we can finally summarize the result of the truncated bulk amplitude in a very compact form:

$$A_{bulk} = \sum_{\{j_l \in \mathbf{Z}/2\}} \prod_l \frac{(2j_l + 1)^{\eta+1}}{(1+\rho^2)^{2j_l N_l}} \cdot \prod_{\alpha=1}^{|C_T|} \left[F_\rho^2 \left(\sum_{l \in \Phi_\alpha} 2j_l \right) \cdot \left(\sum_{l \in \Phi_\alpha} 2j_l + 1 \right)^{\eta-1} \right] \cdot \prod_{k=1}^{|V|-1} \left[F_\rho^2 \left(\sum_{l \in \Theta_k} 2j_l \right) \right], \tag{6.13}$$

in which there are $|F| - |C_T|$ free summations of spins from the residual loops. The power of $(1+\rho^2)^{2j_l N_l}$ can be counted by the number of propagators n_l in each residual loop, and the number of gauge fixed propagators $\tilde{n}_\beta$ in the fundamental cycle associated with the original propagator β:

$$N_l \equiv 4n_l + 2 \sum_{\beta=1}^{n_l} \tilde{n}_\beta, \tag{6.14}$$

Actually from the simplified diagram we can immediately read out the number N_l. This is because n_l counts the number of nodes on the residual loop l and the summation $\sum_{\beta=1}^{n_l} \tilde{n}_\beta$ counts the total number of dashed lines directly connected with the residual loop l.

The convenience of Eq.(6.13) is such that given any 2-complex which belongs to the set Ω_Γ, one can immediately write down the truncated bulk amplitude by simply counting the combinatorics in its simplified diagram without any calculation. Let us look at a concrete example.

The left figure in Fig.6.5 shows the cable diagram of two fully contracted 4-simplices, i.e. a super melon. In this case, $|V| = 2, |E| = 5, |F| = 10$. The optimal tree of the graph only contains one branch, which can be any of the five propagators. By gauge fixing edge E and removing the fundamental cycles through loop identities, we arrive at the corresponding simplified diagram, the right figure in Fig.6.5. In this case there are 4 fundamental cycles. After applying 4 truncated loop identities, there are $|F| - |C_T| = 6$ loops left that originally shared 4 propagators, which correspond to the shared nodes A, B, C, D among loops in the simplified diagram. Each loop identity gives rise to a non-local correlation between the gauge-fixed propagator and the residual loops and they are represented by the blue dashed lines.
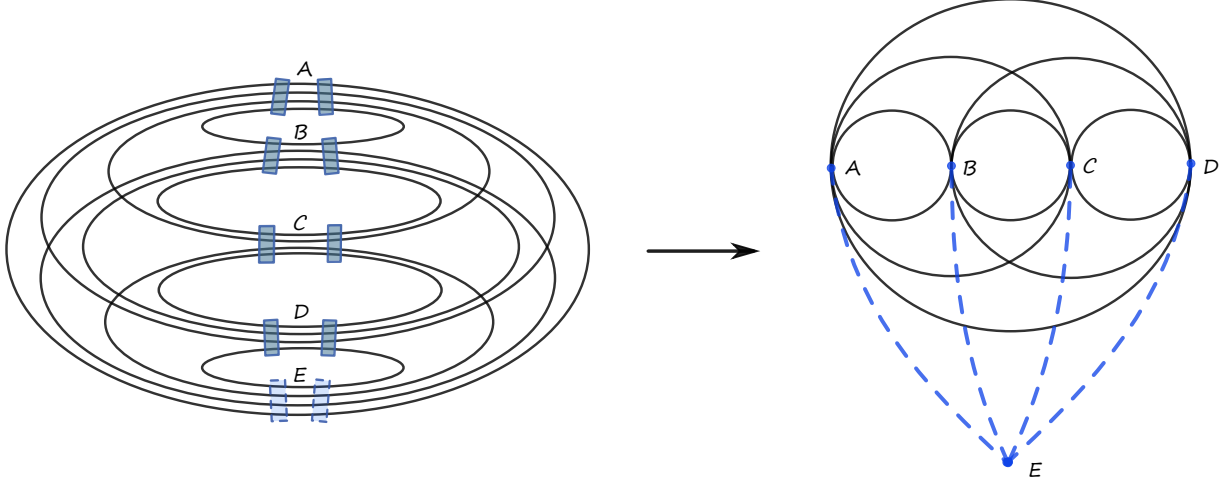
Figure 6.5: Left figure: the cable diagram of a super melon (fully contracted two 4-simplices); right figure: the simplified diagram. Optimal tree of this diagram only contains one branch and there are $|C_T| = 4$ fundamental cycles corresponding to an optimal tree. We choose E as the branch to be gauge fixed. After applying the corresponding 4 loop identities there are $|F| - |C_T| = 6$ residual loops. In the simplified diagram, the 6 residual loops coupled among the 4 shared nodes correspond to 4 original propagators. The 4 blue dashed lines represent the non-local correlation produced by 4 loop identities.

Now we can just read out the truncated bulk amplitude from the simplified diagram: for each residual loop, there are two nodes on it, i.e. $n_l = 2$ and two dashed lines directly connected with the loop, i.e. $\sum_{\beta=1}^{n_l} \tilde{n}_\beta = 2$. Thus from Eq.(6.14), we have $N_l = 12$ for all the l. There are 6 independent summations of spins corresponding to the 6 residual loops l:

$$A_{melon} = \sum_{\{j_{AB}, j_{AC}....j_{CD}\}} \prod_l \frac{(2j_l + 1)^{\eta+1}}{(1 + \rho^2)^{24j_l}} \cdot F_\rho^2 \left(\sum_{l \in \Theta_E} 2j_l\right) \cdot \prod_\alpha \left[F_\rho^2 \left(\sum_{l \in \Phi_\alpha} 2j_l\right) \cdot \left(\sum_{l \in \Phi_\alpha} 2j_l + 1\right)^{\eta-1} \right] \quad (6.15)$$

where $\alpha \in \{A, B, C, D\}$, the set $\Theta_E = \{AB, BC, AC, AD, BD, CD\}$,

$$\Phi_A = \{AB, AC, AD\}, \Phi_B = \{AB, BC, BD\}, \Phi_C = \{BC, CD, AC\}, \Phi_D = \{CD, BD, AD\}. \quad (6.16)$$

With this we can see the power of the simplified diagrams for 2-complexes in Ω_Γ – the expression for the truncated amplitude depends only on the combinatorics of these diagrams. In the next section we will generalize the expression (6.13) for the amplitude to arbitrary connected 2-complexes, not only those with optimal spanning trees.

6.3 The general structure

We have just shown that for a certain class of 2-complexes in Ω_Γ, the truncated bulk amplitude can be read out through the combinatorics of their simplified diagrams. The convenience comes from the graph structure of elements of Ω_Γ – the existence of the optimal spanning tree. However, what if we do not choose the optimal spanning tree to fix the gauge? Are the truncated degrees of freedom tree-dependent or not? Would the truncated bulk amplitude still be characterized by formula (6.13)? Moreover, in general for a graph that probably does not contain an optimal spanning tree, can we still express the truncated bulk amplitude in a simple form?

If we choose a non-optimal tree, there exists at least one fundamental cycle which is not a loop formed by a single strand, but a union of multiple loops coupled together in the cable diagram. In this case, we cannot directly apply loop identity to such a fundamental cycle even though it only contains one non-gauge-fixed propagator. We need to generalize the loop identity in section 4.5 to embrace such situations.
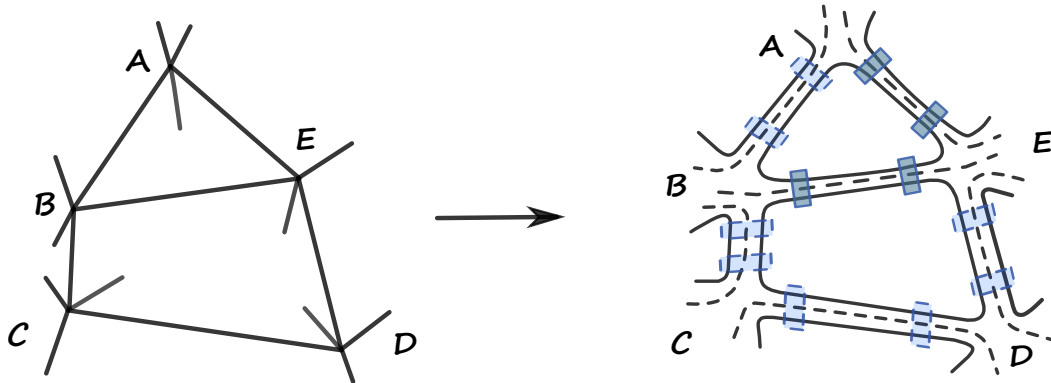
Figure 6.6: With a choice of spanning tree $AB \cup BC \cup CD \cup DE$, one of its fundamental cycle $ABCDE$ nests two loops $ABE \cup BCDE$. We cannot directly apply loop identity for either ABE or $ABCDE$. To integrate out all the loops in the cable diagram, they have to be annihilated in a specific order.

Let us consider an example in Fig.6.6. In this case, if we choose a spanning tree as $AB \cup BC \cup CD \cup DE$, adding an edge AE would create a fundamental cycle $ABCDE$, but it is not a face of the 2-complex. The cycle $ABCDE$ nests two loops $ABE \cup BCDE$ in the cable diagram. To integrate out all the loops in the cable diagram in this case, the loops need to be annihilated in specific order: First we apply loop identity to $BCDE$ because it contains only one original propagator BE. The truncation scheme neglects the mixing strands on edge BE, thus after the truncation we are able to apply loop identity again to ABE. In this way, we are evaluating a nesting of loop

identities. The truncation for ABE is performed after the truncation of loop $BCDE$, thus nesting of loop identities leads to truncation within truncation.

The homogeneity map of the nesting loop identity can be generalized from Eq.(4.38). In our example, for the loop ABE in Fig.6.6, its exponentiated form is

$$L_\tau = \exp \sum_{i=1}^{3} \left(\tilde{\tau}_{AB}[\tilde{z}_i^{AB}|\tilde{w}_i^{AB}\rangle + T_{BE}[z_i^{BE}|w_i^{BE}\rangle + T_{AE}[z_i^{AE}|w_i^{AE}\rangle \right). \tag{6.17}$$

This expression is of the same general structure as the loop identity (4.37) – it is a product of trivial propagators with different weights. The difference resides in the homogeneity map:

$$\mathcal{T}_{AE}^{J} \rightarrow \frac{J!(J+1)^\eta}{(1+\rho^2)^{3J}} \, (\tilde{\tau}_{AB}\tau_{AE}T_{BE})^J \tag{6.18}$$

in which the nested loop and the propagators are tracked by

$$T_{BE}^{J} \rightarrow \frac{J!(J+1)^\eta}{(1+\rho^2)^{4J}} \, (\tilde{\tau}_{BC}\tilde{\tau}_{CD}\tilde{\tau}_{DE}\tau_{BE})^J \,,$$
$$\tau_\alpha^{J} \rightarrow \frac{F_\rho(J)^2}{(1+\rho^2)^{2J}(1+J)!}, \qquad \tilde{\tau}_i^{J} \rightarrow \frac{F_\rho(J/2)^2}{(1+\rho^2)^J}, \tag{6.19}$$

where the indices $\alpha \in \{AE, BE\}$ and $i \in \{AB, BC, CD, DE\}$. Compared with the loop identity (4.38) we have discussed in Section 4.5, the only difference here for the loop ABE is that the homogeneity map for the spinors on edge BE is keeping track of a whole loop identity from loop $BCDE$. When we calculate nesting of loops, we need to apply loop identities in a specific order, and replace the homogeneity map of a gauge-fixed propagator in the second loop ABE to the map which tracks the truncated loop identity in the first loop $BCDE$.

Since the generalization to the nesting of loop identities is straightforward, we can now evaluate the bulk amplitude without an optimal tree. In a general graph, after gauge fixing along a spanning tree, there are $|E| - (|V| - 1)$ original propagators to be integrated. This number is still equal to $|C_T|$, which is the same as in the case of the class of graphs Ω_Γ. The only difference is that we need to consider nesting of loop identities, and annihilate loops in a specific tree-dependent order. After all the $|C_T|$ original propagators are annihilated through generalized loop identities, we have $|F| - |C_T|$ residual loops that have no group integrations to be performed anymore. Performing gaussian integrals of spinors in those loops leads to $|F| - |C_T|$ number of independent summations of spins.

At this stage, the result can be expanded in a power series. If we use e to label edges, each book-keeping parameter τ_e is raised to the power of a summation of a few independent spins

from the residual loops: $\sum_{l \in \tilde{\Theta}_e} 2j_l$. After applying the homogeneity map to obtain the final result, the number of propagators $|E|$ in a graph corresponds to the number of squared hypergeometric functions $F_\rho^2(\sum_{l \in \tilde{\Theta}_e} 2j_l)$ in the amplitude. The set $\tilde{\Theta}_e$ is tree-dependent, and its elements can be straightforwardly obtained through the procedure outlined above. Note that the spin j_l of one residual loop appears in multiple propagators' F_ρ^2. This encodes the non-local feature of the result.

Similarly as in Eq.(6.13), in the general case we can also find out the power of $(1 + \rho^2)$ explicitly, as it comes from two aspects: The first is $(1 + \rho^2)^J$ as part of the normalization in each propagator (Eq.(6.19) and Eq.(4.38)). The second is that when we integrate a spinor along a loop, each gaussian integral gives rise to $(1 + \rho^2)^{-1}$ in the exponential:

$$\int_{\mathbb{C}^2} d\mu_\rho(z) e^{\langle x|z \rangle + \langle z|y \rangle} = \sum_J \frac{\langle x|y \rangle^J}{J!(1 + \rho^2)^J} \tag{6.20}$$

After some algebra, one can check that the coefficient N_l in the power of $(1 + \rho^2)^{-2j_l N_l}$ equals to twice of the number of $2j_l$ appearing in the product of $F_\rho(\sum_{l \in \tilde{\Theta}_e} 2j_l)$.

Thus finally, a general structure of the truncated bulk amplitude for an arbitrary connected 2-complex emerges and we summarize it as following:

$$A_{bulk} = \sum_{\{j_l\} \in Z/2} \prod_e \underbrace{F_\rho^2 \left(\sum_{l \in \tilde{\Theta}_e} 2j_l \right)}_{\#=|E|} \cdot \prod_f [(1 + \rho^2)^{-2j_l N_l} \cdot \underbrace{(2j_l + 1)^{\eta+1}]}_{A:\#=|F|-|C_T|} \cdot \prod_\alpha \underbrace{\left(\sum_{l \in \tilde{\Phi}_\alpha} 2j_l + 1 \right)^{\eta-1}}_{B:\#=|C_T|} \tag{6.21}$$

- There are $|F| - |C_T|$ free summations of spins.

- The number of $F_\rho^2 \left(\sum_{l \in \tilde{\Theta}_e} 2j_l \right)$ is the number of propagators, i.e. $\#F_\rho^2 = |E|$. The set $\tilde{\Theta}_e$ labels faces in the 2-complex and the details of the set $\tilde{\Theta}_e$ are tree-dependent.

- The coefficient N_l in the power of $(1 + \rho^2)^{-2j_l N_l}$ keeps track of the occurrence of each residual loop in the above sets $\tilde{\Theta}_e$. In other words, it tracks the number of times $2j_l$ appears in the product of F_ρ and $\#|2j_l| = N_l/2$.

- The number of $(2j_l + 1)^{\eta+1}$ in the product equals to $|F| - |C_T|$.

- The number of terms in the form of $(\sum_{l \in \tilde{\Phi}_\alpha} 2j_l + 1)^{\eta-1}$ equals to $|C_T|$. $\tilde{\Phi}_\alpha$ is another set which labels the faces in the 2-complex. The details of the set $\tilde{\Phi}_\alpha$ are tree-dependent.

Now we can come back to the questions at the beginning of this section. With different choice of gauge-fixing trees, the values of truncated bulk amplitude are different, which shows as

83

different content in both of the sets $\tilde{\Theta}_e$ and $\tilde{\Phi}_\alpha$ in Eq.(6.21). This is due to the truncation scheme. In the loop identity, the mixing terms get truncated and those degrees of freedom depend on the chosen tree. With nesting of loop identities as we have just discussed (for example Fig.6.6), the truncation within truncation usually leads to worse approximation than the truncation associated with an optimal spanning tree. In Appendix D, using the diagram of 5–1 Pachner move as an example, we evaluate the truncated bulk amplitude with different gauge fixing trees and compare the difference.

We also recall that the truncation scheme is a better approximation for large spins. Hence if the bulk amplitude is convergent, i.e. the most dominant degrees of freedom are given by small spin channel, the truncation is a worse approximation compared to the case when the bulk amplitude is divergent, i.e. large spin channels dominate the amplitude. Even though it is tree dependent, the truncated bulk amplitude of different graphs can be summarized with a same structure Eq.(6.21). In the next section, we will derive a formula for the degrees of divergence based on this result Eq.(6.21). We will see that the tree-dependent information (the details of the sets $\tilde{\Phi}_\alpha$ and $\tilde{\Theta}_m$) only contribute as finite factors in the large spin limit, and the most dominant degrees of freedom can be captured by a simple expression in terms of graph properties.

Chapter 7

Degree of divergence

7.1 The degree of divergence for arbitrary connected 2-complex

In this section, we will show that the degree of divergence can be expressed only in terms of corresponding graph properties. We will summarize the main result first, and then derive it in the later text.

For a connected 2-complex which is dual to a simplicial decomposition of 4-d manifold, the bulk degree of divergence is given by:

$$D(\Gamma) = \Lambda^{(\eta+2)|F|-3|C_T|-3|E|}, \quad \text{when } |F| - |C_T| > 0, \tag{7.1}$$

where Λ is a large spin cut-off. This expression can be rewritten, if we plug in the quantity of $|C_T|$ by Eq.(4.1), as

$$D(\Gamma) = \Lambda^{(\eta+2)|F|-6|E|+3|V|-3}, \quad \text{when } |F| - |E| + |V| - 1 > 0, \tag{7.2}$$

where C_T is the number of fundamental cycles of an arbitrary chosen spanning tree in the graph, $|F|$ is the number of faces in the 2-complex, $|V|$ is the number of vertices and $|E|$ is the number of edges in the bulk.

In section 6 we have seen that to get the bulk amplitude, we need to sum over independent spins in the $|L| = |F| - |C_T|$ residual loops. When $\Lambda \to \infty$, integration is a good approximation of the summation:

$$
\begin{aligned}
A_{bulk}(\Lambda) &\equiv \sum_{j_1 \in \mathbb{Z}/2}^{\Lambda/2} ... \sum_{j_{|L|} \in \mathbb{Z}/2}^{\Lambda/2} f(2j_1, 2j_2, ...2j_{|L|}) \\
&\approx \int_{\epsilon \cdot \Lambda}^{\Lambda} f(j_1, j_2, ..., j_{|L|}) \, dj_1 ... dj_{|L|} \\
&= \Lambda^{|F|-|C_T|} \int_{\epsilon}^{1} f(\Lambda J_1, \Lambda J_2, ..., \Lambda J_{|L|}) \, dJ_1 ... dJ_{|L|},
\end{aligned}
\tag{7.3}
$$

where we use an arbitrary small constant $\epsilon > 0$ as small spin cut-off. When the amplitude is finite, small spin regime dominates the amplitude. However, as we are seeking for the divergences, truncating small spin regime is irrelevant to the result, but it will help us to avoid some poles which come from $1/J^n$ in the asymptotic series expansion.

It is easy to see that only when

$$
|L| = |F| - |C_T| > 0, \quad i.e. |F| - |E| + |V| - 1 > 0
\tag{7.4}
$$

there are free summations in Eq.(6.21), thus it is possible for an amplitude to diverge. In some cases, for example of the diagram in 3–3 Pachner move [105], all the loops can be annihilated by the loop identity, thus there is no divergence associated with the diagram.

To derive (7.1) let us look at the case $\rho = 1$ first. In this case, our hypergeometric function is merely a rational function of factorials. In Appendix C, we have shown that it has asymptotics:

$$
{}_2F_1(-J-1, -J; 2; 1) = \frac{(2J+2)!}{(J+2)! \, (J+1)!} \sim \frac{4^{J+1} e}{\sqrt{\pi} \, J^{3/2}}, \qquad \text{as } J \to \infty.
\tag{7.5}
$$

Note that this asymptotic formula is a good approximation even for small spins. We rewrite the bulk amplitude (6.21) in the form of Eq.(7.3) and then plug in the asymptotics (7.5). For large spins, the asymptotic behavior of the bulk amplitude is given by

$$
\begin{aligned}
A_{bulk}(\Lambda) \sim \Lambda^{|F|-|C_T|} \underbrace{\Lambda^{(|F|-|C_T|)\,(\eta+1)}}_{A} \underbrace{\Lambda^{|C_T|(\eta-1)}}_{B} \left(\frac{4^{\Lambda \sum_l N_l} e^2}{\pi \, \lambda^3} \right)^{|E|} \prod_l 2^{-2\Lambda N_l} \times \\
\times \int_{\epsilon}^{1} \prod_m \left(\sum_{a \in \tilde{\Theta}_m} J_a \right)^{-3} \prod_l J_l^{\eta+1} \prod_\alpha \left(\sum_{b \in \Phi_\alpha} J_b \right)^{\eta-1} dJ_1 ... dJ_{|L|}.
\end{aligned}
\tag{7.6}
$$

86

The integration in the second line is merely a finite number. The underbraced parts A and B result from the corresponding parts in Eq.(6.21). Because the value of N_l equals to twice of the number of $2j_l$ appearing in the product of hypergeometrical functions, we can see that the term of $4^{\sum j_l N_l}$ which comes from the product of the asymptotics (7.5) exactly cancels the factor $\prod_l (1+\rho^2)^{-2j_l N_l}|_{\rho=1}$ in Eq.(6.21). Removing all the trivial constants from the above equation, we immediately arrive at

$$A_{bulk}(\Lambda) \sim \Lambda^{2|F|-\eta|F|-3|C_T|-3|E|}, \tag{7.7}$$

which is exactly the result in Eq.(7.1).

For $0 < \rho < 1$, we have shown in Appendix C that the hypergeometric function has the asymptotic expansion of

$$_2F_1(-J-1,-J;2;\rho^4) \sim \frac{e^{(\frac{3}{2}+J)\zeta_\rho} \cdot \left(1-\rho^4\right)^{\frac{3}{2}+J}}{2\sqrt{\pi}\,\rho^3 \cdot J^{3/2}}, \quad \text{for } 0 < \rho < 1 \text{ as } J \to \infty, \tag{7.8}$$

where $\zeta_\rho \equiv \cosh^{-1}\left[(1+\rho^4)/(1-\rho^4)\right]$. Manifestly, this looks like a complicated function of ρ, but we importantly find that there is a tremendous simplification

$$e^{\zeta_\rho J}\,(1-\rho^4)^J(1+\rho^2)^{-2J} = 1. \tag{7.9}$$

Thus similar to the case $\rho = 1$, the term of $\prod_l e^{j_l N_l \zeta_\rho}\,(1-\rho^4)^{j_l N_l}$ which comes from the numerator of the product of the asymptotics (7.8) cancels the factor $\prod_l(1+\rho^2)^{-2j_l N_l}$ in Eq.(6.21) in the large spin limit. With this cancellation, when we rewrite Eq.(6.21) in the form of Eq.(7.8), we get exactly the same expression (7.6) for the bulk amplitude in the large spin limit. Hence we have just proved that for $0 < \rho \leq 1$, the degree of divergence is characterized by (7.1) and (7.2). Let us collect a few simple examples of the degree of divergence in a table:
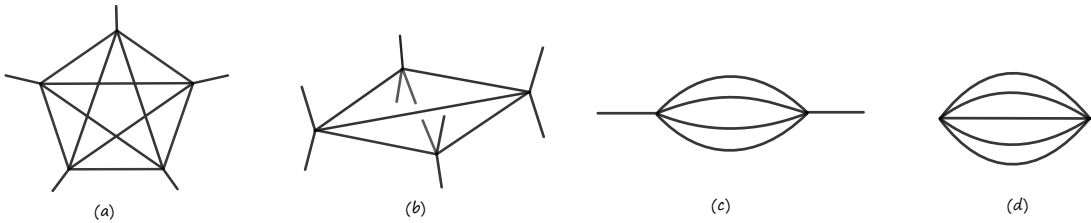
Figure 7.1: A few simple examples we are considering in the following table.

	$|V|$	$|E|$	$|F|$	Degree of divergence
5–1 move (a)	5	10	10	$\Lambda^{10\eta-28}$
4–2 move (b)	4	6	4	$\Lambda^{4\eta-19}$
Elementary melon (c)	2	4	6	$\Lambda^{6\eta-9}$
Fully contracted melon (d)	2	5	10	$\Lambda^{10\eta-7}$

When $\eta = 3$, the 5–1 Pachner move has exactly Λ^2 divergence, which is the expected degree of divergence if the model has diffeomorphism invariance [94, 96]. It is important to note that for this value of η, the 4–2 move is finite. In fact, it does not become divergent until $\eta > 19/4$.

This spin foam model was expected to be less divergent compared with EPRL/FK, due to the difference of imposing the constraint on the propagator rather than the boundary spin network resulting in a more constrained model. This is justified by the case of the elementary melon: the self-energy diagram starts to be divergent when $\eta > 1.5$, which is less divergent compared to previous results in both Riemannian and Lorenzian EPRL/FK model [75, 76]. However, in the range of parameter η when the melons are finite, the 5–1 Pachner Move is also finite, which makes the restoration of diffeomorphism symmetry an obstacle.

7.2   Degree of divergence in terms of topological quantities

To gain some physical insight into the result we have obtained, it is useful to rewrite the degree of divergence in terms of topological and combinatorial quantities. To simplify the discussion, we consider the case of compact 4-d manifolds, which are dual to fully contracted 2-complexes.

If we use N_i to represent the number of i-dimensional simplices in the triangulation, the d-dimensional Euler characteristic χ is defined as

$$\chi = \sum_{i=0}^{d} (-1)^i N_i. \tag{7.10}$$

In the 4-d simplical compact manifold, the link of every 2k-simplex ($k = 1, 2$) is an odd dimensional sphere [92]. Recall that in d dimensions S^d has Euler characteristic $1 + (-1)^d$, hence

$$\sum_{i=2k-1}^{4} (-1)^i \binom{i+1}{2k-1} N_i = 0, \quad k = 1, 2. \tag{7.11}$$

Recall that the number of 4-simplices in the manifold is the number of vertices in the dual 2-complex $N_4 = |V|$, the number of tetrahedra is the number of edges $N_3 = |E|$, and the number

88

of triangles is the number of faces $N_2 = |F|$. Eq.(7.11) gives us the following two independent relations:

$$2|E| = 5|V|, \tag{7.12a}$$

$$2N_1 + 4|E| = 3|F| + 5|V|. \tag{7.12b}$$

Using Eq.(7.10) and Eq.(7.12) we can rewrite the degree of divergence (7.1) in terms of the Euler characteristic χ:

$$\text{In terms of } \chi, |F| \text{ and } |N_0| : \quad D(\Gamma) = \Lambda^{(\eta-4)|F|+3(4N_0-4\chi-1)}. \tag{7.13}$$

Unlike for 2-manifolds, in 4 dimensions we know that Euler characteristic is not enough to specify the topology. There is however another integer characterizing the topology: the *degree* of a graph Γ [86, 87, 88, 89, 90], which respects the formula

$$\frac{2}{(d-1)!}\omega_d(\Gamma) = \frac{d(d-1)}{4}|V| + d - |F|. \tag{7.14}$$

The meaning of this quantity is related with a class of subgraphs: the *jackets*. A jacket of a cable diagram Γ is a subgraph which contains all the vertices V and edges E of Γ, but only a subset of faces. The degree $\omega_d(\Gamma)$ of a graph is the sum of the genera of its jackets [1]. Hence the degree $\omega_d(\Gamma) \geq 0$, while the equality is saturated with Γ dual to a sphere S^d. The reciprocal statement holds only when $d = 2$ [87]. For reviews and discussion of this quantity see [86, 87, 88, 89, 90]. For a 4-d simplicial manifold, the degree of the skeleton of the dual 2-complex Γ and its number of vertices and faces are related by

$$\omega_4(\Gamma)/3 = 3|V| - |F| + 4. \tag{7.15}$$

Thus in 4-d, from equations (7.10), (7.11) and (7.15), it follows that the degree of the graph and the Euler characteristic are related by

$$\omega_4(\Gamma)/3 = 3\chi - 3N_0 + |F|/2 + 4. \tag{7.16}$$

When we fix both the degree $\omega_{4d}(\Gamma)$ and the Euler characteristic χ of a graph, knowing one of the variables $|V|, |F|$ and N_0 will fix the other two.

The degree of divergence formula (7.1) can be rewritten in terms of the degree of the graph $\omega_4(\Gamma)$:

$$\text{in terms of } \omega_{4d}(\Gamma), |F| : \quad D(\Gamma) = \Lambda^{(\eta-2)|F|-4\omega_{4d}(\Gamma)/3+13}, \tag{7.17}$$

---

[1] The genus of a graph is the minimal integer n such that the graph can be embedded in a surface of genus n.

in terms of $\omega_{4d}(\Gamma), |V| : \ D(\Gamma) = \Lambda^{3(\eta-2)|V|-(2+\eta)\omega_{4d}(\Gamma)/3+4\eta+5}$. \hfill (7.18)

If we fix the degree $\omega_{4d}(\Gamma)$ and vary $|V|, |F|$, then $\eta = 2$ marks a transition of behaviors. With $\eta > 2$, $D(\Gamma)$ monotonically increases with $|V|$ and the opposite happens when $\eta < 2$. At $\eta = 2$, the degree of divergence purely depends on $\omega_{4d}(\Gamma)$:

$$D(\Gamma)|_{\eta=2} = \Lambda^{-4\omega_{4d}(\Gamma)/3+13}. \hfill (7.19)$$

From Eq.(7.15) and also from the fact that the degree of a graph is the sum of the genera of its jackets, we know that $\omega_{4d}(\Gamma)/3$ is a non-negative integer. If we fix the number of vertices $|V|$ in the graph, when $\eta < -2$, $D(\Gamma)$ monotonically increases with $\omega_{4d}(\Gamma)$. However, the model is completely convergent with such face weight, which will not give the expected degree of divergence for 5–1 move. In the region $\eta > -2$, $D(\Gamma)$ monotonically decreases with $\omega_{4d}(\Gamma)$ and reaches its maximum with $\omega_{4d}(\Gamma) = 0$. This means that if one uniformly sums over all the possible graphs, the dominant contributions to the partition function are the graphs which are dual to the simplicial manifolds with spherical topology and at the same time with degree $\omega_{4d}(\Gamma) = 0$. In [87] it was shown that this type of graphs with $\omega_{4d}(\Gamma) = 0$ are melonic. It is a class of graphs with maximal $|F|$ at fixed $|V|$, and their elementary subgraph is composed by a couple of simplices glued along all but one of their faces (see Fig.7.1 c). They are the leading order contribution in the large N limit of colored tensor models [87], and have been long suspected to be the most divergent configuration in spin foams [75, 76].

7.3   Physical implications

First let us compare our result with the colored tensor models, in which the dominant graphs and continuum limit have been studied in depth. We will briefly review their results first. In the case of the independent identically distributed model and the Boulatov Ooguri model ([87], [90]), the amplitudes associated with a graph Γ are given by

$$A^{i.i.d.}(\Gamma) = (\lambda\bar{\lambda})^{|V|/2} N^{d-\frac{2}{(d-1)!}\omega(\Gamma)}, \quad A^{B.O.}(\Gamma) = (\lambda\bar{\lambda})^{|V|/2} N^{d-1-\frac{2(d-2)}{d!}\omega(\Gamma)}, \hfill (7.20)$$

where N is a large parameter indicating the tensor size, λ and $\bar{\lambda}$ are coupling constants. Note that in these models the coupling constant has been rescaled by a power of N, so that the amplitude is not increasingly divergent or suppressed by higher number of vertices, and the amplitude of a graph depends solely on its degree [90]. For both of the i.i.d and BO models, it has been shown that the leading order contribution of the $1/N$ expansion [86, 87, 88, 90, 89, 91] is governed by melonic graphs ($\omega(\Gamma) = 0$) [87]. It was further shown in [91] that the melonic dominance leads to branched polymers phase in the continuum limit.

In terms of the dominant graphs, the spin foam model we are studying has the same behavior with the colored tensor models when the face weight $\eta = 2$, as the degree of divergence (7.19) solely depends on a negative power of $\omega_4(\Gamma)$. If one sums over all the diagrams with equal weight as in the colored tensor model, then we predict that the spin foam model has a branched polymers phase in the continuum limit at $\eta = 2$.

When the face weight $\eta \neq 2$ however, the degree of divergence has a non-trivial dependence on $|V|$. When $-2 < \eta < 2$, the amplitude is increasingly suppressed with higher number of vertices $|V|$, which indicates that the most divergent diagram is a single super melon. When $\eta > 2$, the amplitude is increasingly divergent with higher number of vertices $|V|$, which indicates that the coupling constant should be rescaled through renormalization. This region is of physical interest because it contains the range of parameter in which the 5–1 move is divergent while 4–2 is convergent. However, since the dominant diagrams are melonic and they are geometrically degenerate, one might worry that the model is peaked on the configurations which do not describe smooth 4d geometry, if there is no restriction on the set of allowed diagrams.

To address this concern, let us have a look at 3-d gravity first. The degree of divergence for Ponzano-Regge model (3-d $SU(2)$ BF theory) is captured by

$$D_{SU(2)BF}(\Gamma) = \Lambda^{3|F|-3|E|+3|V|-3}. \tag{7.21}$$

The face weight in the model is chosen to be $(2j + 1)$, because it is the only choice which preserves topological invariance. There are different ways of deriving (7.21). In the approach presented in [105] and this paper, we can see that (7.21) arises from the following simple derivation: each residual loop contributes to the degree of divergence a factor of $\delta_{SU(2)}(\mathbb{1}) \sim \Lambda^3$, and in a connected diagram the number of residual loops is given by $|L| = |F| - |C_T| = |F| - |E| + |V| - 1$.

When we discretize 3-d gravity, the residual action of the diffeomorphism group acts at the vertices of the triangulation of a 3-d manifold as vertex translation symmetry. The 4–1 Pachner move has exactly degree of divergence Λ^3, which corresponds to the translation symmetry of placing the free vertex anywhere in the triangulation. A proper Faddeev-Popov gauge fixing procedure divides the amplitude by this divergence [93], thus leaving the model invariant under 4–1 move.

	$|V|$	$|E|$	$|F|$	Degree of divergence
4–1 Pachner move	4	6	4	Λ^3
A fully contracted melon	2	4	6	Λ^9

Now let us rewrite the degree of divergence in terms of topological invariants and the graph degree ω_{3d}. For the simplicial decomposition of 3-d compact manifold, the Euler characteristic is

$$\chi = N_0 - |F| + |E| - |V| \tag{7.22}$$

91

and the degree of the graph is given by

$$2\omega_{3d}(\Gamma) = 3|V| - 2|F| + 6. \tag{7.23}$$

Together with the relation $2|E| = 4|V|$ for a fully contracted 2-complex, we find that the degree of divergence can be equivalently expressed as

$$D_{SU(2)BF}(\Gamma) = \Lambda^{3N_0 - 3\chi - 3} = \Lambda^{3|V|/2 - 3\omega_{3d}(\Gamma) + 6} \tag{7.24}$$

From expression in terms of N_0 and χ, we can see that the divergence is concentrated on the number of free vertices N_0 in the triangulation. From the expression in terms of the degree, we can see that without properly gauge fixing the vertex translation symmetry, the most divergent graphs also have degree $\omega_{3d}(\Gamma) = 0$ and hence are melonic.

As we have discussed in Chapter 2.3, in 3D the gauge fixing procedure introduced in [93] fixes the spins along a maximum tree of bones in the triangulation to be zero. In the approach presented this paper, this maximum tree along the bones in the triangulation precisely corresponds to the residual loops in the simplified diagrams. Setting the spins in those residual loops to zero simply removes all the divergence. Thus the gauge fixing procedure ensures that all the graphs have finite amplitude. Without properly gauge fixing the diffeomorphism symmetry and removing the divergence, one should not rush into the conclusion that the Ponzano-Regge model is peaked on melonic graphs.

The continuum limit of 3-d gravity is fully described by the discrete model, which allows us to identify the gauge symmetry and leaves the model finite. However, the question is very non-trivial in 4-d, since the diffeomorphism symmetry is only expected to be recovered in the continuum limit through renormalization. Nevertheless, considering that the discretized 4-d classical Regge action indeed has the vertex translation symmetry, in the quantum model we might be able to identify some residual gauge symmetry with non-compact gauge orbits, which could be the origin of the divergence in the 5–1 Pachner Move. As we have just shown, with face weight $\eta = 3$ the model has the expected degree of divergence if the diffeomorphism symmetry is recovered. Hence the future research should clarify whether the model indeed contains some residual gauge symmetry which results in the divergence. One would hope that properly identifying and fixing this residual gauge symmetry might completely remove the divergence and change the behavior of melonic dominance, as is the case in 3-d. However, here is the non-trivial part: the vertex translation symmetry is not present in the model yet, and it is only expected to be recovered through renormalization. However, without the proper gauge fixing, the divergence of the model leads to non-geometrical dominant phase of the partition function. Lack of precise residual gauge symmetry and the melonic-dominant phase are two sides of the same coin. Hence it is meaningful to investigate a model which could possibly take diffeomorphisms as a more fundamental role, rather than recovering gauge symmetry through renormalization.

The implications of the result in this paper are different for the two distinct approaches towards continuum limit: summing over all the possible diagrams [27, 124, 125], or refining the partition function on a fixed lattice (a la Dittrich [102, 103, 62]).

For the summation approach, the melonic dominance might be resolved by gauge fixing, as we have just discussed. Another way is by putting a restriction on the space of diagrams which are to be summed over, and discarding the geometrically degenerate cases. Such an approach will result in a different model than the current group field theories. It also requires finding a complete classification of 2-complexes which are dual to non-degenerate geometries and is an interesting mathematical question by itself. A related question is whether the fully contracted diagrams (in the context of group field theory) can be interpreted similarly as in quantum field theory, where the sum of all the vacuum bubbles is a normalization factor for the physical correlation functions.

For the refining approach, there is no concern of the melonic dominance and one can focus on possible phase transitions which have already been indicated by the distinct behaviors of the model in different ranges of η. There indeed exists value of η such that 5–1 move has Λ^2 divergence while 4–2 move is finite. This is a promising sign of recovering diffeomorphism symmetry in the continuum limit.

Chapter 8

Conclusion and discussion

Let us now collect the results and see what we have learnt. We have introduced a new way of imposing holomorphic simplicity constraints in the Riemannian holomorphic Spin Foam model. Instead of constraining the boundary spin network function, as is usually done, we imposed the simplicity constraints on BF projectors. It turned out to have the same asymptotics as the seminal EPRL-FK model [126, 127, 63]. This model allows for more general graphs than the usual models built from vertex amplitudes, and dramatically simplified computation when we evaluate amplitudes.

Some new techniques have been developed for evaluating amplitudes, including the homogeneity map, loop identity and its truncation. Applying those techniques, we have analytically computed 4D Pachner moves for the first time in a simplicity-constrained Spin Foam model of 4–dimensional Quantum Gravity. For both the 4–2 and 5–1 moves, there is an insertion of a non-local operators in the final coarse grained simplices, with a mixing of strands leading to non-geometrical and non-local configuration. This means that the model does not have vertex translation symmetry as an expected residual of diffeomorphisms.

From the viewpoint of real-space renormalization group however, such non-local operators are expected to appear in each step of coarse graining, and have to be truncated to local ones in a controlled manner. Indeed, we have found that there exists a very natural and simple truncation scenario to restrict the dynamics in the geometrical form. It removes the mixing of strands in the coarse-grained simplices, thus allowing the result to remain geometrical, and hence making the coarse graining Pachner moves structure preserving.

We then push the result to be more general – evaluating arbitrary amplitudes. First, for a certain class of graphs with optimal spanning trees, we derived a simple expression to capture the dominant degrees of freedom in the partition function. Using it, one can simply read out the evaluation of truncated bulk amplitude through combinatorial properties of a graph.

We then generalized the result to arbitrary graphs and studied their structure. With the gauge fixing choice along a generic choice of spanning trees, we need to evaluate nesting of loop identities which leads to truncation within truncation. However, with the choice of an optimal spanning tree, the error of truncation is minimized. We then showed that even though the truncated degrees of freedom depend on the choice of gauge-fixing tree, the dominant degrees of freedom are tree-independent and can be captured by a simple expression.

Using the asymptotic expansion of the hypergeometrical functions, we extracted a simple formula for the exact degree of divergence for arbitrary 2-complexes, in which the variables are the number of vertices $|V|$, number of faces $|F|$ and the number of edges $|E|$. The dependence on Barbero-Immirzi parameter has dropped out in the asymptotic analysis. The only parameter in the degree of divergence formula is the power of the face weight η. When the face weight is $(2j + 1)^3$, i.e. $\eta = 3$, the 5–1 Pachner move has Λ^2 divergence, which is the expected degree of divergence if diffeomorphism symmetry is recovered.

To gain some physical insight, we expressed the degree of divergence formula in terms of Euler chracteristic χ and the degree of graph $\omega(\Gamma)$. We found that for the face weight $\eta > -2$, the most divergent graphs are the ones that have spherical topology and degree $\omega_{4d}(\Gamma) = 0$. It has been shown in [87] that this type of graphs are melonic, which is a class of graphs with maximal number of faces at fixed number of vertices. When the face weight $\eta = 2$, the degree of divergence (7.19) solely depends on a negative power of $\omega_{4d}(\Gamma)$. If one sums over all the diagrams with equal weight as in the colored tensor models, then we predict that the spin foam model has a branched polymers phase in the continuum limit at $\eta = 2$. When $\eta < 2$, the amplitude is increasingly suppressed with higher number of vertices $|V|$, which indicates that the most divergent diagram is a single super melon ($\eta > -2$). In the region of parameter of physical interest (the 5–1 move is divergent while 4–2 is convergent), the amplitude is increasingly divergent with higher number of vertices $|V|$. We might need to introduce a new coupling constant for the vertex, and it should be rescaled through renormalization. If we do not put restriction on the allowed

diagrams, one might be concerned that the model is peaked on geometrically degenerate melonic configurations.
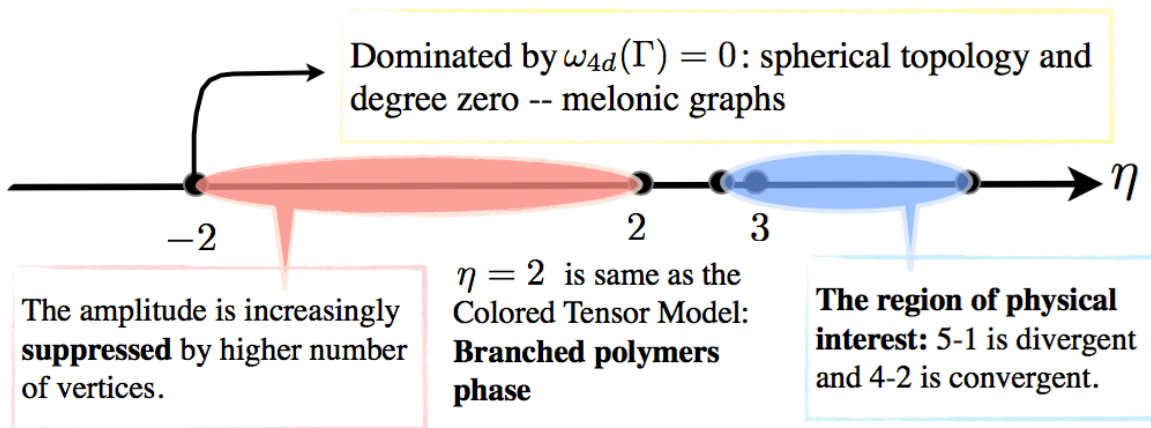
Figure 8.1: Indication of different phases in terms of the power of face weight η.

Whether the continuum limit of Spin Foams should be defined via refining on a fixed 2-complex, or through summation over foams, has been debated in the field for a long time. If one takes the point of view that the continuum limit of Spin Foams should be defined through refining the partition function on a fixed lattice [102, 103, 62], then the melonic diagrams are excluded by definition and one can focus on possible phase transitions which are already indicated by the distinct behaviors of the model in different ranges of η. If one takes the point of view that the continuum limit of the model should be defined through summing over all possible diagrams corresponding to the same boundary (such as in group field theory and colored tensor models), then the melonic dominance is more worrisome. One way to resolve it is by restricting the space of diagrams which are to be summed over, and exclude the geometrically degenerate cases. Hence future research should address a complete classification of 2-complexes which are dual to non-degenerate 4D geometries. Another idea is that the fully contracted diagrams can be interpreted similarly as in quantum field theory, where the sum of all the vacuum bubbles is a normalization factor for the physical correlation functions.

Another way to understand the melonic dominance comes from the important lesson in 3D quantum gravity. In Ponzano-Regge model, one can identify a vertex translation symmetry, which is a residue of diffeomorphism symmetry resulting from discretization. Without a proper Faddeev-Popov procedure, we have checked that the most divergent diagrams in the model are also melonic. We expect that in 4D, the residual gauge symmetry with non-compact gauge orbits could be the origin of the divergence in the 5–1 move. One might expect that properly identifying

and fixing this residual gauge symmetry might completely remove the divergence and change the behavior of melonic dominance. However, here is the non-trivial part: as the model does not yet have exact residual gauge symmetry, one cannot perform the gauge fixing procedure. Hence it is meaningful to investigate a model which could possibly take diffeomorphisms as a more fundamental role, rather than recovering gauge symmetry through renormalization.

Future Outlook

First, it will be an important step to generalize the techniques and results in this thesis to a Spin Foam model with Lorentzian signature. This is not straightforward since there is no holomorphic representation for SL(2,ℂ), hence we cannot write a Spin Foam model with a Gaussian measure in Lorentizan case. However, some techniques can be carried over: there has been new development of decomposing the amplitudes in gauge group SL(2,ℂ) into SU(2) intertwiners at the vertices and integrals over boosts at the edges [132]. The Riemannian case we have studied was a nice test ground, and we expect that the generic behavior of non-local coupling under coarse graining, together with the broken vertex translation symmetry for flat solutions will carry over to the Lorentzian case. One hope is that imposing causal structure in the Lorentzian signature might change the non-geometrical dominant behavior, result in a different phase with Riemannian case. For example, it has been shown in 4D Dynamical Triangulations that the Euclidean model suffers from only having a crumpled phase and branched polymer phase [133]. However, the inclusion of causal structure in the Lorentzian model extended the phase diagram by a genuinely four-dimensional de Sitter phase.

The analysis of dominant contribution to the partition function actually signals an ambiguous part at the fundamental construction of the Spin Foam framework. Originally, the partition function of a given boundary state was defined as a weighted sum of $Z(\Gamma)$: $Z(\partial\mathcal{M}) := \sum_{\Gamma} w(\Gamma)Z(\Gamma)$ and the weight $w(\Gamma)$ was suggested as a symmetry factor of the diagram. As this intuitive but naive summation would lead to melonic dominant phase, it is important to figure out what are the fundamental rules to determine the measure $w(\Gamma)$ of the graph space in the Spin Foam framework. This is also a crucial element for the study of renormalization in the summation approach.

Most importantly, there is the paradoxical situation we are facing: the residual gauge symmetry is not present in the model yet, and it is only expected to be recovered through renormalization. However, without properly gauge fixing, the divergence of the model leads to non-geometrical dominant phase of the partition function. Lack of precise residual gauge symmetry and the melonic-dominant phase are two sides of the same coin. It is worth rethinking the insights from canonical loop quantum gravity, and construct a path integral formalism that takes diffeomorphism invariance as a defining characteristic, rather than hoping to recover the gauge symmetry through renormalization.

Bibliography

[1] R. H. Brandenberger, "Lectures on the theory of cosmological perturbations," Lect. Notes Phys. **646**, 127 (2004) [hep-th/0306071].

[2] T. P. Hack, "On the Backreaction of Scalar and Spinor Quantum Fields in Curved Space-times," arXiv:1008.1776 [gr-qc].

[3] G. 't Hooft, "On the Quantum Structure of a Black Hole," Nucl. Phys. B **256**, 727 (1985). doi:10.1016/0550-3213(85)90418-3

[4] S. W. Hawking, M. J. Perry and A. Strominger, "Soft Hair on Black Holes," Phys. Rev. Lett. **116**, no. 23, 231301 (2016) doi:10.1103/PhysRevLett.116.231301 [arXiv:1601.00921 [hep-th]].

[5] S. W. Hawking, M. J. Perry and A. Strominger, "Superrotation Charge and Supertranslation Hair on Black Holes," arXiv:1611.09175 [hep-th].

[6] W. G. Unruh, "Notes on black hole evaporation," Phys. Rev. D **14**, 870 (1976). doi:10.1103/PhysRevD.14.870

[7] F. Cachazo, S. He and E. Y. Yuan, "Scattering of Massless Particles in Arbitrary Dimensions," Phys. Rev. Lett. **113**, no. 17, 171601 (2014) doi:10.1103/PhysRevLett.113.171601 [arXiv:1307.2199 [hep-th]].

[8] F. Cachazo, S. He and E. Y. Yuan, "Scattering of Massless Particles: Scalars, Gluons and Gravitons," JHEP **1407**, 033 (2014) doi:10.1007/JHEP07(2014)033 [arXiv:1309.0885 [hep-th]].

[9] M. H. Goroff and A. Sagnotti, "The Ultraviolet Behavior of Einstein Gravity," Nucl. Phys. B **266**, 709 (1986). doi:10.1016/0550-3213(86)90193-8

[10] A. Perez, "The Spin Foam Approach to Quantum Gravity," Living Rev. Rel. **16**, 3 (2013) [arXiv:1205.2019 [gr-qc]].

[11] E. Witten, "Anti-de Sitter space and holography," Adv. Theor. Math. Phys. **2**, 253 (1998) [hep-th/9802150].

[12] P. Kovtun, D. T. Son and A. O. Starinets, "Viscosity in strongly interacting quantum field theories from black hole physics," Phys. Rev. Lett. **94**, 111601 (2005) doi:10.1103/PhysRevLett.94.111601 [hep-th/0405231].

[13] F. Brnner, D. Parganlija and A. Rebhan, "Glueball Decay Rates in the Witten-Sakai-Sugimoto Model," Phys. Rev. D **91**, no. 10, 106002 (2015) Erratum: [Phys. Rev. D **93**, no. 10, 109903 (2016)] doi:10.1103/PhysRevD.93.109903, 10.1103/PhysRevD.91.106002 [arXiv:1501.07906 [hep-ph]].

[14] S. Ryu and T. Takayanagi, "Holographic derivation of entanglement entropy from AdS/CFT," Phys. Rev. Lett. **96**, 181602 (2006) doi:10.1103/PhysRevLett.96.181602 [hep-th/0603001].

[15] T. Faulkner, M. Guica, T. Hartman, R. C. Myers and M. Van Raamsdonk, "Gravitation from Entanglement in Holographic CFTs," JHEP **1403**, 051 (2014)

[16] S. Hossenfelder, "Experimental Search for Quantum Gravity," arXiv:1010.3420 [gr-qc].

[17] R. Gambini and J. Pullin, "Emergence of stringlike physics from Lorentz invariance in loop quantum gravity," Int. J. Mod. Phys. D **23**, no. 12, 1442023 (2014) doi:10.1142/S0218271814420231 [arXiv:1406.2610 [gr-qc]].

[18] D . M. T. Benincasa and F. Dowker, "The Scalar Curvature of a Causal Set," Phys. Rev. Lett. **104**, 181301 (2010) doi:10.1103/PhysRevLett.104.181301 [arXiv:1001.2725 [gr-qc]].

[19] G. Amelino-Camelia, L. Freidel, J. Kowalski-Glikman and L. Smolin, "The principle of relative locality," Phys. Rev. D **84**, 084010 (2011)

[20] L. Freidel, R. G. Leigh and D. Minic, "Metastring Theory and Modular Space-time," JHEP **1506**, 006 (2015) doi:10.1007/JHEP06(2015)006 [arXiv:1502.08005 [hep-th]].

[21] C. Rovelli and L. Smolin, "Loop Space Representation of Quantum General Relativity," Nucl. Phys. B **331**, 80 (1990). doi:10.1016/0550-3213(90)90019-A

[22] C. Rovelli and L. Smolin, Phys. Rev. D **52**, 5743 (1995) doi:10.1103/PhysRevD.52.5743 [gr-qc/9505006].

[23] C. Rovelli, "Quantum gravity," Cambridge University Press (2007)

[24] C. Rovelli, "Zakopane lectures on loop gravity," PoS QGQGS **2011**, 003 (2011) [arXiv:1102.3660 [gr-qc]].

[25] C. Rovelli and L. Smolin, Phys. Rev. Lett. **61**, 1155 (1988). doi:10.1103/PhysRevLett.61.1155

[26] T. Thiemann, "Modern canonical quantum general relativity," gr-qc/0110034.

[27] C. Rovelli and F. Vidotto, "Covariant Loop Quantum Gravity : An Elementary Introduction to Quantum Gravity and Spinfoam Theory," Cambridge Monographs on Mathematical Physics, Cambridge University Press, 2014

General Spin Foam

[28] G. Ponzano and T. Regge, "Semiclassical limit of Racah coefficients", Spectroscopic and group theoretical methods in physics (1968) p.1-58, ed. F. Bloch, North-Holland Publ. Co. (Amsterdam)

[29] M. P. Reisenberger and C. Rovelli, "'Sum over surfaces' form of loop quantum gravity," Phys. Rev. D **56**, 3490 (1997) doi:10.1103/PhysRevD.56.3490 [gr-qc/9612035].

[30] J. C. Baez, "Spin foam models," Class. Quant. Grav. **15**, 1827 (1998) doi:10.1088/0264-9381/15/7/004 [gr-qc/9709052].

[31] E. R. Livine, "The Spinfoam Framework for Quantum Gravity,"

[32] C. Rovelli, "The Basis of the Ponzano-Regge-Turaev-Viro-Ooguri quantum gravity model in the loop representation basis," Phys. Rev. D **48**, 2702 (1993) doi:10.1103/PhysRevD.48.2702 [hep-th/9304164].

[33] L. Crane, "Topological field theory as the key to quantum gravity," In *Riverside 1993, Proceedings, Knots and quantum gravity* 121-132 [hep-th/9308126].

[34] J. W. Barrett, "Quantum gravity as topological quantum field theory," J. Math. Phys. **36**, 6161 (1995) doi:10.1063/1.531239 [gr-qc/9506070].

[35] M. P. Reisenberger, gr-qc/9711052.

[36] L. Freidel and K. Krasnov, "Spin foam models and the classical action principle," Adv. Theor. Math. Phys. **2**, 1183 (1999) [hep-th/9807092].

[37] J. W. Barrett and L. Crane, "Relativistic spin networks and quantum gravity," J. Math. Phys. **39**, 3296 (1998) doi:10.1063/1.532254

[38] J. W. Barrett and L. Crane, "A Lorentzian signature model for quantum general relativity," Class. Quant. Grav. **17**, 3101 (2000) doi:10.1088/0264-9381/17/16/302 [gr-qc/9904025].

[39] A. Barbieri, "Quantum tetrahedra and simplicial spin networks," Nucl. Phys. B **518**, 714 (1998) doi:10.1016/S0550-3213(98)00093-5 [gr-qc/9707010].

[40] J. C. Baez and J. W. Barrett, "The Quantum tetrahedron in three-dimensions and four-dimensions," Adv. Theor. Math. Phys. **3**, 815 (1999) [gr-qc/9903060].

[41] J. Iwasaki, "A Lattice quantum gravity model with surface - like excitations in four-dimensional space-time," gr-qc/0006088.

[42] R. Gambini and J. Pullin, "A Finite spin foam-based theory of three-dimensional and four-dimensional quantum gravity," Phys. Rev. D **66**, 024020 (2002) doi:10.1103/PhysRevD.66.024020 [gr-qc/0111089].

[43] L. Freidel and K. Krasnov, "A New Spin Foam Model for 4d Gravity," Class. Quant. Grav. **25**, 125018 (2008) [arXiv:0708.1595 [gr-qc]].

[44] J. Engle, R. Pereira and C. Rovelli, "The Loop-quantum-gravity vertex-amplitude," Phys. Rev. Lett. **99**, 161301 (2007) [arXiv:0705.2388 [gr-qc]].

[45] J. Engle, R. Pereira and C. Rovelli, "Flipped spinfoam vertex and loop gravity," Nucl. Phys. B **798**, 251 (2008) [arXiv:0708.1236 [gr-qc]].

[46] J. Engle, E. Livine, R. Pereira and C. Rovelli, "LQG vertex with finite Immirzi parameter," Nucl. Phys. B **799**, 136 (2008) [arXiv:0711.0146 [gr-qc]].

[47] L. Smolin, "Linking topological quantum field theory and nonperturbative quantum gravity," J. Math. Phys. **36**, 6417 (1995) doi:10.1063/1.531251 [gr-qc/9505028].

[48] L. Smolin, "Quantum gravity with a positive cosmological constant," hep-th/0209079.

[49] V. G. Turaev and O. Y. Viro, "State sum invariants of 3 manifolds and quantum 6j symbols," Topology **31**, 865 (1992). doi:10.1016/0040-9383(92)90015-A

[50] M. Han, "Cosmological Constant in LQG Vertex Amplitude," Phys. Rev. D **84**, 064010 (2011) doi:10.1103/PhysRevD.84.064010 [arXiv:1105.2212 [gr-qc]].

[51] W. J. Fairbairn and C. Meusburger, "Quantum deformation of two four-dimensional spin foam models," J. Math. Phys. **53**, 022501 (2012) doi:10.1063/1.3675898 [arXiv:1012.4784 [gr-qc]].

[52] Y. Ding and M. Han, "On the Asymptotics of Quantum Group Spinfoam Model," arXiv:1103.1597 [gr-qc].

[53] M. Han, "4-dimensional Spin-foam Model with Quantum Lorentz Group," J. Math. Phys. **52**, 072501 (2011) doi:10.1063/1.3606592 [arXiv:1012.4216 [gr-qc]].

[54] H. M. Haggard, M. Han, W. Kaminski and A. Riello, "SL(2,C) Chern-Simons Theory, Flat Connections, and Four-dimensional Quantum Geometry," arXiv:1512.07690 [hep-th].

[55] E. Bianchi, E. Magliaro and C. Perini, "LQG propagator from the new spin foams," Nucl. Phys. B **822**, 245 (2009) doi:10.1016/j.nuclphysb.2009.07.016 [arXiv:0905.4082 [gr-qc]].

[56] C. Rovelli and F. Vidotto, "Planck stars," Int. J. Mod. Phys. D **23**, no. 12, 1442026 (2014) doi:10.1142/S0218271814420267 [arXiv:1401.6562 [gr-qc]].

[57] M. Christodoulou, C. Rovelli, S. Speziale and I. Vilensky, "Planck star tunneling time: An astrophysically relevant observable from background-free quantum gravity," Phys. Rev. D **94**, no. 8, 084035 (2016) doi:10.1103/PhysRevD.94.084035 [arXiv:1605.05268 [gr-qc]].

[58] A. Barrau, B. Bolliet, F. Vidotto and C. Weimer, "Phenomenology of bouncing black holes in quantum gravity: a closer look," JCAP **1602**, no. 02, 022 (2016) doi:10.1088/1475-7516/2016/02/022 [arXiv:1507.05424 [gr-qc]].

[59] E. Bianchi, C. Rovelli and F. Vidotto, "Towards Spinfoam Cosmology," Phys. Rev. D **82**, 084035 (2010) doi:10.1103/PhysRevD.82.084035 [arXiv:1003.3483 [gr-qc]].

[60] B. Dittrich, "Diffeomorphism symmetry in quantum gravity models," Adv. Sci. Lett. **2**, 151 doi:10.1166/asl.2009.1022 [arXiv:0810.3594 [gr-qc]].

[61] B. Bahr and B. Dittrich, "(Broken) Gauge Symmetries and Constraints in Regge Calculus," Class. Quant. Grav. **26**, 225011 (2009) doi:10.1088/0264-9381/26/22/225011 [arXiv:0905.1670 [gr-qc]].

[62] B. Dittrich, "The continuum limit of loop quantum gravity - a framework for solving the theory," arXiv:1409.1450 [gr-qc].

[63] M. X. Han and M. Zhang, "Asymptotics of Spinfoam Amplitude on Simplicial Manifold: Euclidean Theory," Class. Quant. Grav. **29**, 165004 (2012) [arXiv:1109.0500 [gr-qc]].

[64] M. Han and M. Zhang, "Asymptotics of Spinfoam Amplitude on Simplicial Manifold: Lorentzian Theory," Class. Quant. Grav. **30**, 165012 (2013) doi:10.1088/0264-9381/30/16/165012 [arXiv:1109.0499 [gr-qc]].

[65] M. Han and T. Krajewski, "Path Integral Representation of Lorentzian Spinfoam Model, Asymptotics, and Simplicial Geometries," Class. Quant. Grav. **31**, 015009 (2014) doi:10.1088/0264-9381/31/1/015009 [arXiv:1304.5626 [gr-qc]].

[66] M. Han, "On Spinfoam Models in Large Spin Regime," Class. Quant. Grav. **31**, 015004 (2014) doi:10.1088/0264-9381/31/1/015004 [arXiv:1304.5627 [gr-qc]].

[67] M. Han, "Semiclassical Analysis of Spinfoam Model with a Small Barbero-Immirzi Parameter," Phys. Rev. D **88**, 044051 (2013) doi:10.1103/PhysRevD.88.044051 [arXiv:1304.5628 [gr-qc]].

[68] U. Pachner, "P.L. homeomorphic manifolds are equivalent by elementary shellings," European Journal of Combinatorics 12 (2), 129145 (1991)

[69] E. R. Livine and J. Tambornino, "Holonomy Operator and Quantization Ambiguities on Spinor Space," Phys. Rev. D **87**, no. 10, 104014 (2013) [arXiv:1302.7142 [gr-qc]].

[70] F. Hellmann and W. Kaminski, "Holonomy spin foam models: Asymptotic geometry of the partition function," JHEP **1310**, 165 (2013) doi:10.1007/JHEP10(2013)165 [arXiv:1307.1679 [gr-qc]].

[71] K. G. Wilson, "Confinement of Quarks," Phys. Rev. D **10**, 2445 (1974). doi:10.1103/PhysRevD.10.2445

[72] T. Regge, "General Relativity Without Coordinates," Nuovo Cim. **19**, 558 (1961). doi:10.1007/BF02733251

[73] M. Rocek and R. M. Williams, "Quantum Regge Calculus," Phys. Lett. **104B**, 31 (1981). doi:10.1016/0370-2693(81)90848-0

[74] C. Perini, C. Rovelli and S. Speziale, "Self-energy and vertex radiative corrections in LQG," Phys. Lett. B **682**, 78 (2009) [arXiv:0810.1714 [gr-qc]].

[75] T. Krajewski, J. Magnen, V. Rivasseau, A. Tanasa and P. Vitale, "Quantum Corrections in the Group Field Theory Formulation of the EPRL/FK Models," Phys. Rev. D **82**, 124069 (2010) doi:10.1103/PhysRevD.82.124069 [arXiv:1007.3150 [gr-qc]].

[76] A. Riello, "Self-energy of the Lorentzian Engle-Pereira-Rovelli-Livine and Freidel-Krasnov model of quantum gravity," Phys. Rev. D **88**, no. 2, 024011 (2013) [arXiv:1302.1781 [gr-qc]].

[77] L. Freidel and D. Louapre, "Ponzano-Regge model revisited II: Equivalence with Chern-Simons," gr-qc/0410141.

[78] J. W. Barrett and I. Naish-Guzman, "The Ponzano-Regge model and Reidemeister torsion," gr-qc/0612170.

[79] V. Bonzom and M. Smerlak, "Bubble divergences from cellular cohomology," Lett. Math. Phys. **93**, 295 (2010) [arXiv:1004.5196 [gr-qc]].

[80] V. Bonzom and M. Smerlak, "Bubble divergences: sorting out topology from cell structure," Annales Henri Poincare **13**, 185 (2012) [arXiv:1103.3961 [gr-qc]].

[81] L. Freidel, R. Gurau and D. Oriti, "Group field theory renormalization - the 3d case: Power counting of divergences," Phys. Rev. D **80**, 044007 (2009) [arXiv:0905.3772 [hep-th]].

[82] S. Carrozza and D. Oriti, "Bounding bubbles: the vertex representation of 3d Group Field Theory and the suppression of pseudo-manifolds," Phys. Rev. D **85**, 044004 (2012) doi:10.1103/PhysRevD.85.044004 [arXiv:1104.5158 [hep-th]].

[83] A. Baratin, L. Freidel and R. Gurau, "Weighting bubbles in group field theory," Phys. Rev. D **90**, no. 2, 024069 (2014) doi:10.1103/PhysRevD.90.024069 [arXiv:1405.2808 [hep-th]].

[84] S. Carrozza and D. Oriti, "Bubbles and jackets: new scaling bounds in topological group field theories," JHEP **1206**, 092 (2012) doi:10.1007/JHEP06(2012)092 [arXiv:1203.5082 [hep-th]].

[85] A. Baratin, S. Carrozza, D. Oriti, J. Ryan and M. Smerlak, "Melonic phase transition in group field theory," Lett. Math. Phys. **104**, 1003 (2014) doi:10.1007/s11005-014-0699-9 [arXiv:1307.5026 [hep-th]].

[86] R. Gurau, "The 1/N expansion of colored tensor models," Annales Henri Poincare **12**, 829 (2011) doi:10.1007/s00023-011-0101-8 [arXiv:1011.2726 [gr-qc]].

[87] R. Gurau, "The complete 1/N expansion of colored tensor models in arbitrary dimension," Annales Henri Poincare **13**, 399 (2012) doi:10.1007/s00023-011-0118-z [arXiv:1102.5759 [gr-qc]].

[88] R. Gurau and V. Rivasseau, "The 1/N expansion of colored tensor models in arbitrary dimension," Europhys. Lett. **95**, 50004 (2011) doi:10.1209/0295-5075/95/50004 [arXiv:1101.4182 [gr-qc]].

[89] V. Bonzom, R. Gurau, A. Riello and V. Rivasseau, "Critical behavior of colored tensor models in the large N limit," Nucl. Phys. B **853**, 174 (2011) doi:10.1016/j.nuclphysb.2011.07.022 [arXiv:1105.3122 [hep-th]].

[90] R. Gurau and J. P. Ryan, "Colored Tensor Models - a review," SIGMA **8**, 020 (2012) doi:10.3842/SIGMA.2012.020 [arXiv:1109.4812 [hep-th]].

[91] R. Gurau and J. P. Ryan, "Melons are branched polymers," Annales Henri Poincare **15**, no. 11, 2085 (2014) doi:10.1007/s00023-013-0291-3 [arXiv:1302.4386 [math-ph]].

[92] D. Gabrielli, "Polymeric phase of simplicial quantum gravity," Phys. Lett. B **421**, 79 (1998) doi:10.1016/S0370-2693(98)00022-7 [hep-lat/9710055].

[93] L. Freidel and D. Louapre, "Diffeomorphisms and spin foam models," Nucl. Phys. B **662**, 279 (2003) [gr-qc/0212001].

[94] A. Baratin and L. Freidel, "Hidden Quantum Gravity in 4-D Feynman diagrams: Emergence of spin foams," Class. Quant. Grav. **24**, 2027 (2007) doi:10.1088/0264-9381/24/8/007 [hep-th/0611042].

[95] V. Bonzom and B. Dittrich, "Bubble divergences and gauge symmetries in spin foams," Phys. Rev. D **88**, 124021 (2013) doi:10.1103/PhysRevD.88.124021 [arXiv:1304.6632 [gr-qc]].

[96] B. Dittrich and S. Steinhaus, "Path integral measure and triangulation independence in discrete gravity," Phys. Rev. D **85**, 044032 (2012) [arXiv:1110.6866 [gr-qc]].

[97] B. Dittrich, W. KamiÅski and S. Steinhaus, "Discretization independence implies non-locality in 4D discrete quantum gravity," Class. Quant. Grav. **31**, no. 24, 245009 (2014) doi:10.1088/0264-9381/31/24/245009 [arXiv:1404.5288 [gr-qc]].

[98] B. Bahr and B. Dittrich, "Breaking and restoring of diffeomorphism symmetry in discrete gravity," AIP Conf. Proc. **1196**, 10 (2009)

[99] R. Oeckl, "Renormalization for spin foam models of quantum gravity," In *Rio de Janeiro 2003, Recent developments in theoretical and experimental general relativity, gravitation, and relativistic field theories, pt. C* 2296-2300 [gr-qc/0401087].

[100] R. Oeckl, "Renormalization of discrete models without background," Nucl. Phys. B **657**, 107 (2003) [gr-qc/0212047].

[101] B. Bahr, B. Dittrich and S. Steinhaus, "Perfect discretization of reparametrization invariant path integrals," Phys. Rev. D **83**, 105026 (2011) doi:10.1103/PhysRevD.83.105026 [arXiv:1101.4775 [gr-qc]].

[102] B. Dittrich, "From the discrete to the continuous: Towards a cylindrically consistent dynamics," New J. Phys. **14**, 123004 (2012) [arXiv:1205.6127 [gr-qc]].

[103] B. Bahr, "On background-independent renormalization of spin foam models," arXiv:1407.7746 [gr-qc].

[104] B. Dittrich, L. Freidel and S. Speziale, "Linearized dynamics from the 4-simplex Regge action," Phys. Rev. D **76**, 104020 (2007) doi:10.1103/PhysRevD.76.104020

[105] A. Banburski, L. Q. Chen, L. Freidel and J. Hnybida, "Pachner moves in a 4d Riemannian holomorphic Spin Foam model," Phys. Rev. D **92**, no. 12, 124014 (2015) doi:10.1103/PhysRevD.92.124014 [arXiv:1412.8247 [gr-qc]].

[106] A. Banburski and L. Q. Chen, "A simpler way of imposing simplicity constraints," arXiv:1512.05331 [gr-qc].

[107] L. Q. Chen, "Bulk amplitude and degree of divergence in 4d spin foams," Phys. Rev. D **94**, no. 10, 104025 (2016) doi:10.1103/PhysRevD.94.104025 [arXiv:1602.01825 [gr-qc]].

[108] E.R. Livine and S. Speziale, "A new spinfoam vertex for quantum gravity", Phys.Rev.D76 (2007) 084028 [arXiv:0705.0674]

[109] E. R. Livine and S. Speziale, "Consistently Solving the Simplicity Constraints for Spinfoam Quantum Gravity," Europhys. Lett. **81**, 50004 (2008) [arXiv:0708.1915 [gr-qc]].

[110] L. Freidel, K. Krasnov and E. R. Livine, "Holomorphic Factorization for a Quantum Tetrahedron," Commun. Math. Phys. **297**, 45 (2010) [arXiv:0905.3627 [hep-th]].

[111] L. Freidel and E. R. Livine, "The Fine Structure of SU(2) Intertwiners from U(N) Representations," J. Math. Phys. **51**, 082502 (2010) [arXiv:0911.3553 [gr-qc]].

[112] L. Freidel and E. R. Livine, "U(N) Coherent States for Loop Quantum Gravity," J. Math. Phys. **52**, 052502 (2011) [arXiv:1005.2090 [gr-qc]].

[113] M. Dupuis and E. R. Livine, "Revisiting the Simplicity Constraints and Coherent Intertwiners," Class. Quant. Grav. **28**, 085001 (2011) [arXiv:1006.5666 [gr-qc]].

[114] E. F. Borja, L. Freidel, I. Garay and E. R. Livine, "U(N) tools for Loop Quantum Gravity: The Return of the Spinor," Class. Quant. Grav. **28**, 055005 (2011) [arXiv:1010.5451 [gr-qc]].

[115] M. Dupuis and E. R. Livine, "Holomorphic Simplicity Constraints for 4d Spinfoam Models," Class. Quant. Grav. **28**, 215022 (2011) [arXiv:1104.3683 [gr-qc]].

[116] E. R. Livine and J. Tambornino, "Spinor Representation for Loop Quantum Gravity," J. Math. Phys. **53**, 012503 (2012) [arXiv:1105.3385 [gr-qc]].

[117] M. Dupuis, L. Freidel, E. R. Livine and S. Speziale, "Holomorphic Lorentzian Simplicity Constraints," J. Math. Phys. **53**, 032502 (2012) [arXiv:1107.5274 [gr-qc]].

[118] M. Dupuis and E. R. Livine, "Holomorphic Simplicity Constraints for 4d Riemannian Spinfoam Models," J. Phys. Conf. Ser. **360**, 012046 (2012) [arXiv:1111.1125 [gr-qc]].

[119] M. Dupuis, S. Speziale and J. Tambornino, "Spinors and Twistors in Loop Gravity and Spin Foams," PoS QGQGS **2011**, 021 (2011) [arXiv:1201.2120 [gr-qc]].

[120] B. Dittrich and S. Speziale, "Area-angle variables for general relativity," New J. Phys. **10**, 083006 (2008) doi:10.1088/1367-2630/10/8/083006 [arXiv:0802.0864 [gr-qc]].

[121] L. Freidel and J. Hnybida, "On the exact evaluation of spin networks," J. Math. Phys. **54**, 112301 (2013) doi:10.1063/1.4830008 [arXiv:1201.3613 [gr-qc]].

[122] L. Freidel and J. Hnybida, "A Discrete and Coherent Basis of Intertwiners," Class. Quant. Grav. **31**, 015019 (2014) doi:10.1088/0264-9381/31/1/015019 [arXiv:1305.3326 [math-ph]].

[123] J. Hnybida, "Generating Functionals for Spin Foam Amplitudes," PhD Thesis, arXiv:1411.2049 [math-ph].

[124] L. Freidel, "Group field theory: An Overview," Int. J. Theor. Phys. **44**, 1769 (2005) doi:10.1007/s10773-005-8894-1 [hep-th/0505016].

[125] D. Oriti, "The Group field theory approach to quantum gravity," In *Oriti, D. (ed.): Approaches to quantum gravity* 310-331 [gr-qc/0607032].

[126] F. Conrady and L. Freidel, "On the semiclassical limit of 4d spin foam models," Phys. Rev. D **78**, 104023 (2008) [arXiv:0809.2280 [gr-qc]].

[127] J. W. Barrett, R. J. Dowdall, W. J. Fairbairn, H. Gomes and F. Hellmann, "Asymptotic analysis of the EPRL four-simplex amplitude," J. Math. Phys. **50**, 112504 (2009) [arXiv:0902.1170 [gr-qc]].

[128] V. Bargmann, "On the Representations of the Rotation Group," Rev. Mod. Phys. **34**, 829 (1962).

[129] J. Schwinger, "On Angular Momentum," U.S. Atomic Energy Commission. (unpublished) NYO-3071, (1952).

[130] W. Kocay, D.L. Kreher, "Graphs, Algorithms, and Optimization, Discrete Mathematics and Its Applications", CRC Press (2004).

[131] L. Freidel and E. R. Livine, "Spin networks for noncompact groups," J. Math. Phys. **44**, 1322 (2003) [hep-th/0205268].

[132] S. Speziale, "Boosting Wigners nj-symbols," J. Math. Phys. **58**, no. 3, 032501 (2017) doi:10.1063/1.4977752 [arXiv:1609.01632 [gr-qc]].

[133] A. Gorlich, "Causal Dynamical Triangulations in Four Dimensions," arXiv:1111.6938 [hep-th].

[134] F. W. J. Olver, D. W. Lozier, R. F. Boisvert, and C. W. Clark, editors. NIST Handbook of Mathematical Functions. Cambridge University Press, New York, NY, 2010. Print companion to [DLMF].

Appendices

Appendix A

A.1 Gaussian integration

In this appendix we compile a list of useful Gaussian spinor integrals. Consider first a standard Gaussian integral over the complex line $\mathbb{C}$

$$\int_{\mathbb{C}} \frac{\mathrm{d}^2\alpha}{\pi^2} e^{-|\alpha|^2 + \bar{x}\alpha + y\bar{\alpha}} = e^{\bar{x}y}. \tag{A.1}$$

This easily generalizes to a Gaussian integration over spinors on $\mathbb{C}^2$ with the Bargmann measure $\mathrm{d}\mu(z) = \pi^{-2} e^{-\langle z|z\rangle} \mathrm{d}^4 z$ giving us the integral that allows us to contract strands on cable graphs

$$\int_{\mathbb{C}^2} \mathrm{d}\mu(z) e^{\langle x|z\rangle + \langle z|y\rangle} = e^{\langle x|y\rangle}. \tag{A.2}$$

It is interesting to note that this contraction also works with anti-holomorphic spinors $|z]$, since $[x|y] = \langle y|x\rangle$. We have thus

$$\int_{\mathbb{C}^2} \mathrm{d}\mu(z) e^{\langle x|z] + [z|y\rangle} = e^{\langle x|y\rangle}. \tag{A.3}$$

As with usual Gaussian integrations, we can calculate Gaussian spinor integrals of arbitrary polynomials. The special case worth mentioning is of course how delta function acts on holomorphic functions

$$\int_{\mathbb{C}^2} \mathrm{d}\mu(z) f(z) e^{\langle z|w\rangle} = f(w). \tag{A.4}$$

Let us now consider the integrals that are crucial to the computations in the thesis – integrals with a matrix A. First consider the more familiar case of integrals over vectors of n complex numbers

$$\int_{\mathbb{C}^n} \prod_{i=1}^{n} \frac{\mathrm{d}^2\alpha_i}{\pi^2} e^{-\sum_{i,j} \bar{\alpha}_i . A_{ij}\alpha_j} = \frac{1}{\det(A)} \tag{A.5}$$

This again trivially extends to the integrals over spinors. The expression useful for our thesis is

$$\int_{\mathbb{C}^{2n}} \prod_{i=1}^{n} d\mu(z_i) e^{\sum_{i,j} \langle z_i | A_{ij} | z_j \rangle} = \frac{1}{\det(\mathbb{1} - A)}. \tag{A.6}$$

Recall that for the constrained model we had to change the measure of integration over spinors to $d\mu_\rho(z) = (1 + \rho^2)^2 \pi^{-2} e^{-(1+\rho^2)\langle z | z \rangle} d^4 z$. It is easy to check that this is normalized properly as

$$\int_{\mathbb{C}^2} \frac{(1 + \rho^2)^2 d^4 z}{\pi^2} e^{-(1+\rho^2)\langle z | z \rangle} = 1. \tag{A.7}$$

This change of measure leads to very simple changes to the above integrals. In particular, for a contraction we have

$$\int_{\mathbb{C}^2} d\mu_\rho(z) e^{\langle x | z \rangle + \langle z | y \rangle} = e^{(1+\rho^2)^{-1} \langle x | y \rangle}. \tag{A.8}$$

Hence for every contraction of spinors we pick up a factor of $1/(1 + \rho^2)$. Thus for a loop on which we have three spinors we get the factor of $(1 + \rho^2)^{-3}$ – this appears all the time in loop identity and Pachner moves calculations.

A.2 Mapping SU(2) to spinors

Lemma A.2.1. *Let $f \in L^2(SU(2))$ be homogeneous of degree $2J$, i.e. $f(\lambda g) = \lambda^{2J} f(g)$. Given a spinor by $|z\rangle$ define $g(z) = (|0\rangle\langle 0| + |0][0|)g(z) = |0\rangle\langle z| + |0][z|$ where $|0\rangle = (1, 0)^t$. Then*

$$\int_{\mathbb{C}^2} d\mu(z) f(g(z)) = \Gamma(J + 2) \int_{SU(2)} dg\, f(g). \tag{A.9}$$

Proof. We can relate the inner product (3.1) to the standard $L^2(SU(2))$ inner product by parametrizing the spinor as

$$|z\rangle = \begin{pmatrix} r \cos\theta e^{i\phi} \\ r \sin\theta e^{i\psi} \end{pmatrix}, \tag{A.10}$$

where $r \in (0, \infty)$, $\theta \in [0, \pi/2)$, $\phi \in [0, 2\pi)$, $\psi \in [0, 2\pi)$. The Lebesgue measure in these coordinates is $d^4 z = r^3 \sin\theta \cos\theta dr\, d\phi\, d\theta\, d\psi$. Now using the homogeneity property $f(g(z)) = r^{2J} f(\widetilde{g}(z))$ we have

$$\int_{\mathbb{C}^2} d\mu(z) f(g(z)) = \int_0^\infty dr\, r^{3+2j} e^{-r^2} \int_0^{\pi/2} d\theta \sin\theta \cos\theta \int_0^{2\pi} d\phi \int_0^{2\pi} d\psi\, f(\widetilde{g}(z)), \tag{A.11}$$

111

where $\widetilde{g}(z) \in SU(2)$. Performing the intgral over r we get

$$\int dr\, r^{3+2J} e^{-r^2} = \frac{1}{2}\Gamma(J+2) \qquad (A.12)$$

and so

$$\int_{\mathbb{C}^2} d\mu(z) f(g(z)) = \Gamma(J+2) \int_{SU(2)} dg\, f(g), \qquad (A.13)$$

where dg is the normalized Haar measure on $SU(2)$. In our case J is an integer so $\Gamma(J+2) = (J+1)!$. $\square$

A.3 Group averaging the SU(2) projector

In this appendix we recall the calculation in [121] which shows that we can perform the integration over g explicitly for the BF projector (3.13), which we prove in the following theorem.

Theorem A.3.1. *The projector (3.13) can be expressed as a power series in the holomorphic spinor invariants as*

$$P(z_i; w_i) = \sum_{[k]} \frac{1}{(J+1)!} \prod_{i<j} \frac{([z_i|z_j\rangle[w_i|w_j\rangle)^{k_{ij}}}{k_{ij}!}. \qquad (A.14)$$

where the sum is over sets of $n(n-1)/2$ non-negative integers k_{ij} with $1 \le i < j \le n$.

Proof. Expanding (3.13) in a power series

$$\int_{SU(2)} dg\, e^{[z_i|g|w_i\rangle} = \sum_{j_i} \int dg \prod_i \frac{[z_i|g|w_i\rangle^{2j_i}}{(2j_i)!}, \qquad (A.15)$$

we see that each term in the sum is homogeneous of degree $2J = \sum_i(2j_i)$. This fact allows us to use Lemma A.2.1 detailed in Appendix A.2 which says that we can replace the integral over $SU(2)$ with a Gaussian integral paying a factor of $1/(J+1)!$ as in

$$(J+1)! \int dg \prod_i \frac{[z_i|g|w_i\rangle^{2j_i}}{(2j_i)!} = \int d\mu(\alpha) \prod_i \frac{([z_i|0\rangle\langle\alpha|w_i\rangle + [z_i|0][\alpha|w_i\rangle)^{2j_i}}{(2j_i)!}. \qquad (A.16)$$

Now resum over j_i to get

$$\sum_{j_i}(J+1)! \int dg \prod_i \frac{[z_i|g|w_i\rangle^{2j_i}}{(2j_i)!} = \int d\mu(\alpha) e^{\sum_i([z_i|0\rangle\langle\alpha|w_i\rangle + [z_i|0][\alpha|w_i\rangle)} = e^{\sum_{i,j}[z_i|0][0|z_j\rangle[w_i|w_j\rangle}, \qquad (A.17)$$

112

where we've performed the Gaussian integration in the second equality. Using the antisymmetry $[w_i|w_j\rangle = -[w_j|w_i\rangle$ and recognizing the identity $1 = |0\rangle\langle 0| + |0][0|$ in

$$\sum_{i,j}[z_i|0][0|z_j\rangle[w_i|w_j\rangle = \sum_{i<j}[z_i\,(|0\rangle\langle 0| + |0][0|)\,|z_j\rangle[w_i|w_j\rangle = \sum_{i<j}[z_j|z_i\rangle[w_i|w_j\rangle. \qquad (A.18)$$

Finally we have

$$\sum_{j_i}(J+1)! \int dg \prod_i \frac{[z_i|g|w_i\rangle^{2j_i}}{(2j_i)!} = e^{\sum_{i<j}[z_j|z_i\rangle[w_i|w_j\rangle} = \sum_{[k]}\prod_{i<j}\frac{([z_i|z_j\rangle[w_i|w_j\rangle)^{k_{ij}}}{k_{ij}!} \qquad (A.19)$$

and since $J = \sum_{i<j}k_{ij}$ is just the total homogeneity of each term we can move the $(J+1)!$ to the RHS and complete the proof. $\qquad\square$

A.4   Proof of Lemma (4.4.1)

Proof. For a 2×2 matrix $2\det M = \text{Tr}(M)^2 - \text{Tr}(M^2)$. If one consider $M = \mathbb{1} - \sum_i C_i|A_i\rangle[B_i|$, we have

$$\text{Tr}(M^2) = 2 - 2\sum_i C_i[B_i|A_i\rangle + \sum_{i,j} C_iC_j[B_i|A_j\rangle[B_j|A_i\rangle$$

and

$$\text{Tr}(M)^2 = 4 - 4\sum_i C_i[B_i|A_i\rangle + \sum_{i,j} C_iC_j[B_i|A_i\rangle[B_j|A_j\rangle,$$

therefore

$$2\det(M) = 2 - 2\sum_i C_i[B_i|A_i\rangle + \sum_{i,j} C_iC_j\left([B_i|A_i\rangle[B_j|A_j\rangle - [B_i|A_j\rangle[B_j|A_i\rangle\right)$$

and using $[A_i|B_i\rangle[B_j|A_j\rangle - [A_i|B_j\rangle[B_i|A_j\rangle = [A_i|A_j\rangle[B_j|B_i\rangle$ gives the result. $\qquad\square$

Appendix B

Explicit calculation of the constrained loop identity

In this appendix we explicitly show how to calculate the constrained loop identity (4.32). Let us consider the loop composed of two pairs of partially gauge-fixed propagators $\mathbb{1}_\rho \circ \mathbb{1}_\rho$ and one pair of propagators $P_\rho \circ P_\rho$. To calculate this loop, let us use the homogenized propagators $\mathbb{1}_{\tilde{\tau}} \circ \mathbb{1}_{\tilde{\tau}}$ and $G_\tau \circ G_\tau$ instead and at the end of the calculation use the homogeneity maps (4.30) and (4.31), which we recall are given by

$$\mathbb{1}_{\tilde{\tau}} \circ \mathbb{1}_{\tilde{\tau}} = e^{\tilde{\tau} \sum_i [\tilde{z}_i | \tilde{w}_i\rangle} \quad \text{with} \quad \tilde{\tau}^J \to \frac{F_\rho(J/2)^2}{(1+\rho^2)^J} \quad \text{for} \quad \mathbb{1}_{\tilde{\tau}} \circ \mathbb{1}_{\tilde{\tau}} \to \mathbb{1}_\rho \circ \mathbb{1}_\rho$$

for a pair of gauge-fixed propagators and by

$$G_\tau \circ G_\tau = e^{\tau \sum_{i<j} [z_i|z_j\rangle[w_i|w_j\rangle} \quad \text{with} \quad \tau^J \to \frac{F_\rho(J)^2}{(1+\rho^2)^{2J}(J+1)!} \quad \text{for} \quad G_\tau \circ G_\tau \to P_\rho \circ P_\rho.$$

for the pair of propagators P_ρ. We will also insert a face weight by tracking the homogeneity of spin in the loop by a factor of τ'. The contractions of the spinors around the loop are as follows: $|w_4\rangle = |\tilde{w}_4^2]$, $|\tilde{z}_4^2\rangle = |\tilde{z}_4^1]$ and $|\tilde{w}_4^1\rangle = |z_4]$. The cable diagram with all the labels is shown in Fig. B.1.
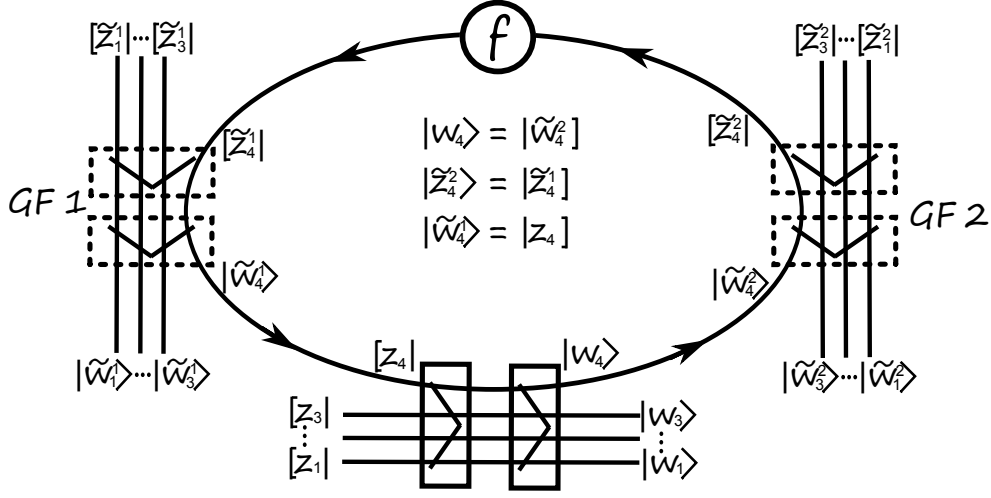
Figure B.1: Cable diagram with all the labels for the constrained loop identity.

We can thus finally calculate the loop identity:

$$\int d\mu_\rho(z_4, w_4, \tilde{z}_4^1) G_\tau^2(z_1, \ldots, \tau' z_4; w_1, \ldots, \check{w}_4^2) \mathbb{1}_{\tilde{\tau}_1}^2(\tilde{z}_1^1, \ldots, \tilde{z}_4^1; \tilde{w}_1^1, \ldots, \check{z}_4) \mathbb{1}_{\tilde{\tau}_2}^2(\tilde{z}_1^2, \ldots, \check{z}_4^1; \tilde{w}_1^2, \ldots, \tilde{w}_4^2)$$

$$= \frac{e^{\tau \sum_{i<j<4}[z_i|z_j\rangle[w_i|w_j\rangle + \sum_{i<4} \tilde{\tau}_1[\tilde{z}_i^1|\tilde{w}_i^1\rangle + \tilde{\tau}_2[\tilde{z}_i^2|\tilde{w}_i^2\rangle}}{1 - \frac{\tau\tilde{\tau}_1\tilde{\tau}_2\tau'}{(1+\rho^2)^3} \sum_{i<4}[z_i|w_i\rangle + \left(\frac{\tau\tilde{\tau}_1\tilde{\tau}_2\tau'}{(1+\rho^2)^3}\right)^2 \sum_{i<j<4}[z_i|z_j\rangle[w_i|w_j\rangle}$$

$$= \exp\left(\tau \sum_{i<j<4}[z_i|z_j\rangle[w_i|w_j\rangle + \sum_{i<4} \tilde{\tau}_1[\tilde{z}_i^1|\tilde{w}_i^1\rangle + \tilde{\tau}_2[\tilde{z}_i^2|\tilde{w}_i^2\rangle\right) \times$$

$$\times \sum_{N,M} \frac{(N+M)!}{N!M!} \left(\frac{\tau\tilde{\tau}_1\tilde{\tau}_2\tau'}{(1+\rho^2)^3}\right)^{N+2M} \left(\sum_{i<4}[z_i|w_i\rangle\right)^N \left(-\sum_{i<j<4}[z_i|z_j\rangle[w_i|w_j\rangle\right)^M .$$

The factor of $1/(1+\rho^2)^3$ arises from the three spinor integrations. Compared to the toy loop, the result is thus an exchange of $\frac{\tau\tau'}{1+\rho^2} \to \frac{\tau\tilde{\tau}_1\tilde{\tau}_2\tau'}{(1+\rho^2)^3}$ and the addition of the trivial propagation of the gauge-fixed strands. Before we can use the homogeneity maps we have to expand the exponentials in a power series. Doing this we arrive at

$$\sum_{A,B,C,M,N} \frac{(-1)^M(N+M)!}{A!B!C!M!N!} \left(\frac{\tau\tilde{\tau}_1\tilde{\tau}_2\tau'}{(1+\rho^2)^3}\right)^{N+2M} \tilde{\tau}_1^A \tilde{\tau}_2^B \tau^C \times$$

$$\times \left(\sum_{i<4}[\tilde{z}_i^1|\tilde{w}_i^1\rangle\right)^A \left(\sum_{i<4}[\tilde{z}_i^2|\tilde{w}_i^2\rangle\right)^B \left(\sum_{i<4}[z_i|w_i\rangle\right)^N \left(\sum_{i<j<4}[z_i|z_j\rangle[w_i|w_j\rangle\right)^{M+C} .$$

115

Relabeling $N \rightarrow J$ and $M + C \rightarrow J'$ and using the above homogeneity maps for $\tau, \tilde{\tau}_1, \tilde{\tau}_2$ and $\tau'^{2j} \rightarrow (2j+1)^{\eta}$, we recover the result for the constrained loop identity (4.32).

Appendix C

The asymptotics of certain types of the hypergeometrical functions and the modified Bessel functions

The hypergeometric function has asymptotic formula [134] :

$$
\begin{aligned}
{}_2F_1(a + \lambda, \ b - \lambda; \ c; \ \frac{1}{2} - \frac{1}{2}u) = \\
2^{(a+b-1)/2} \sqrt{\zeta \sinh \zeta} \ (\lambda + \frac{a}{2} - \frac{b}{2})^{1-c} \ \frac{(u+1)^{(c-a-b-1)/2}}{(u-1)^{c/2}} \times \\
\times [I_{c-1}\left(\zeta(\lambda + \frac{a}{2} - \frac{b}{2})\right)(1 + O(\lambda^{-2})) + \\
+ \frac{I_{c-2}\left(\zeta(\lambda + a/2 - b/2)\right)}{2\lambda + a - b} \ ((c - \frac{1}{2}) \ (c - \frac{3}{2})(\frac{1}{\zeta} - \coth \zeta) + \\
+ \frac{1}{2}(2c - a - b - 1)(a + b - 1) \tanh \frac{\zeta}{2} + O(\lambda^{-2}))], \\
\text{for } |\arg (u - 1)| < \pi, \ \lambda \to \infty
\end{aligned}
\tag{C.1}
$$

where $\zeta \equiv \cosh^{-1} u$.

Together with Pfaff transformation:

$$
{}_2F_1(a, b; c; u) = (1 - u)^{-b} \cdot {}_2F_1(b, c - a; c; \frac{u}{u - 1})
\tag{C.2}
$$

we can get that for $0 < \rho < 1$,

$$
\begin{aligned}
{}_2F_1(-J-1, -J; 2; \rho^4) = \\
\frac{(1-\rho^4)^{J+3/2}}{4\sqrt{2}\,\rho^5\,\zeta^{1/2}\,(3+2J)^2} \Big[I_1\Big(\big(\tfrac{3}{2}+J\big)\zeta\Big) \cdot (8\zeta\,\rho^2\,(3+2J) + O(J^{-2})) - \\
- 3I_0\Big(\big(\tfrac{3}{2}+J\big)\zeta\Big) \cdot (\zeta\,(1+\rho^4) - 2\rho^2 + O(J^{-2}))\Big], \qquad J \to \infty
\end{aligned}
\tag{C.3}
$$

where

$$
\zeta \equiv \cosh^{-1}\left(\frac{1+\rho^4}{1-\rho^4}\right)
\tag{C.4}
$$

The asymptotic expansion of hypergeometric function involves the modified Bessel function of the first kind[134] :

$$
I_\nu(\omega) = \sum_{k=0}^{\infty} \frac{(\tfrac{1}{2}\omega)^{2k+\nu}}{k!\,\Gamma(\nu+k+1)}, \quad \omega \in \mathbb{C}
\tag{C.5}
$$

which is one of the two linearly independent solutions of the modified Bessel's Equation. $I_\nu(\omega)$ enjoys the asymptotic expansion:

$$
I_\nu(\omega) = \frac{e^\omega}{\sqrt{2\pi\omega}}\left(1 - \frac{4\nu^2 - 1}{8\omega} + O(\omega^{-2})\right), \text{ for } |\arg \omega| < \frac{\pi}{2},\ |\omega| \to \infty
\tag{C.6}
$$

Thus Eq.(C.3) together with Eq.(C.6), we get

$$
\begin{aligned}
{}_2F_1(-J-1, -J; 2; \rho^4) = \\
\frac{e^{(\tfrac{3}{2}+J)\zeta}\,(1-\rho^4)^{\tfrac{3}{2}+J}}{16\sqrt{2\pi}(3+2J)^{7/2}\zeta^2\rho^5} \cdot [6\rho^2 - 3\zeta\left(1+\rho^4\right) - \\
- 4\zeta^2(3+2J)\left(3+3\rho^4 - 24\rho^2 - 16\,J\rho^2\right) + O(J^{-2})].
\end{aligned}
\tag{C.7}
$$

We will see from the following plot that the expansion above is an excellent approximation to the hypergeometrical function even at small spins

After removing some constant terms due to J being large, and simplifying the expression, we finally arrive at

$$
{}_2F_1(-J-1, -J; 2; \rho^4) \sim \frac{e^{(\tfrac{3}{2}+J)\zeta} \cdot \left(1-\rho^4\right)^{\tfrac{3}{2}+J}}{2\sqrt{\pi}\,\rho^3 \cdot J^{3/2}}, \quad \text{for } 0 < \rho < 1 \text{ as } J \to \infty,
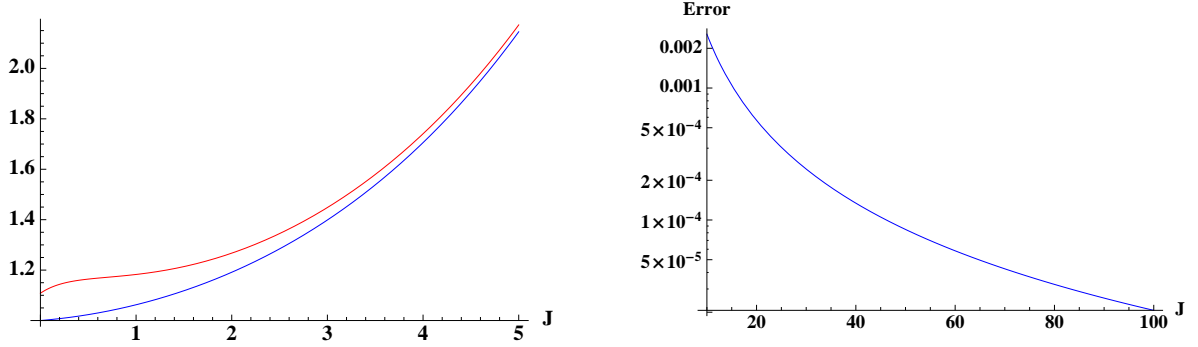\tag{C.8}
$$

118

Figure C.1: The left graph shows a comparison between $_2F_1(-J-1,-J;2;\rho^4)$ (in blue line) and its expansion Eq.(C.7) (in red line) with small spins and $\rho = 1/2$. The right graph shows the error of using the expansion Eq.(C.7) to approximate the hypergeometrical function when $\rho = 1/2$.

where $\zeta \equiv \cosh^{-1}\left[(1+\rho^4)/(1-\rho^4)\right]$. As we will see in Fig.C.2, the asymptotic expression is only a bad approximation with very small spins,

For $\rho = 1$, the asymptotics are much simpler, due to the fact that $_2F_1(-J-1,-J;2;1)$ has very simple factorial expression:

$$_2F_1(-J-1,-J;2;1) = \frac{(2J+2)!}{(J+2)!\,(J+1)!}. \tag{C.9}$$

With Stirling's approximation of factorials

$$n! \sim \sqrt{2\pi n}\left(\frac{n}{e}\right)^n \text{ as } n \to \infty \tag{C.10}$$

we have

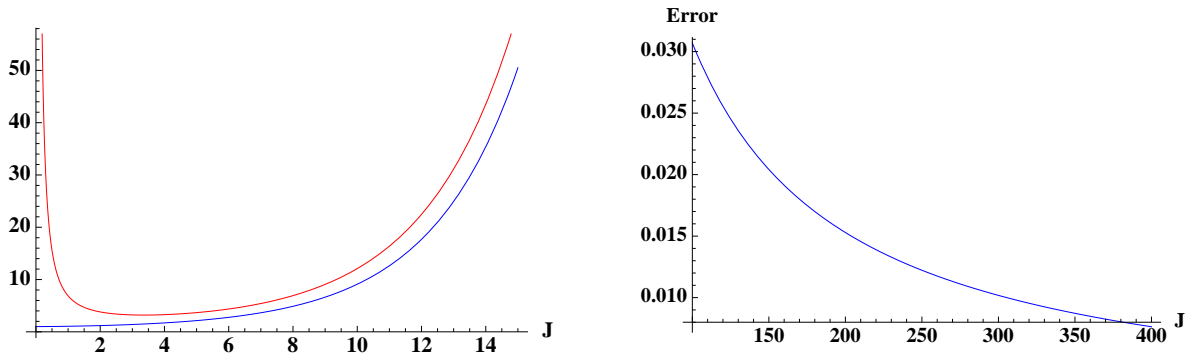$$_2F_1(-J-1,-J;2;1) \sim \frac{4^{J+1}e}{\sqrt{\pi}\cdot J^{3/2}}, \text{ as } J \to \infty. \tag{C.11}$$

119

Figure C.2: The left graph shows a comparison between $_2F_1(-J-1,-J;2;\rho^4)$ (in blue line) and its asymptotic expression Eq. (C.8) (in red line) with small spins and $\rho = 1/2$. The right graph shows the error of using the asymptotic expression Eq. (C.8) to approximate the hypergeometrical function.

Appendix D

The truncated bulk amplitude of the 5–1 move with different gauge fixing trees

In this appendix, we will use 5–1 Pachner move as an example to illustrate that using different choice of gauge fixing trees to compute truncated bulk amplitude gives rise to different result. Both of the results have the same structure as in Eq.(6.21), the differences lie in the sets[1] Φ, Θ and the N_l which essentially keep track of the number of elements in the sets.

A class of optimal spanning trees in the 5-1 cable diagram is taking any of the five vertices as root, and the four edges connected to this vertex as branches. For example, in Fig.D.1, the spanning tree is $AE \cup BE \cup CE \cup DE$. There are $|C_T| = |E| - |V| + 1 = 6$ fundamental cycles. All of them are single-strand loops and contain one original propagator per loop. Applying six corresponding truncated loop identities, we graphically arrive at the simplified diagram. Thus we can read out the truncated bulk amplitude

$$A_{bulk} = \sum_{\{j_l \in \mathbf{Z}/2\}} \prod_l \frac{(2j_l + 1)^{\eta+1}}{(1 + \rho^2)^{2j_l N_l}} \cdot \prod_{\alpha=1}^{|C_T|} \left[F_\rho^2 \left(\sum_{l \in \Phi_\alpha} 2j_l \right) \cdot \left(\sum_{l \in \Phi_\alpha} 2j_l + 1 \right)^{\eta-1} \right] \cdot \prod_{k=1}^{|V|-1} \left[F_\rho^2 \left(\sum_{l \in \Theta_k} 2j_l \right) \right] \quad \text{(D.1)}$$

where $N_l \equiv 4n_f + 2\sum_{\alpha=1}^{n_l} \tilde{n}_\alpha = 4 \times 3 + 2 \times 6 = 24$

$$\Phi_{AB} = \{ABD, ABC\}, \Phi_{AD} = \{ABD, ACD\}, \Phi_{AC} = \{ABC, ACD\},$$
$$\Phi_{BD} = \{ABD, ABC\}, \Phi_{BC} = \{ABC, BCD\}, \Phi_{CD} = \{BCD, ACD\} \quad \text{(D.2)}$$

---

[1]Formally, these have to be multisets because a single element can appear multiple times.
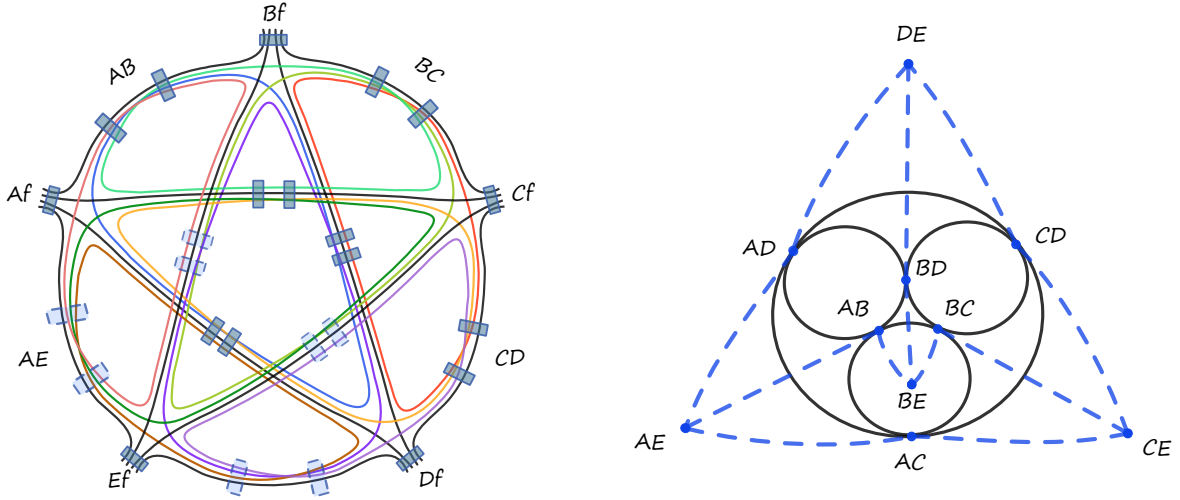
Figure D.1: The cable diagram of 5–1 Pachner move and simplified diagram. The optimal tree contains four branches and there are $|C_T| = 6$ fundamental cycles. The four gauge-fixed propagators are represented as 4 blue dots in the simplified diagram. After applying the corresponding 6 truncated loop identities there are $|F| - |C_T| = 4$ residual loops. Each loop identity creates 2 non-local connections (the dashed lines in the simplified diagram) with the 6 shared points, which correspond to 6 original propagators.

$$\Theta_{AE} = \{ABD, ABC, ACD\}, \quad \Theta_{BE} = \{ABD, ABC, BCD\}$$
$$\Theta_{CE} = \{ABC, BCD, ACD\}, \quad \Theta_{DE} = \{ABD, BCD, ACD\}$$

(D.3)

Now let us redo the calculation with another spanning tree: $AB \cup AE \cup DE \cup CD$. This is not an optimal tree, i.e. some fundamental cycles are not single loops formed by strands. For example: adding the branch BC into the spanning tree creates a cycle $ABCDE \in C_T$, however, $ABCDE \notin F$. It is the same for the edges AC, BD: both of their cycles $ABDE, ACDE \notin F$.

This type of gauge fixing structure leads to nesting of loop identities. For example, we can apply truncated loop identity to loop ADE. Without any mixing of strands due to the truncation, we can apply truncated loop identity again to loop ACD. The truncation within truncation leads to a worse approximation compared with the optimal tree above. The final result of truncated bulk amplitude has the same structure as Eq.(D.1), but the summation of spins in the hypergeometrical functions are different.

$$\Phi_{AC} = \{ABC, AEC\}, \quad \Phi_{AD} = \{ABC, AEC, ABD\},$$
$$\Phi_{BC} = \{BCD, ABC\}, \quad \Phi_{BD} = \{ABD, BCD\}, \tag{D.4}$$
$$\Phi_{BE} = \{BCD, BCD, ABC, ABD\}, \quad \Phi_{CE} = \{BCD, ABC, AEC\}$$

$$\Theta_{AB} = \{BCD, ABC, ABD\}, \quad \Theta_{AE} = \{BCD, ABC, AEC, ABD\}$$
$$\Theta_{CD} = \{BCD, ABC, AEC, \}, \quad \Theta_{DE} = \{BCD, ABC, AEC, ABD\} \tag{D.5}$$

We can count the occurence of each residual loop in the above sets. We find that $N_{BCD} = N_{ABC} = 36$, $N_{AEC} = N_{ABD} = 24$. One can numerically check that the value of truncated amplitude with a choice of arbitrary spanning tree is smaller than the value corresponding to the optimal tree. This is due to the fact that the nesting of loop identities makes the truncation a worse approximation. As we have shown in Section 7.2, when the amplitude is divergent this difference disappears. The degree of divergence is a tree-independent quantity.

123